

NAVAL POSTGRADUATE SCHOOL

Monterey, California



THESIS

DECADAL VARIABILITY OF THERMOHALINE STRUCTURE AT THE SHEBA SITE

by

Robin D. Tyner

June 1999

Thesis Advisor:
Second Reader:

Timothy P. Stanton
Robert H. Bourke

Approved for public release; distribution is unlimited.

REPORT DOCUMENTATION PAGE

Form Approved
OMB No. 0704-0188

Public reporting burden for this collection of information is estimated to average 1 hour per response, including the time for reviewing instruction, searching existing data sources, gathering and maintaining the data needed, and completing and reviewing the collection of information. Send comments regarding this burden estimate or any other aspect of this collection of information, including suggestions for reducing this burden, to Washington headquarters Services, Directorate for Information Operations and Reports, 1215 Jefferson Davis Highway, Suite 1204, Arlington, VA 22202-4302, and to the Office of Management and Budget, Paperwork Reduction Project (0704-0188) Washington DC 20503.

1. AGENCY USE ONLY (Leave blank)

2. REPORT DATE

June 1999

3. REPORT TYPE AND DATES COVERED

Master's Thesis

4. TITLE AND SUBTITLE

DECADAL VARIABILITY OF THERMOHALINE STRUCTURE AT THE SHEBA SITE

5. FUNDING NUMBERS

6. AUTHOR(S)

Tyner, Robin D.

7. PERFORMING ORGANIZATION NAME(S) AND ADDRESS(ES)

Naval Postgraduate School
Monterey, CA 93943-5000

8. PERFORMING
ORGANIZATION REPORT
NUMBER

9. SPONSORING / MONITORING AGENCY NAME(S) AND ADDRESS(ES)

National Science Foundation
Office of Polar Programs, OPP-9701391

10. SPONSORING /
MONITORING
AGENCY REPORT NUMBER

11. SUPPLEMENTARY NOTES

The views expressed in this thesis are those of the author and do not reflect the official policy or position of the Department of Defense or the U.S. Government.

12a. DISTRIBUTION / AVAILABILITY STATEMENT

Approved for public release; distribution unlimited.

12b. DISTRIBUTION CODE

13. ABSTRACT (maximum 200 words)

Recent studies have documented changes in the thermohaline layer of the Canadian Basin. This study analyzes a year long set of temperature and salinity profiles from the SHEBA ice station, in comparison with the 40-year climatology from the EWG digital atlas, the most complete Arctic data compilation available. Significant anomalies were observed, including warming and shoaling of the Pacific layer south and east of the Chukchi Cap, absence of a Pacific layer north of the Chukchi Cap, upper halocline freshening, and large mixed layer salinity decreases in the Beaufort Sea in contrast to increases north of and over the Chukchi Cap. These anomalies suggest a shift in synoptic scale advective patterns in response to a weakened Beaufort High pressure system and a strengthened and expanded Eurasian Low pressure system. These circulation changes may restrict the flow of Pacific water through Herald Canyon, focusing it more through Barrow Canyon. Ice cover/thickness changes may also contribute to the observed anomalies.

14. SUBJECT TERMS

decadal variability, upper halocline, temperature, salinity, SHEBA, Beaufort Gyre, Canada Basin

15. NUMBER OF
PAGES

112

16. PRICE CODE

17. SECURITY CLASSIFICATION OF
REPORT

Unclassified

18. SECURITY CLASSIFICATION OF
THIS PAGE

Unclassified

19. SECURITY CLASSIFI- CATION
OF ABSTRACT

Unclassified

20. LIMITATION
OF ABSTRACT

UL

**DECADAL VARIABILITY OF THERMOHALINE STRUCTURE AT THE
SHEBA SITE**

Robin D. Tyner
Lieutenant Commander, United States Navy
B.S., United States Naval Academy, 1988
M.B.A., New Hampshire College, 1996

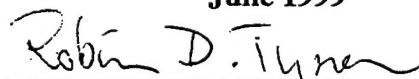
Submitted in partial fulfillment of the
requirements for the degree of

**MASTER OF SCIENCE IN METEOROLOGY AND PHYSICAL
OCEANOGRAPHY**

from the

**NAVAL POSTGRADUATE SCHOOL
June 1999**

Author:

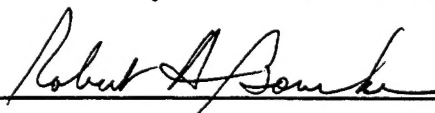


Robin D. Tyner

Approved by:



Timothy P. Stanton, Thesis Advisor



Robert H. Bourke, Second Reader



Roland W. Garwood, Jr., Chairman
Department of Oceanography

ABSTRACT

Recent studies have documented changes in the thermohaline layer of the Canadian Basin. This study analyzes a year long set of temperature and salinity profiles from the SHEBA ice station, in comparison with the 40-year climatology from the EWG digital atlas, the most complete Arctic data compilation available. Significant anomalies were observed, including warming and shoaling of the Pacific layer south and east of the Chukchi Cap, absence of a Pacific layer north of the Chukchi Cap, upper halocline freshening, and large mixed layer salinity decreases in the Beaufort Sea in contrast to increases north of and over the Chukchi Cap. These anomalies suggest a shift in synoptic scale advective patterns in response to a weakened Beaufort High pressure system and a strengthened and expanded Eurasian Low pressure system. These circulation changes may restrict the flow of Pacific water through Herald Canyon, focusing it more through Barrow Canyon. Ice cover/thickness changes may also contribute to the observed anomalies.

TABLE OF CONTENTS

I.	INTRODUCTION	1
A.	OVERVIEW	1
B.	METHODOLOGY	1
II.	BACKGROUND OCEANOGRAPHY	3
A.	OCEANOGRAPHIC FEATURES	3
B.	VERTICAL STRUCTURE	8
III.	ANALYSIS OF EWG CLIMATOLOGICAL ATLAS	17
A.	ATLAS DESCRIPTION	17
B.	DESCRIPTION OF THE REGIONAL/DECADAL ANALYSIS	18
C.	REGIONAL ANALYSIS OF 15/50/100 M DEPTH LEVELS	29
D.	ANALYSIS OF REGIONAL DECADAL MEAN PROFILES	43
E.	WINTER-SUMMER COMPARISONS	51
F.	HISTORICAL VARIABILITY SUMMARY	52
IV.	ANALYSIS OF SHEBA DATA IN COMPARISON WITH HISTORICAL DATA	57
A.	OVERVIEW	57
B.	DECADAL AND GRID BOX COMPARISONS	61
C.	SHEBA ANALYSIS SUMMARY	70
V.	DISCUSSION AND CONCLUSIONS	77
A.	COMPARISON SUMMARY OF SHEBA AND HISTORICAL DATA	77
B.	SHEBA ANOMALIES AND PROPOSED EXPLANATIONS	79
C.	POTENTIAL EFFECTS OF OBSERVED ANOMALIES	90
D.	RELATED TOPICS FOR FURTHER INVESTIGATION	91
APPENDIX A. SUMMARY PLOTS OF MAR-MAY AND JUL-SEP HISTORICAL DATA FROM THE EWG DIGITAL ATLAS FOR TEMPERATURE AND SALINITY		93
LIST OF REFERENCES		97
INITIAL DISTRIBUTION LIST		101

ACKNOWLEDGEMENTS

This thesis could not have been completed without the funding provided by the National Science Foundation, which made the collection of data used in this thesis possible. Assistance from the following persons was also vital to the successful completion of this thesis: Timothy Stanton for his vision, expertise, and encouragement, Dr. Robert Bourke for his outstanding polar oceanography instruction, editing skills, and encouragement, and Jim Stockton for computer systems support, and Mike Cook and Paul Jessen for programming expertise.

I. INTRODUCTION

A. OVERVIEW

During the Surface Heat Budget of the Arctic (SHEBA) program, the Canadian ice breaker CCGS Des Groseilliers entered the Beaufort Sea pack ice and drifted with the ice cover from September 1997 to September 1998, frozen into the pack ice for much of the year. As one of a myriad scientific experiments conducted during SHEBA, a continuous time series of temperature and salinity profiles was collected. This study analyzes the temperature and salinity profiles collected in the upper 150 m of the water column, averaged over one meter depth intervals and one day time intervals, and compares them to the most robust climatological data base available for this region of the Arctic Ocean. Significant changes and anomalies revealed are examined and discussed.

B. METHODOLOGY

The first step in this project was an extensive literature search including books, Polar Oceanography course notes, and scientific journal articles that described physical and dynamic features and properties of the Arctic Ocean, specifically the Canadian Basin. This background reading provided an overview of well-accepted mechanisms for known processes, proposed theories for less-well understood processes, and insight into uncertain and ongoing spatial and temporal changes in Arctic features and circulations patterns. A synopsis of this background material is provided in Chapter II as a brief overview of the oceanography of the western Arctic basin.

Environmental Working Group (EWG) digital climatological atlases for both winter and summer,

containing 45 years of temperature and salinity statistical data were obtained. Climatological vertical profiles were constructed from horizontal statistical fields of temperature and salinity at all available depths at and above 150 m. Although individual profiles were not available, the robustness and completeness of this data set, combined with the thoroughness of applied quality control procedures, made it reasonable to conduct an historical analysis. The ensemble means provided were of sufficient resolution to make meaningful comparisons on a decadal scale. Analysis of this data provided valuable insight into the decadal and inter-decadal variability of the western Arctic Ocean, suggesting locations where long term, low frequency variability dominates. Chapter III details the analysis of this climatological data.

Mean profiles (upper 150 m) of the SHEBA data were constructed over the same geographic regions and temporal spans used by the EWG digital atlas. These profiles were analyzed in comparison with the historical profiles, in order to discern whether anomalies were present, and if so, to determine their scale in relation to historically documented variability. This analysis and comparison is covered in Chapter IV.

Finally, in Chapter V, the findings from Chapter IV are discussed in more detail, and explanations are presented. Results from this study were compared with results from other recent experiments and publications. Conclusions were drawn, incorporating information from other published works where applicable. The findings of this study pointed to several related topics that warrant additional research and analysis.

II. BACKGROUND OCEANOGRAPHY

A. OCEANOGRAPHIC FEATURES

The Arctic Ocean is divided into two major basins, the Canadian Basin and the Eurasian Basin, which are separated by the Lomonosov Ridge. These basins are often loosely referred to as the western Arctic and eastern Arctic, respectively. The Canadian Basin is further separated by the Alpha-Mendeleev Ridge into the Canada Basin and the Makarov Basin. The Eurasian Basin is subdivided by the Nansen-Gakkel Ridge into the the Amundsen Basin and the Nansen Basin. Within the southern Canada Basin is the Beaufort Sea, with a maximum depth of 3800 m - the deepest part of the Canada Basin. South of the Canada Basin lie the relatively shallow Chukchi and East Siberian Seas. The geography and bathymetry of the above-mentioned features are all illustrated in Figure 2.1, adapted from Swift et al., 1997.

The bathymetry of the Beaufort and Chukchi Seas exerts a significant influence on the predominant physical processes of the region, including currents, halocline maintenance and eddy formation. The Chukchi Sea, just west of the Beaufort Sea and north of the Bering Strait, has a maximum depth of only 50 m. The bathymetric slope between the Chukchi Sea and the western Beaufort Sea, and between the Beaufort Sea and the narrow continental shelf to the south, is extremely steep. The Chukchi Cap, or Chukchi Plateau, a large subsurface plateau just north of the Chukchi Sea, has a depth of approximately 500 m and a very steep eastern slope. The eastern Beaufort Sea has a gentler bathymetric slope as it approaches the MacKenzie shelf of northwest Canada.

The broad, clockwise Beaufort Gyre extends across most of the Canada Basin to a depth of about 150 m. It is the

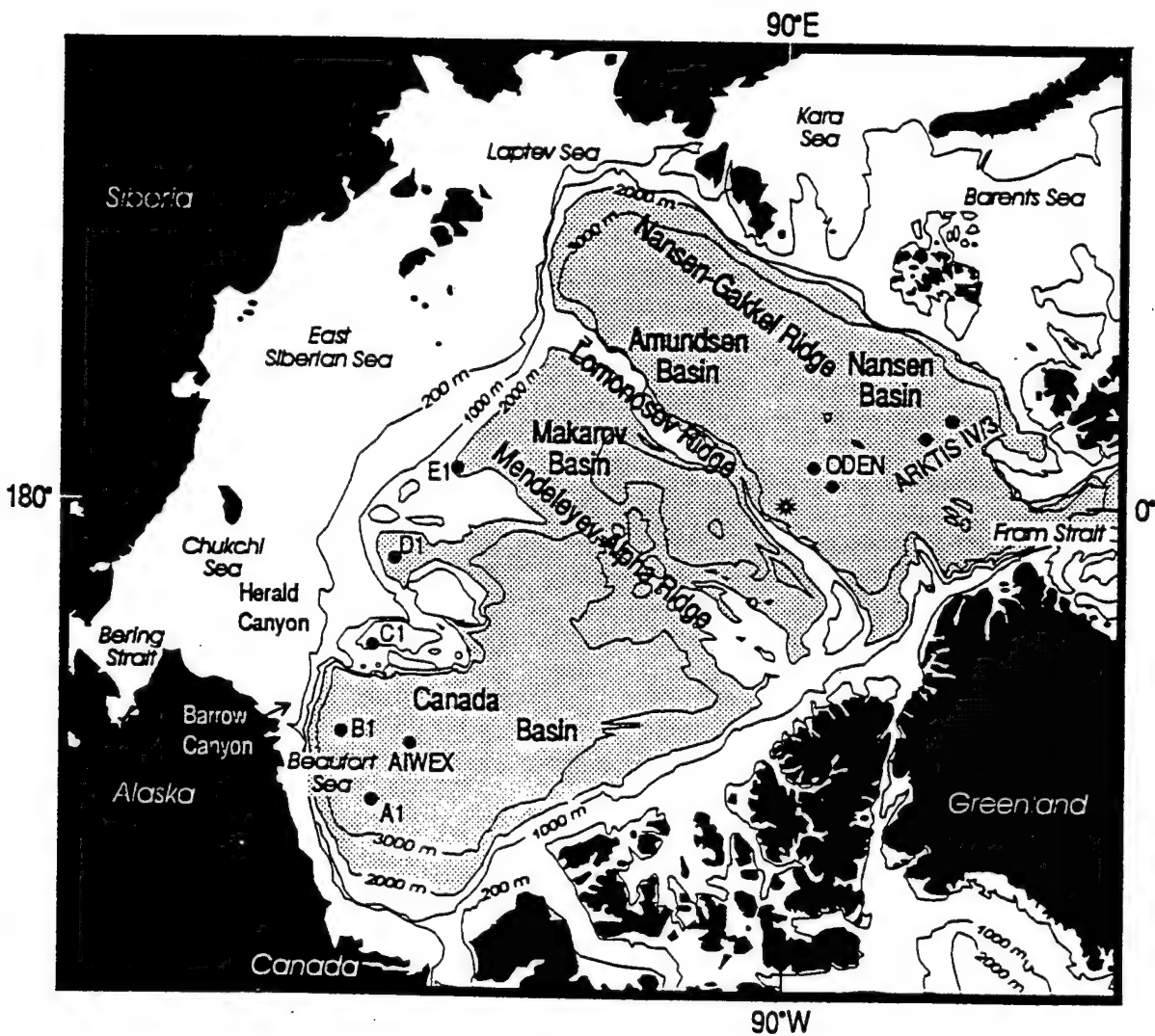


Figure 2.1. Geography and bathymetry of the western Arctic Ocean. Also shown are station locations from Larsen-93, AIWEX, Oden-91, and ARKTIS IV/3 (from McLaughlin et al. 1996).

oceanic response to the anti-cyclonic wind circulation around the semi-permanent high pressure system, the Beaufort High, centered over the Canada Basin. Ekman convergence driven by the geostrophic wind pattern causes downwelling, which slightly depresses the pycnocline, halocline, and thermocline in the center of the gyre. This downwelling is roughly proportional to the strength (pressure gradient) and areal extent of the high pressure cell. The location and strength of the high are also related to the extent of transport of Bering Sea water into the Arctic.

Warm, saline, northerly inflow of Pacific water into the Canada Basin occurs year round through Bering Strait. It is most pronounced in summer when maximum surface temperatures may reach 6°-10°C (Bourke, 1982; Coachman and Aagard, 1974), with summer salinities seldom exceeding 31 psu (Bourke, 1982). In winter temperatures are near freezing (-1.5 to -1.7°C), and salinities range from 32 to 34 psu. The flow splits into two major branches, with several smaller offshoots, following the bottom topography of the Chukchi Sea. The northwesterly branch follows Herald Canyon, and the northeasterly branch follows the deeper, narrower Barrow Canyon (Figure 2.2). The northeasterly branch, a narrow high-speed current along western Alaska, is known as the Alaskan Coastal Current. Summer ice melt is strongly enhanced by the warm northward flow across the Chukchi Shelf and along the Alaskan coastline. Therefore, the retreat of the ice edge in summer generally corresponds to bottom topography, but is also influenced by local surface wind stress (Bourke, 1982; Paquette and Bourke, 1981).

The warm Alaskan Coastal Current flows north along the western and northern Alaska coastlines at approximately 0.4 m/s. It is concentrated at the surface in the Chukchi Sea due to its relatively low density, but as it approaches deeper water, the denser water beneath it flows downslope,

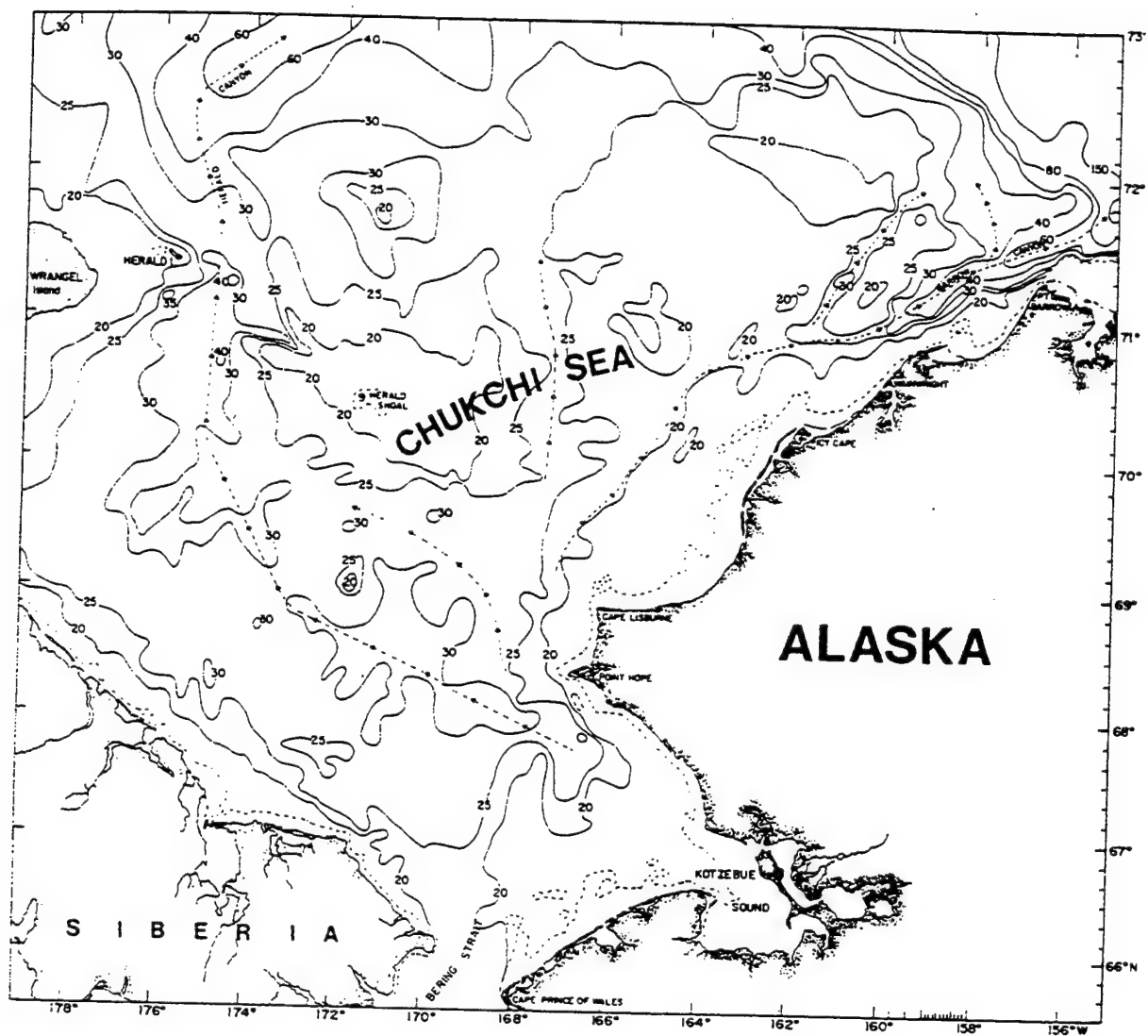


Figure 2.2. Geography/bathymetry of the Chukchi Sea and Bering Strait. The arrows suggest steering of the broad northward flow through various troughs and canyons, including Barrow Canyon and Herald Canyon (from Paquette and Bourke, 1981).

and the current itself finds a deeper equilibrium level at 30-50 m depth on the Beaufort Sea shelf (Paquette and Bourke, 1974). The Alaskan Coastal Current eventually feeds the cyclonic Beaufort Undercurrent, which flows eastward in excess of 0.1 m/s at depths up to 150 m on the continental shelf (Carmack, 1990; Aagaard, 1984).

Fronts in this region are generally associated with currents carrying relatively warm Bering Sea water, or with the marginal ice zone (MIZ). Two types of summertime fronts can occur near the ice on the shallow shelves. A nearly vertical upper-layer temperature and salinity front develops in the top 10-20 m roughly at the interface between the ice edge and the oncoming warm water. A lower-layer "front" develops south of and below the upper layer front in regions where incoming warm water overlies deeper cold water (Bourke, 1982).

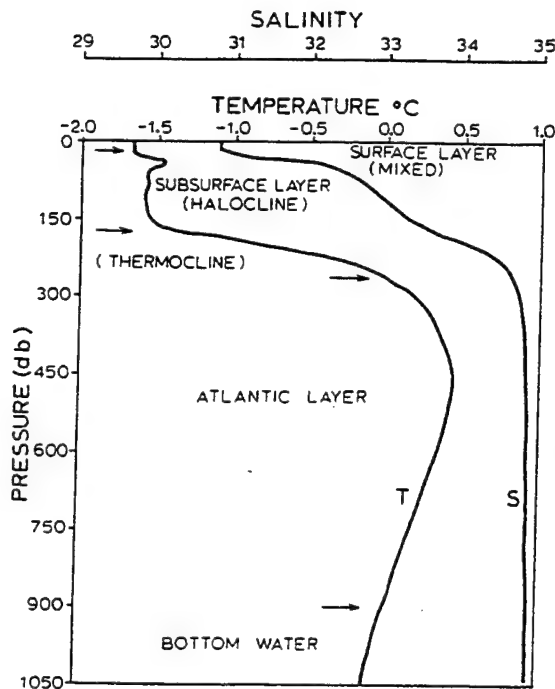
Beaufort Sea eddies, or sub-mesoscale coherent vortices (SCV's), have been observed at depths from 5m to 500 m, and are estimated to cover 20-30% of the Beaufort Sea (D'Asaro, 1988a). They are most commonly warm, anticyclonic, and above 250 m in the Beaufort Sea, with maximum properties centered at 100-150 m depth. These eddies have anomalous water properties (temperature, density, nutrients, etc.) that correspond to the warm Bering Sea inflow, and are too large to have been generated in the Beaufort Sea. Therefore, the eddies must be generated at the edge of the Beaufort Sea and advected into the interior (D'Asaro, 1988b; Manley and Hunkins, 1985; Hunkins, 1974). In his study of four eddies found during the Arctic Internal Wave Experiment (AIWEX), D'Asaro (1988a) noted that anticyclonic eddies above 250 m were centered on temperature maxima of waters originating in the Pacific Ocean, while cyclonic eddies were centered below 300 m near the Atlantic water temperature maximum. Anticyclonic Beaufort Sea eddies are about 10-20 km in diameter, and have a mean rotational speed of

approximately 0.24 m/s. They have no surface signature. The upper surface of these eddies often coincides with the base of the mixed layer (Manley and Hunkins, 1985).

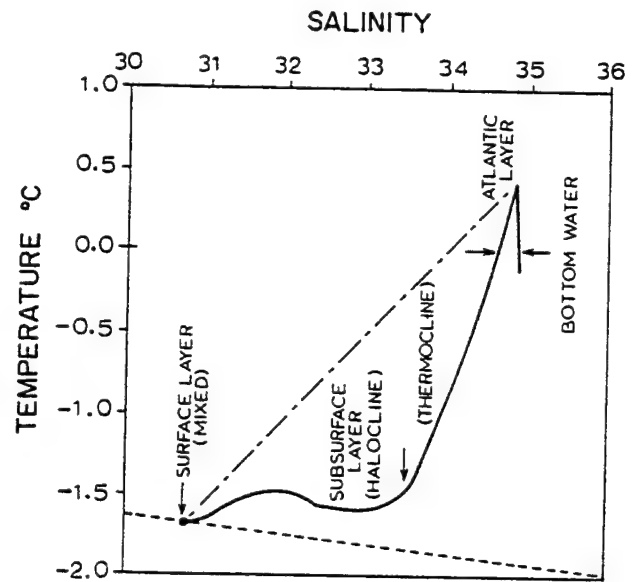
SCV's are probably generated in Barrow Canyon, and perhaps even Herald Canyon, where water flows from the Chukchi Sea into the Beaufort Sea (D'Asaro, 1988b; Hunkins, 1974). They originate with a positive potential vorticity, $q \propto (\zeta + f)$, where the relative vorticity (ζ) is approximately $-1.5f$ to $-2.5f$. Friction reduces the potential vorticity of the flow on the inshore side of a coastally trapped current (i.e., the flow through Barrow Canyon) until $q < 0$. When the flow separates from the coast, the vorticity in the boundary layer separates into vortices, which undergo geostrophic adjustment to become SCV's. The cores of these vortices, where $q < 0$, are unstable, and entrain surrounding water with positive vorticity, until they eventually attain zero potential vorticity well away from the coast in the Beaufort Sea (D'Asaro, 1988b).

B. VERTICAL STRUCTURE

The water mass structure of the Arctic Ocean generally consists of three vertical layers: surface, intermediate, and deep, capped by a layer of ice. The specific characteristics of these three layers vary significantly throughout the Arctic. The focus of this thesis is the surface layer of the Canada Basin, primarily in the western Beaufort Sea and Chukchi Cap regions, with some interest in the interrelationships with the neighboring Chukchi Sea, the intermediate layer below, and the overlying ice cover. The following discussion of surface and intermediate layer features, shown in Figures 2.3(a) and 2.3(b), is primarily based on historical data and analyses, i.e., prior to the 1990's. Recently observed characteristics and changes will be addressed in Chapter V.



(a)



(b)

Figure 2.3. Principal water masses in the Canadian Basin, depicted by (a) typical T/S profiles; and (b) correlation in T-S space. (Following Melling and Lewis, 1982).

Because of the near-freezing water temperatures in the Arctic, and the small thermal expansion coefficient of sea water at these temperatures and salinities, density is controlled primarily by salinity. The halocline closely corresponds to the pycnocline, and temperature can be considered a water mass tracer. The very small contribution of temperature fluctuations to density near the freezing point of seawater for salinities found in the Arctic Ocean is illustrated in Figure 2.4.

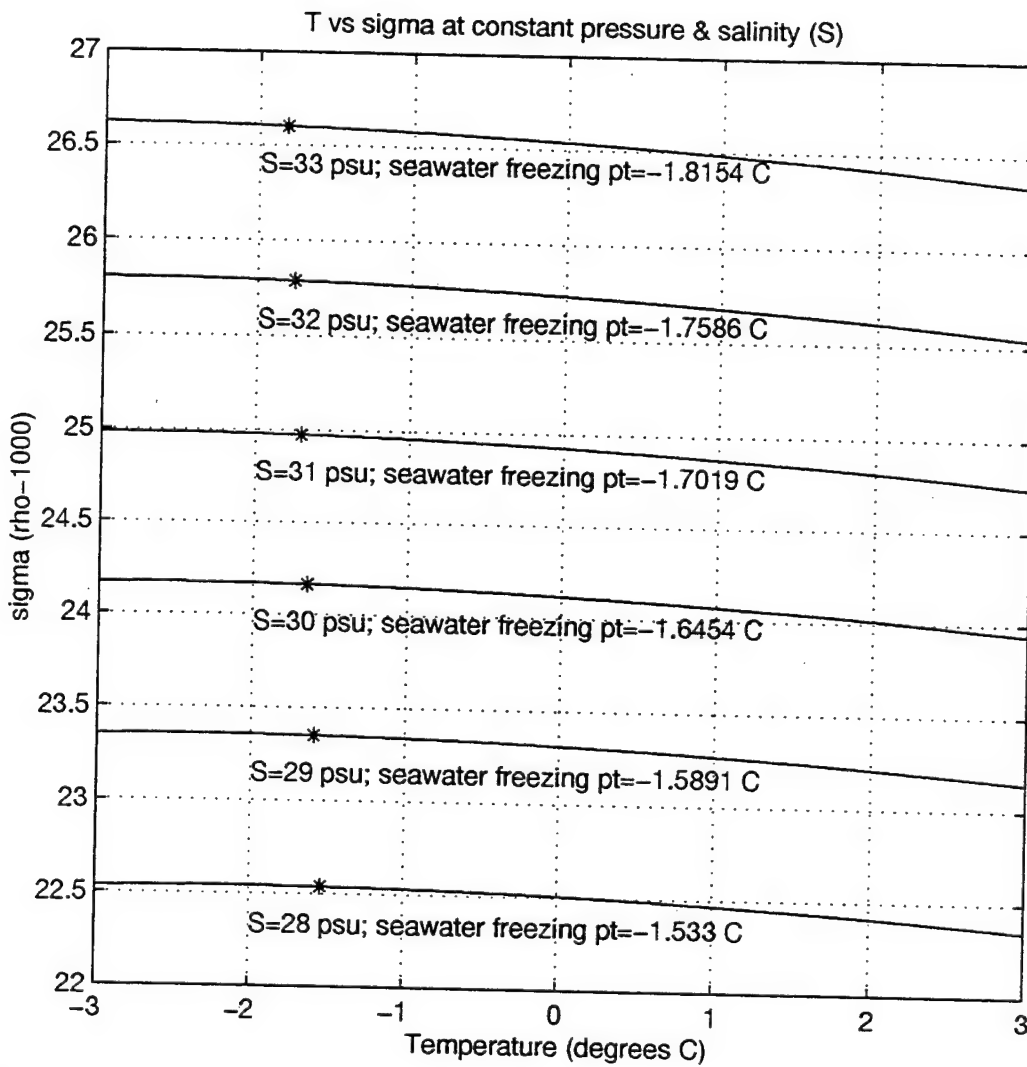


Figure 2.4. Plot of density (sigma zero) versus temperature at various salinity levels. The freezing point at various salinities is represented by an asterisk (*). Note that temperatures near the freezing point have virtually no effect on density.

The surface layer can be sub-divided into the surface mixed layer and subsurface layer. The surface mixed layer in the Canada Basin extends to a depth of approximately 40-50 m, depending on the extent of convective and wind stress mixing. The characteristics of the mixed layer have a seasonal cycle. By the end of winter it is isothermal, with a temperature at the freezing point (approximately -1.7°C), and isohaline, with salinity <31 psu. During summer, solar insolation warms the water column and ice melt decreases the near-surface salinity. By the end of summer a distinct seasonal halocline/pycnocline is formed below 20-25 m, which prevents turbulent mixing and effectively caps the "lower mixed layer", trapping its heat (Maykut and McPhee, 1995; McPhee et al., 1998). During fall, solar insolation decreases rapidly and water above the summer halocline cools. Mixing by winter storms then breaks down the seasonal halocline, releases the trapped heat, and deepens the isothermal/isohaline mixed layer. Whether or not all of the trapped heat is released, and whether or not the mixed layer returns to its previous year's depth, depends on the severity and duration of the winter cooling season.

The subsurface layer, from approximately 40 m - 150 m, coincides with the upper halocline. The upper halocline is formed by summer ice melt and river runoff at the surface, overlying denser water originating in the Bering Sea and modified on the Chukchi and East Siberian shelves (Jones and Anderson, 1986). The upper halocline is maintained and strengthened by the wintertime lateral advection of high salinity water from the shelves, which is formed primarily by brine rejection during ice formation (Aagaard et al., 1981; Melling and Lewis, 1982). A secondary mechanism for maintaining the halocline is the upwelling of Atlantic waters in canyons and its subsequent cooling (Aagaard et al., 1981; Melling and Lewis, 1982). However, Jones and Anderson (1986) suggest that nitrate values found in the

Atlantic layer are too large to be reduced to the nitrate values observed in the upper halocline, which reduces the probable contribution of this mechanism.

The temperature in the subsurface layer normally remains below -1°C , but a notable temperature maximum (T_{max}) is present around 75 m associated with warm summertime inflow of Pacific water through the Bering Strait (Coachman and Barnes, 1961). Figure 2.5 shows the distribution of this maximum temperature in the Pacific layer. This T_{max} normally has a salinity of approximately 31.9 psu (Jones and Anderson, 1986). The diffusive instability is possible above this temperature maximum, allowing the Bering Sea water to supply a small amount of heat to the overlying mixed layer (Padman and Dillon, 1987; Carmack and Aagaard, 1973). Wintertime inflow through the Bering Strait is cooler and denser, due to colder atmospheric temperatures and minimal river and melt water input. This winter inflow lies below the summertime inflow, forming a temperature minimum at approximately 150 m.

A nutrient (silicate, phosphate, nitrate) maximum associated with the Bering Sea inflow is found within the subsurface layer at a salinity of 33.1 psu, at approximately 100 m depth (Jones and Anderson, 1986; Swift et al., 1997; Carmack et al., 1997). Jones and Anderson (1986) propose that this maximum forms in the Chukchi Sea, where high ice productivity, combined with relatively long residence times on shelves fed by nutrient-rich Bering Sea water, provide an opportunity for the $S=33.1$ psu water to become enriched with nutrients.

The intermediate layer extends from about 150 m to 900 m. This layer is dominated by water of Atlantic origin, and has traditionally been defined as waters with a temperature greater than 0°C . The upper half of this layer contains the main thermocline and the lower halocline - the thermohaline staircase (Padman and Dillon, 1987). An NO minimum of

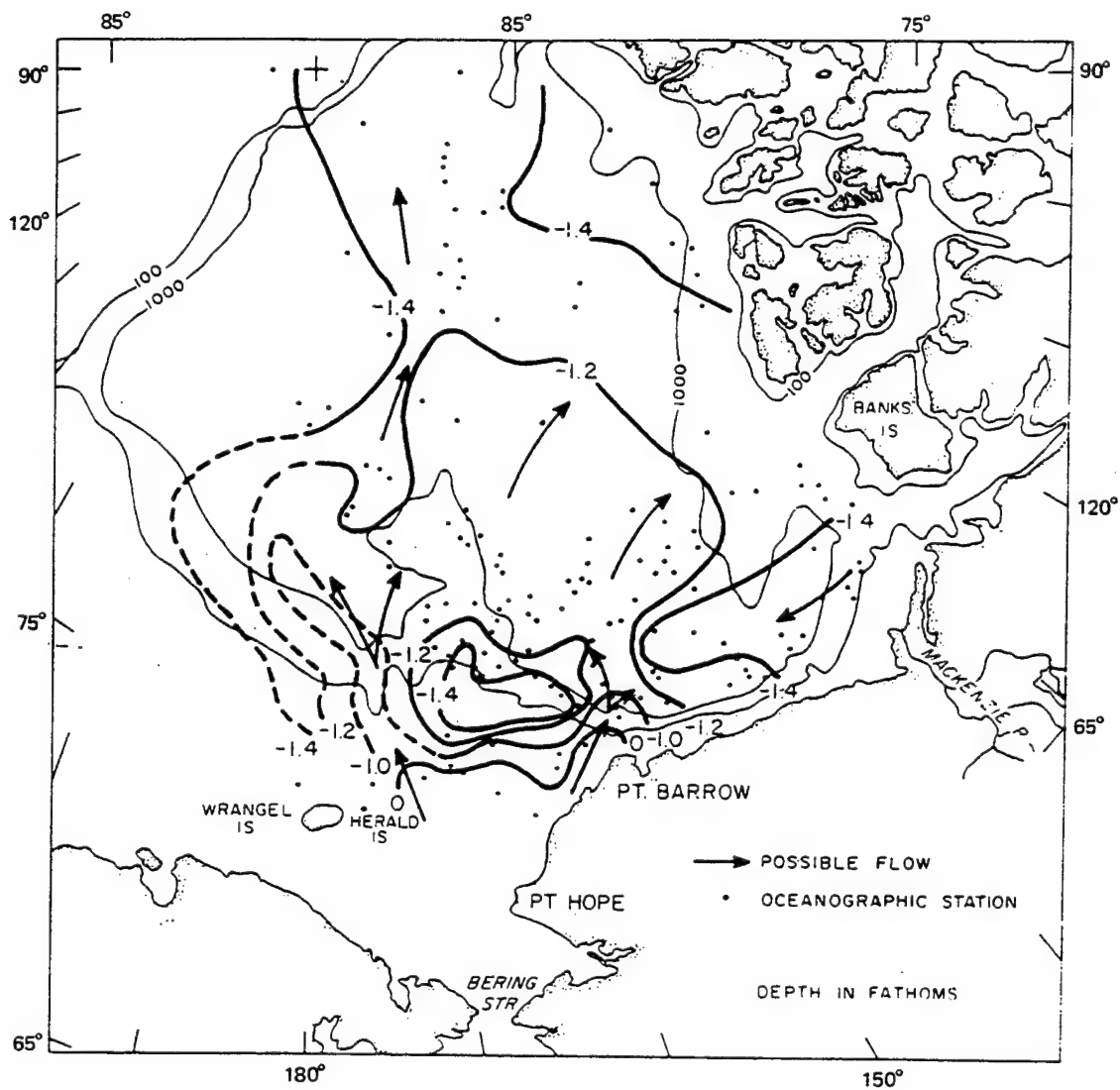


Figure 2.5. Isotherms of maximum temperature between 50 and 100 m (waters of Pacific origin) in the Canadian Basin. At shallow stations (west of Point Barrow) temperature at -32 psu is used. All maximum temperatures in the Beaufort Sea are below -1.0°C (from Coachman and Aagaard, 1974).

Atlantic origin is found at $S=34.2$ psu, near the top of the intermediate layer. Jones and Anderson [1986] propose that this minimum is formed on the shelves of the Barents and Kara Seas during winter ice production.

The intermediate layer is the warmest layer of the Arctic ocean, but its heat is effectively trapped by the strong halocline/pycnocline, as the stable stratification inhibits turbulent mixing. Weak vertical heat exchange may still occur by breaking internal waves or by conduction at the molecular level - an extremely slow process. Because temperature and salinity both increase with depth, the diffusive instability is possible. Padman and Dillon [1987] found that the diffusive heat fluxes between 300 m and 420 m, although not uniform, were approximately 0.05 W/m^2 - at least two orders of magnitude smaller than dominant Arctic ocean heat flux processes.

The Beaufort Sea is almost completely ice-covered (~97%) in winter, reducing to approximately 85% ice cover in summer. The mean ice thickness is 2-3 m, roughly in annual thermodynamic equilibrium balance. Most of the ice in the Beaufort Sea is multi-year ice. The Chukchi Sea is normally ice-covered from November to late June, when the ice edge rapidly retreats to 72° - 75° N (Bourke, 1982). The Beaufort Sea ice cover drifts with the Beaufort Gyre - clockwise at about 0.02 m/s . The stronger the Beaufort high pressure center over this gyre, the stronger the Ekman convergence becomes at the surface. This causes ice convergence against land masses and the building of pressure ridges.

Brine rejection during winter freezing increases the salinity at the ice-water interface. This denser water sinks through the fresher mixed layer, thus convectively overturning the upper water column and building the halocline (Aagaard et al., 1981; Melling and Lewis, 1982). This process achieves its greatest impact over latent heat polynyas, where thin surface ice layers are repeatedly

formed, displaced by surface winds, and then reformed (Aagaard et al., 1981; Cavalieri and Martin, 1994). Cavalieri and Martin, (1994) found that Alaskan coastal polynyas between Cape Lisburne and Point Barrow, along with Siberian coastal polynyas in the vicinity of Anadyr Strait and the Gulf of Anadyr, account for nearly 50% of the total dense water production in the Arctic Basin.

The ice cover presents a significant barrier to vertical heat transfer between the ocean and atmosphere. It acts as a heat sink for the relatively warm ocean, and effectively halts sensible and latent heat exchange between the atmosphere and the ocean. Molecular conduction, the only means for heat transfer through the ice, is extremely slow. A typical value for the molecular heat conductivity of ice (k_i) is $2.1 \text{ W m}^{-1} \text{ K}^{-1}$, depending on the ice salinity and temperature ($k_i \cong k_{\text{pure ice}} + \beta \cdot S_i / T$, where $\beta = 0.137 \text{ W/m}$, T = the temperature of the ice, and S_i = the salinity of the ice) (Untersteiner, 1961). This is much smaller than the typical turbulent diffusivity of water. The thermal insulating properties of ice actually inhibit its growth rate as it gets thicker. Within leads and polynyas, however, the lack of thick ice permits significant heat fluxes from the ocean to the much colder atmosphere.

III. ANALYSIS OF EWG CLIMATOLOGICAL ATLAS

A. ATLAS DESCRIPTION

Winter and summer climatological atlases of the Arctic Ocean were constructed by a team of U.S. and Russian scientists working together under the Environmental Working Group (EWG) of the U.S.-Russian Joint Commission on Economic and Technical Cooperation, referred to as the Gore-Chernomyrdin Commission. They were released in March 1997 and August 1998, respectively. These atlases are the first consolidation of nearly all Arctic data resources worldwide, including Russian data and newly declassified USN data which was previously unavailable to U.S. scientists. Data sources include the Arctic and Antarctic Research Institute (AARI) Expeditions, Russian National Ocean Data Center (ODC), Russian Naval Ocean Data Center, Murmansk Polar Institute for Fishery and Oceanography, U.S. National Ocean Data Center (NODC), Canada Institute for Ocean Science (IOS), and SALARGOS buoy data released by the U.S. Naval Oceanographic Office (NAVOCEANO) (EWG, 1997; EWG, 1998). Due to access restrictions imposed on the original data, individual profiles are not stored in the atlas. Instead, statistical fields (used for this research project) and objectively analyzed fields of temperature and salinity were calculated from the data over decadal time intervals and provided in the atlas.

The atlases contain statistics for 45 years of winter (December through May) and summer (June through November) temperature and salinity data, organized by depth and decade. Statistics were calculated for 200 km by 200 km grid cells covering the Arctic region. (Smaller grid cells were used when possible, mostly in the summer atlas, in smaller scale regions with large numbers of observations). This statistical data is stored in the atlases as horizontal

fields by depth and decade for the following periods: December through February, March through May, June, July through September, and October through November. The March through May data is considered representative of the winter season, and the July through September data is considered representative of the summer season.

Due to the diverse sources of the data, strict objective and subjective quality control methods were applied to this consolidated database. The following four data record checks were made on the headers of each observation: time (hours between 00 and 24, minutes between 00 and 59), coordinates (latitude between 60° and 90°, longitude between ±180°, minutes between 00 and 59), distance between stations (ensure ship/aircraft speed between stations was possible), and bottom depths (within limits of bathymetric database). Parameter checks were conducted for temperature, salinity, and potential density to ensure the values in each observation were values possible in Arctic seawater. A statistical check was applied independently to data at each standard depth. Observations with values more than three standard deviations from the mean value were discarded. Additionally, expert control was done using code developed by subject matter experts.

B. DESCRIPTION OF THE REGIONAL/DECADAL ANALYSIS

Figure 3.1 shows the relation between Canada Basin latitudes/longitudes and the x/y coordinates (distances in km referenced from the North Pole) used in the atlases. Each grid cell is 200 km by 200 km. The SHEBA drift track, three representative latitude lines, a rough outline of the Alaskan coast, and a 500 m depth contour are plotted on this figure for reference. The grid cells over the SHEBA drift track are designated SHa through SHh, in the order which

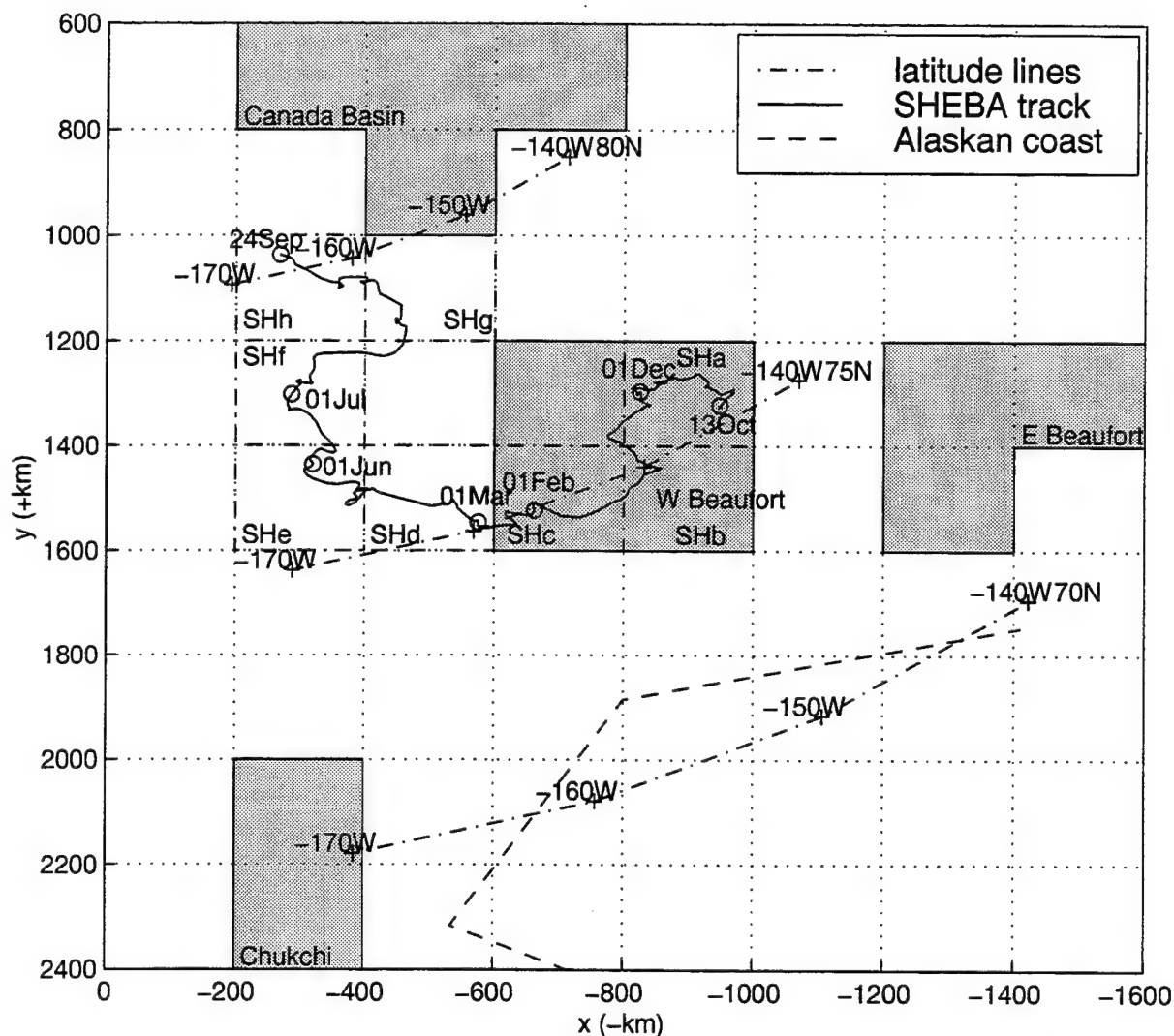


Figure 3.1. Regions of the Canada Basin surrounding the SHEBA site. This map is presented in x/y km coordinates, consistent with those used by the EWG digital atlas. Grid cells are 200 km by 200 km. The SHEBA drift track and a rough outline of the northern Alaskan coastline are plotted for reference. Shaded grid cells represent geographic regions with similar oceanographic features (eastern and western Beaufort Sea, northern Canada Basin, Chukchi Sea). Individual SHEBA boxes are outlined and labelled SHa-h.

SHEBA drifted through them. (Note that two boxes through which SHEBA drifted are omitted. The SHEBA track only crossed a small corner of these two boxes, for which very little statistical data was available). Grid cells over areas with similar oceanographic features were grouped to represent broader regional areas surrounding the SHEBA site (Chukchi Sea, western Beaufort Sea, eastern Beaufort Sea, northern Canada Basin), and are shaded gray. Cells with no data or non-robust data (based on less than five observations) and cells which overlaid coastlines were not used.

Figures 3.2 and 3.3 are used to provide an historical understanding of regional differences in and surrounding the Beaufort Sea. Figures 3.2a-d show the statistical mean late-winter (Mar-May) temperatures and salinities at 15 m, 50 m, and 100 m within each grid box for each decade from the 1950's to the 1980's. Figures 3.3a-d show mean summer (Jul-Sep) data for these same depths and decades. Data for two decades is shown on each figure. Within each grid box, the three rows correspond to the three depth levels and the two columns represent decadal means (either 1950's/1960's or 1970's/1980's). Mean values are only indicated for grid boxes containing at least five observations at that specific depth level and decade. Note that data was not available or was non-robust for many depths/decades. Data at 15 m is considered representative of the mixed layer. Data above 15 m frequently had large standard deviations, and was more likely influenced by small scale air-sea interactions and/or sea ice cover. The 50 m and 100 m levels are both within the upper halocline and are more representative of advective changes and long-term trends in temperature and salinity.

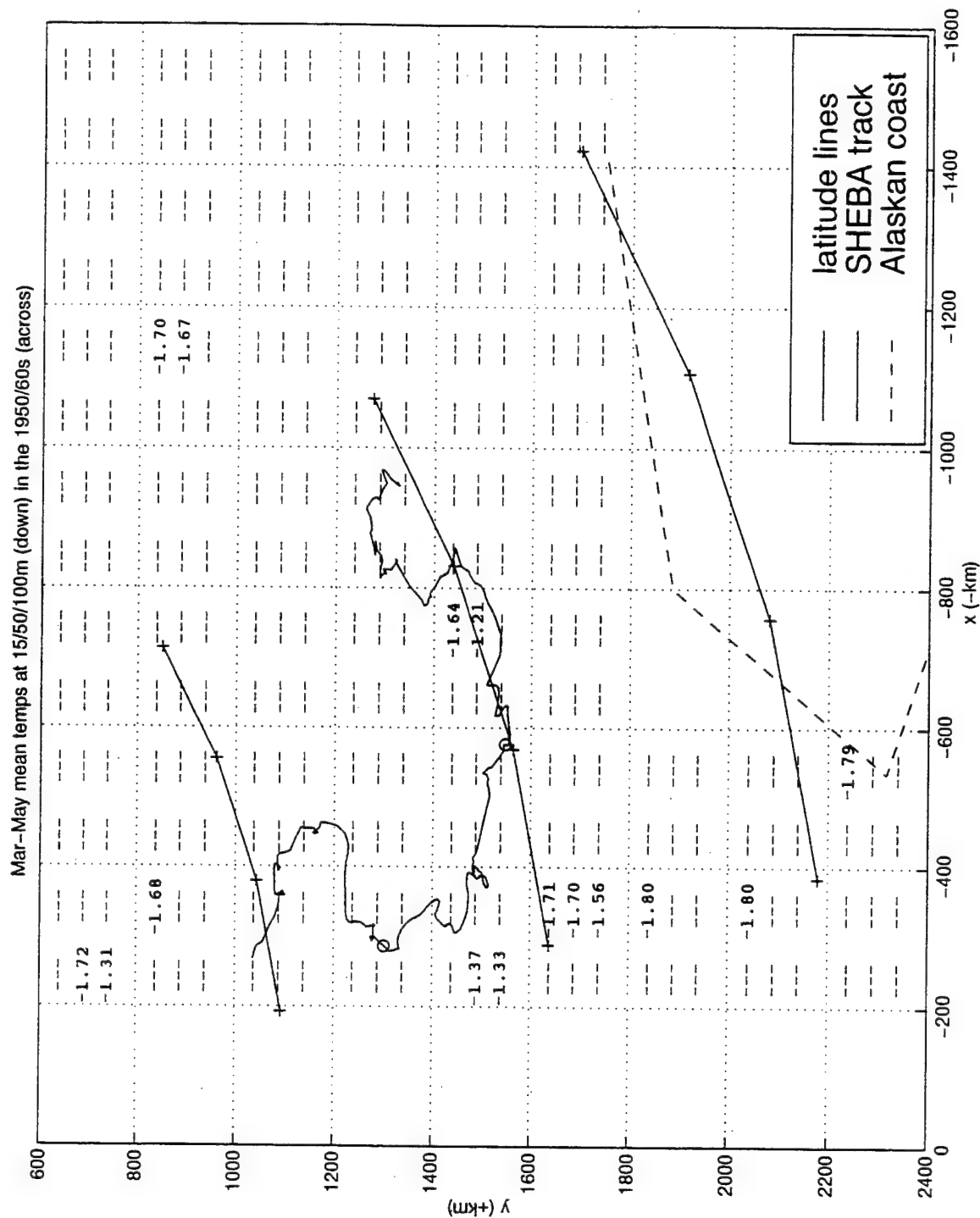


Figure 3.2 (a). Mar-May mean historical temperatures from the EWG digital atlas for each grid box at 15 m (first row), 50 m (second row), and 100 m (third row) during the 1950's (first column) and 1960's (second column).

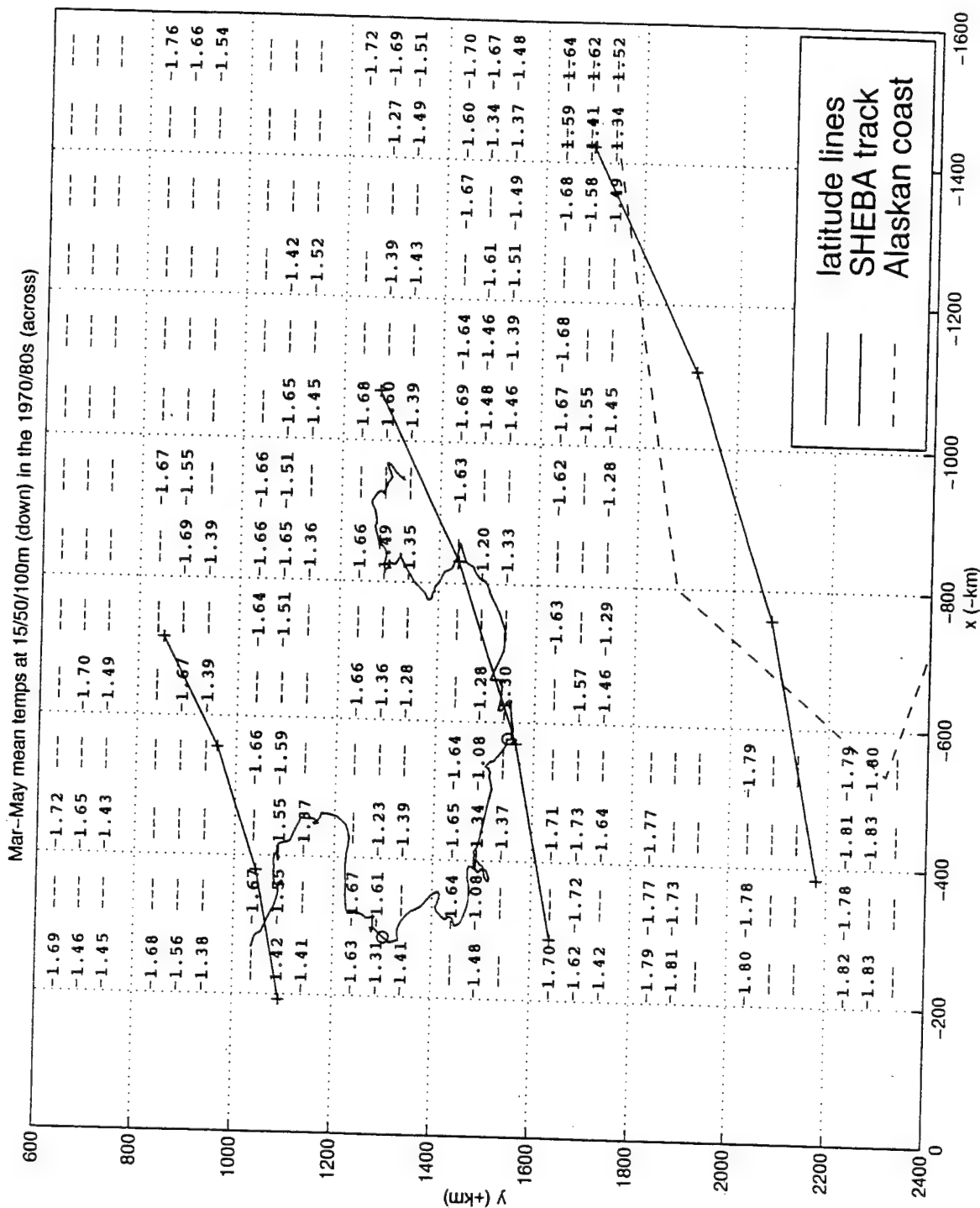


Figure 3.2 (b). Mar-May mean historical temperatures from the EWG digital atlas for each grid box at 15 m (first row), 50 m (second row), and 100 m (third row) during the 1970's (first column) and 1980's (second column).

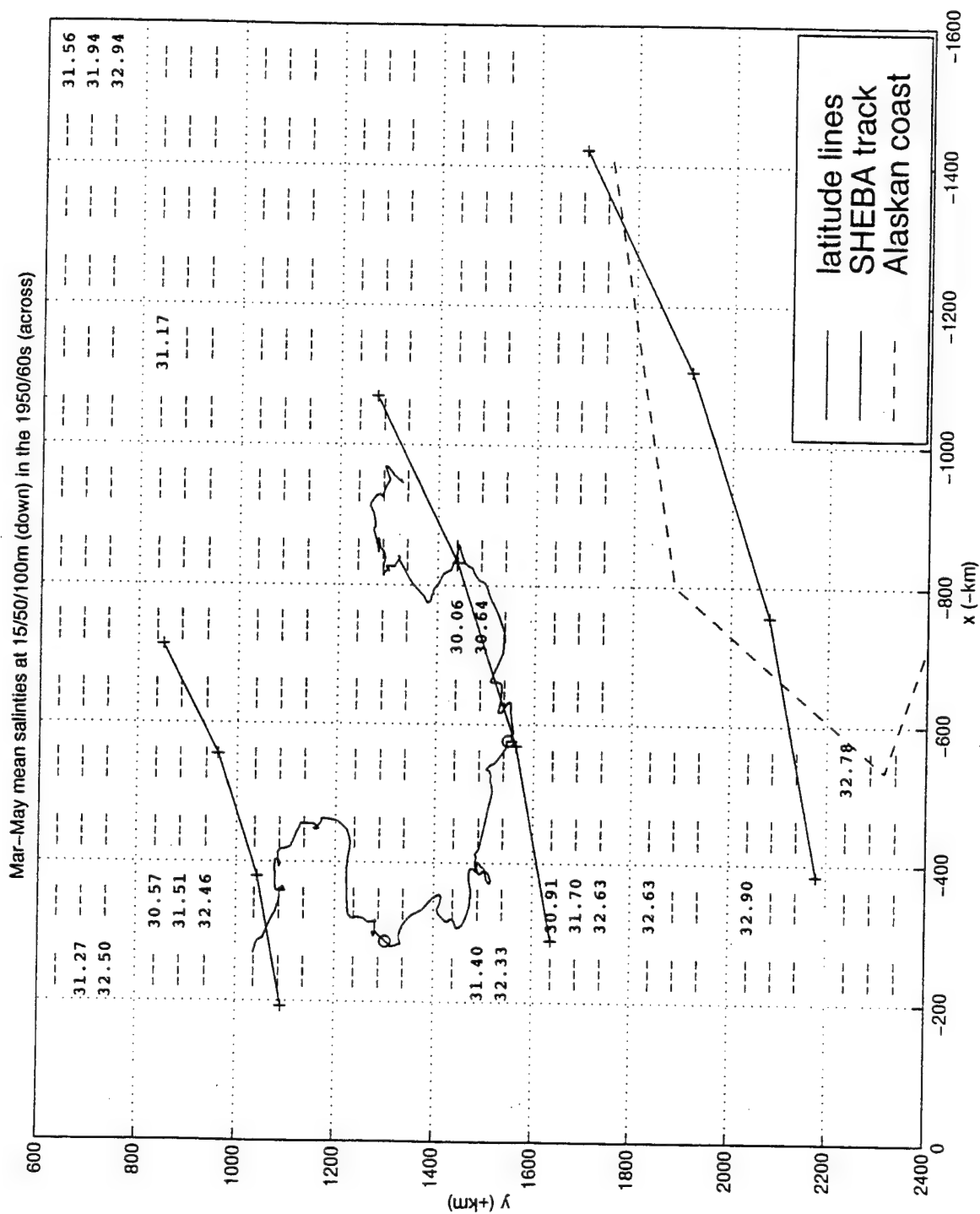


Figure 3.2 (c). Mar-May mean historical salinities from the EWG digital atlas for each grid box at 15 m (first row), 50 m (second row), and 100 m (third row) during the 1950's (first column) and 1960's (second column).

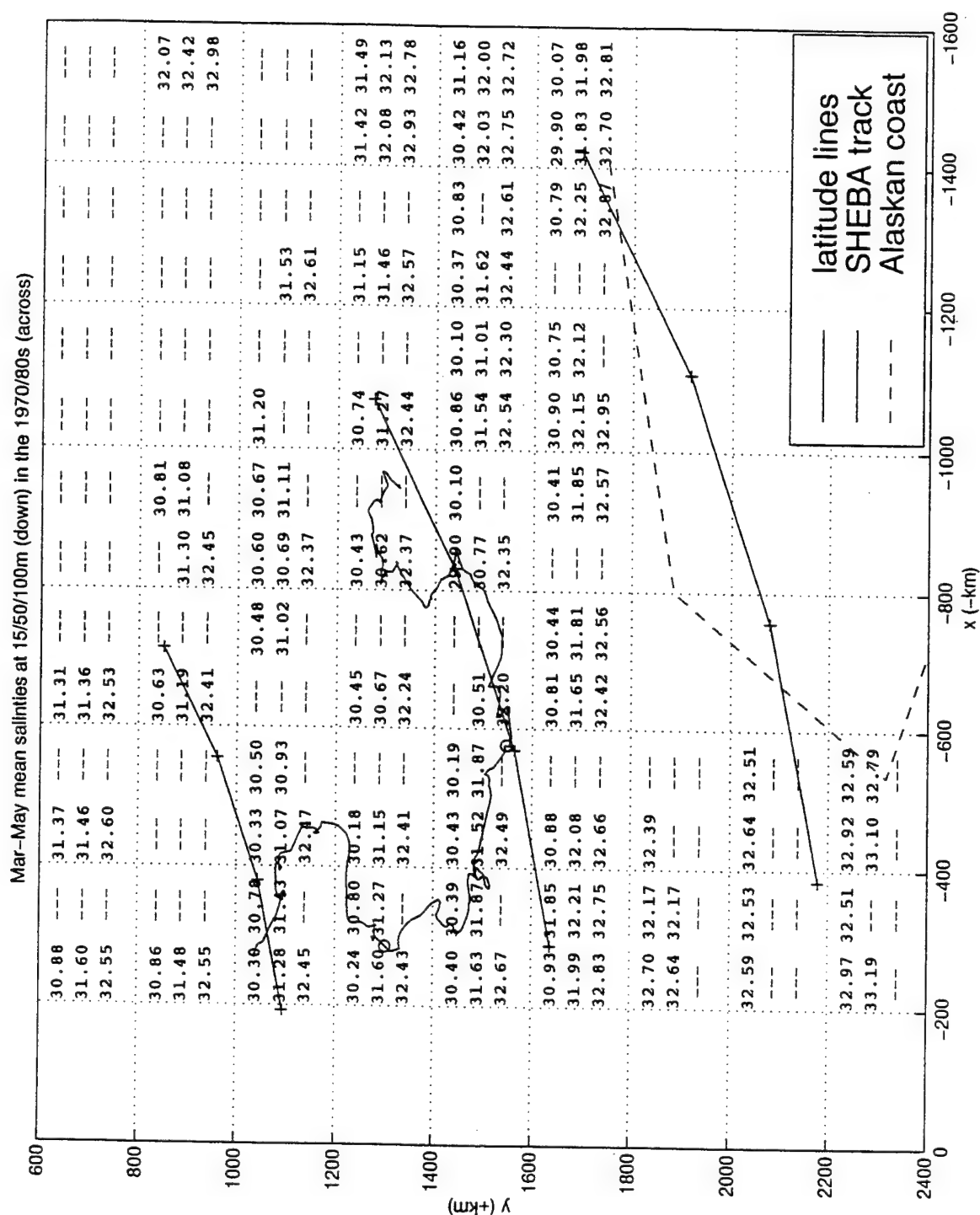


Figure 3.2 (d). Mar-May mean historical salinities from the EWG digital atlas for each grid box at 15 m (first row), 50 m (second row), and 100 m (third row) during the 1970's (first column) and 1980's (second column).

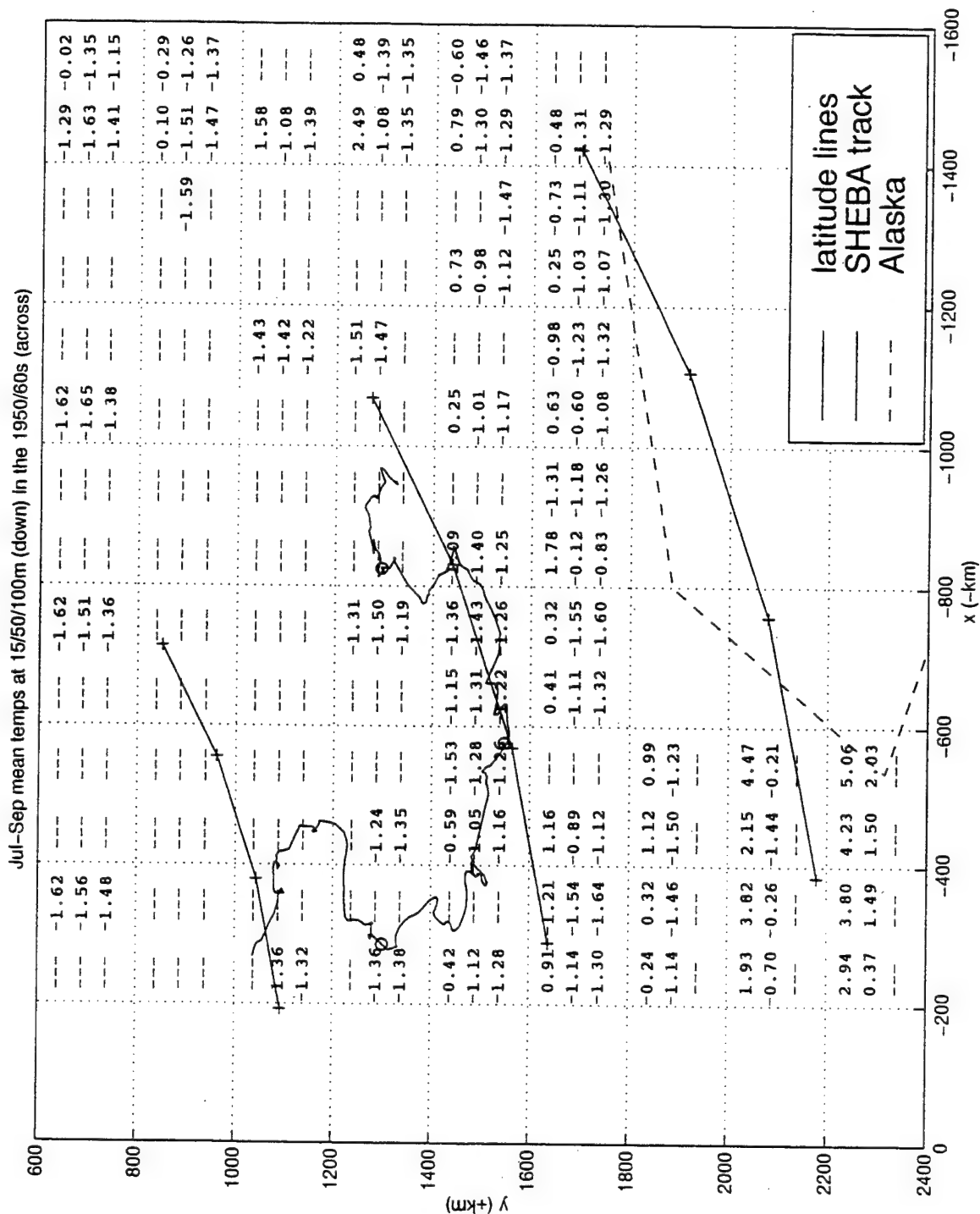


Figure 3.3 (a). Jul-Sep mean historical temperatures from the EWG digital atlas for each grid box at 15 m (first row), 50 m (second row), and 100 m (third row) during the 1950's (first column) and 1960's (second column).

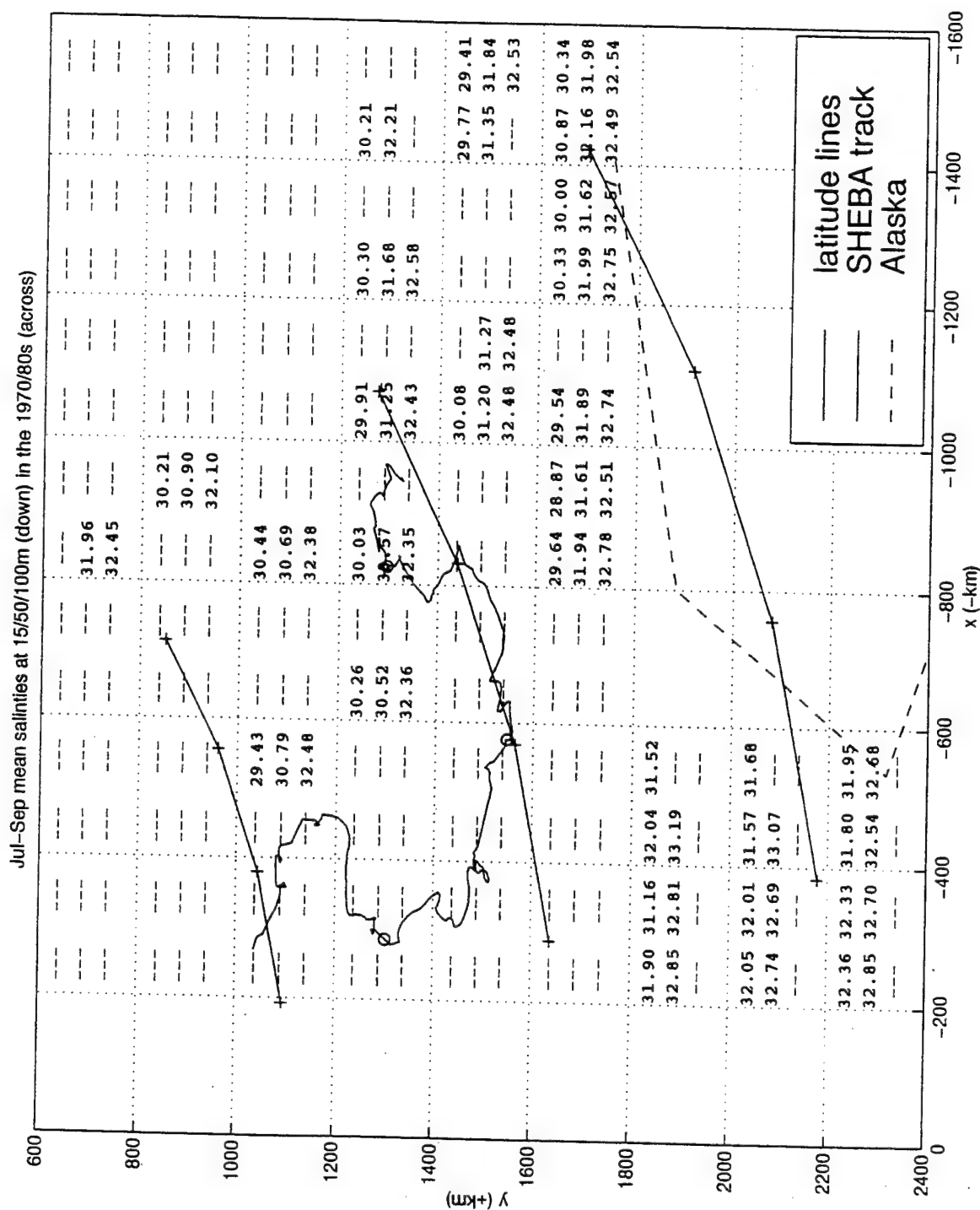


Figure 3.3 (d). Jul-Sep mean historical salinities from the EWG digital atlas for each grid box at 15 m (first row), 50 m (second row), and 100 m (third row) during the 1970's (first column) and 1980's (second column).

Figures 3.4a-d and 3.5a-e are late winter (Mar-May) and summer (Jul-Sep) vertical profiles of temperature and salinity for grouped grid boxes in the Chukchi Sea, eastern Beaufort Sea, western Beaufort Sea, and northern Canada Basin. These profiles were generated from the statistical (mean) data fields in the digital atlas at 0 (surface), 5, 10, 15, 25, 50, 75, 100 and 150 m depths, as available. The specific grid boxes used for each region are shaded in Figure 3.1. The horizontal ranges around each observation are \pm one standard deviation. Although the digital atlas provides other statistical quantities (median, kurtosis, first and third quartiles) for individual 200 km by 200 km boxes (by depth and decade), these statistics could not be converted into regional statistics due to the lack of information about individual observations. The extra plot for the Jul-Sep period (Figure 3.5b) shows mean temperature profiles for the Chukchi and eastern Beaufort Seas on an expanded (warmer) scale than the standard scale selected for all other vertical profile plots.

C. REGIONAL ANALYSIS OF 15/50/100 M DEPTH LEVELS

This section summarizes regional, decadal averaged temperature and salinity conditions for both Mar-May and Jul-Sep at 15 m, 50 m, and 100 m depths in the Canada Basin, summarized in Figures 3.2a-d and 3.3a-d. Mar-May temperature and salinity data from the 1950's and 1960's is extremely sparse over much of the basin. Data coverage over the northern Canada Basin (including the northwestern Beaufort Sea and the northern portion of the Chukchi Cap) is even less during the Jul-Sep period than the Mar-May period.

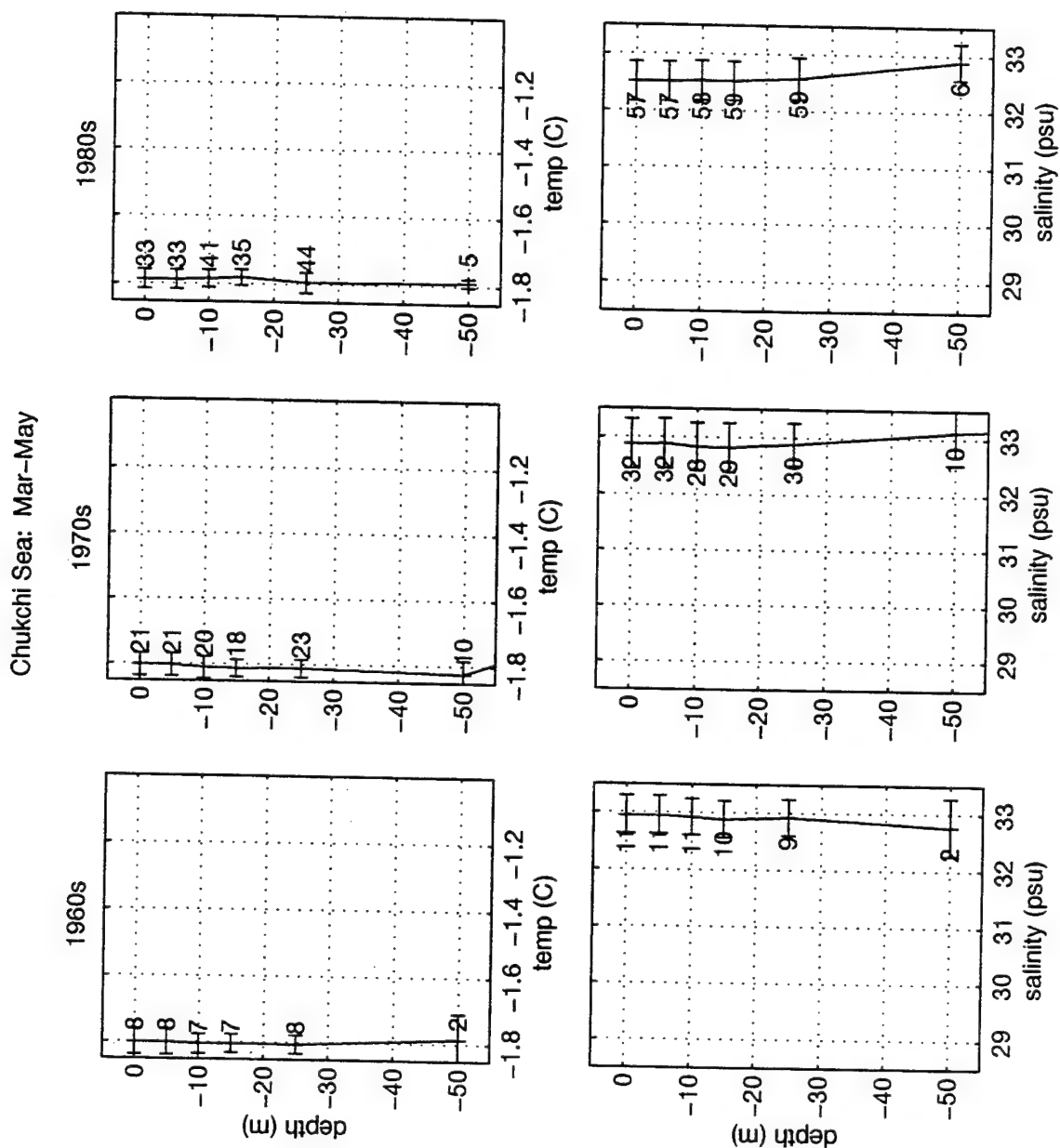


Figure 3.4 (a). Mar-May mean temperature and salinity profiles for the Chukchi Sea during the 1960's, 70's and 80's. Mean values/standard deviations are from the EWG digital atlas. The number of observations used to generate the mean at each depth is annotated for each data point.

E Beaufort Sea: Mar-May

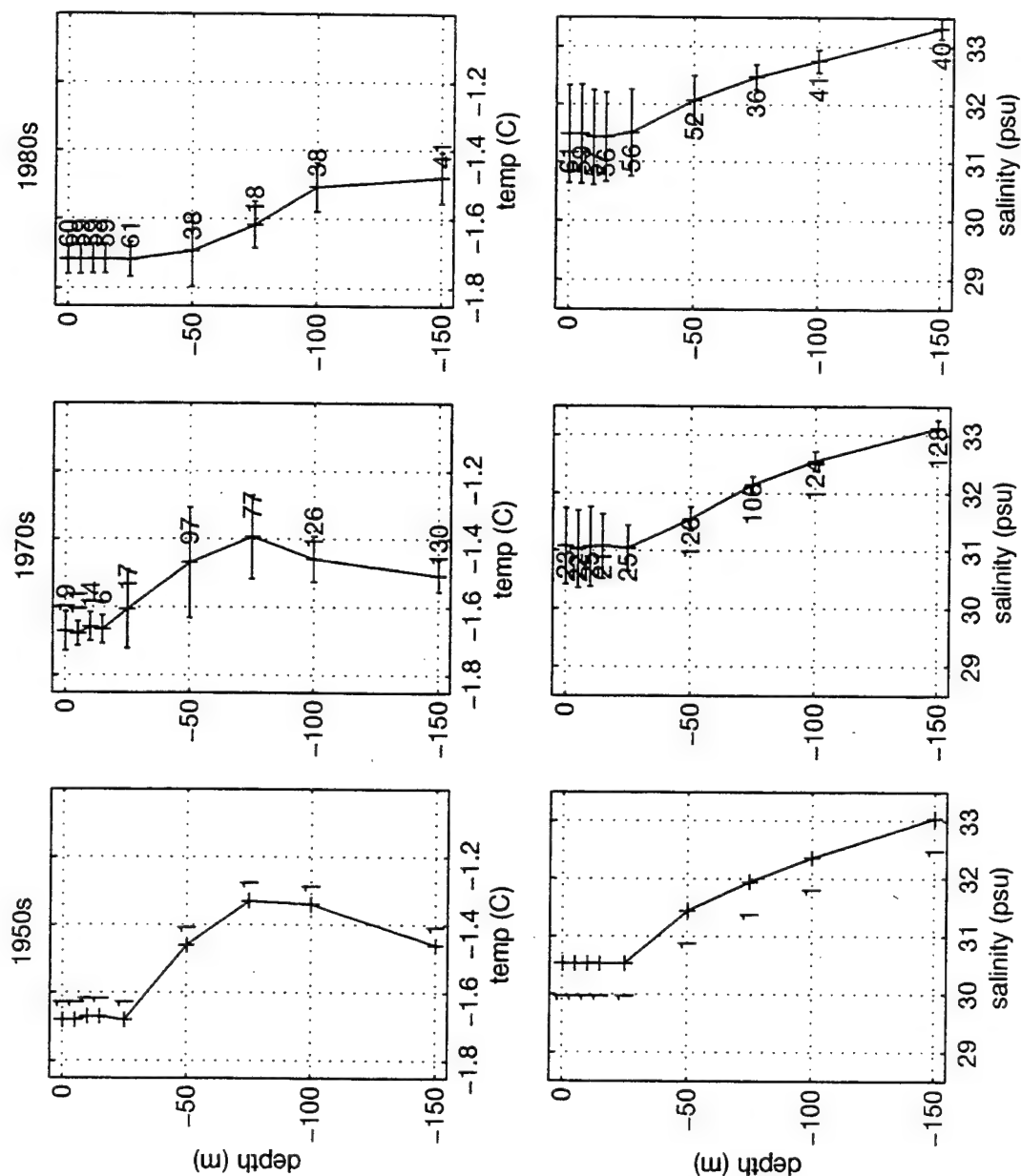


Figure 3.4 (b). Mar-May mean temperature and salinity profiles for the eastern Beaufort Sea during the 1950's, 70's and 80's. Mean values/standard deviations are from the EWG digital atlas. The number of observations at each depth is annotated for each data point.

W Beaufort Sea: Mar-May

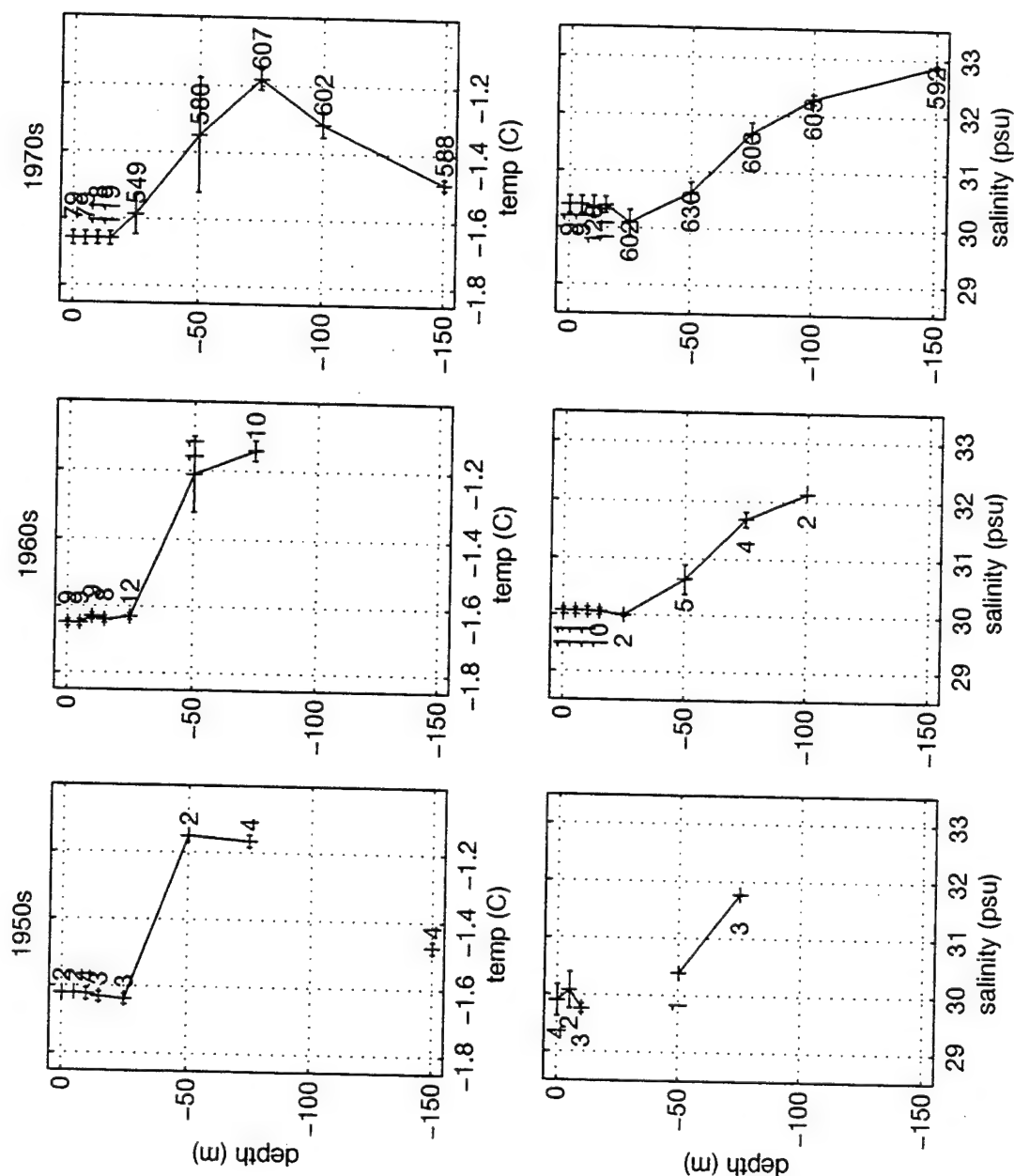


Figure 3.4 (c). Mar-May mean temperature and salinity profiles for the western Beaufort Sea during the 1950's, 60's and 70's. Mean values/standard deviations are from the EWG digital atlas. The number of observations at each depth is annotated for each data point.

N Canada Basin: Mar-May

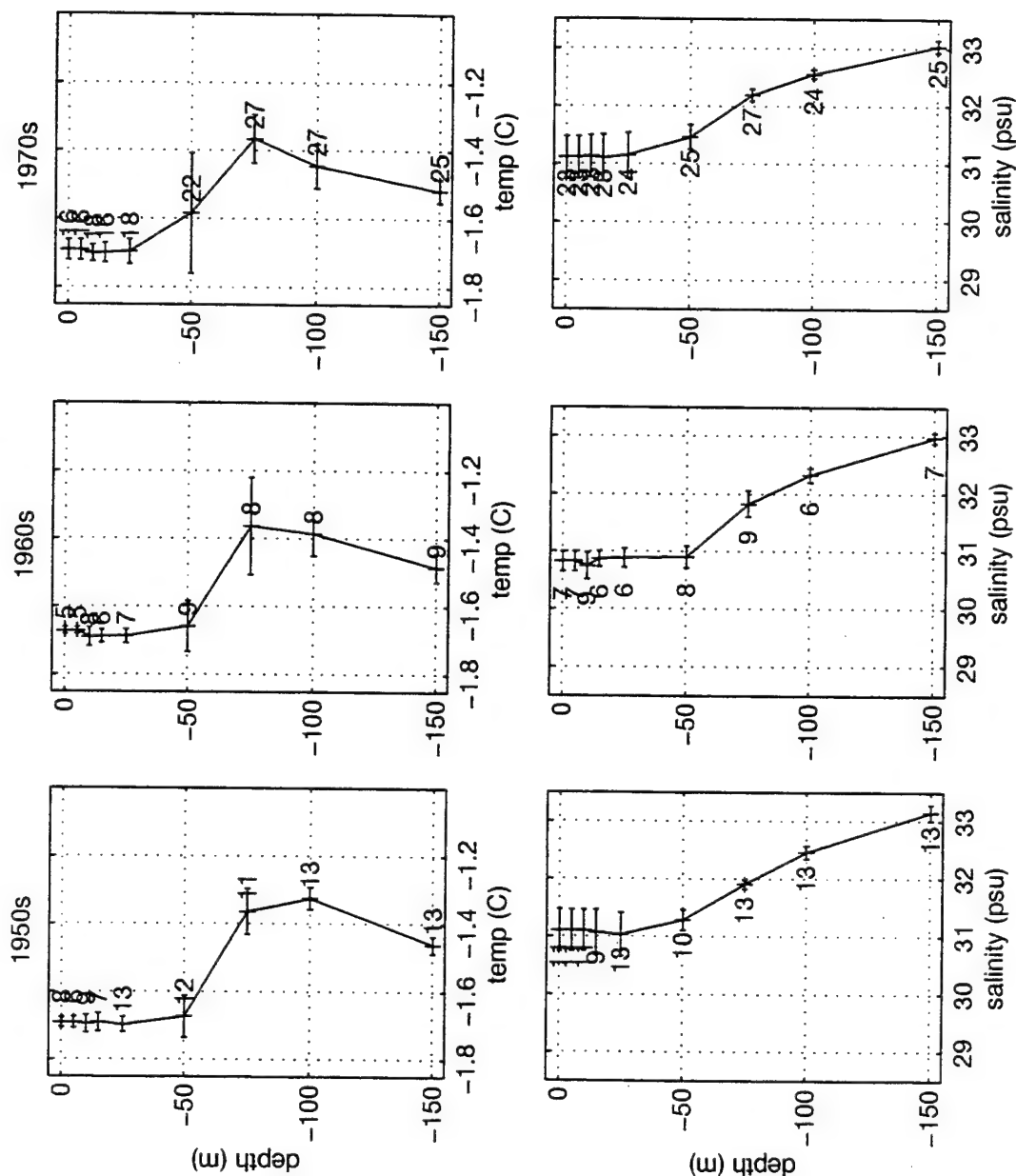


Figure 3.4 (d). Mar-May mean temperature and salinity profiles for the northern Canada Basin during the 1950's, 60's and 70's. Mean values/standard deviations are from the EWG digital atlas. The number of observations at each depth is annotated for each data point.

Chukchi Sea: Jul-Sep

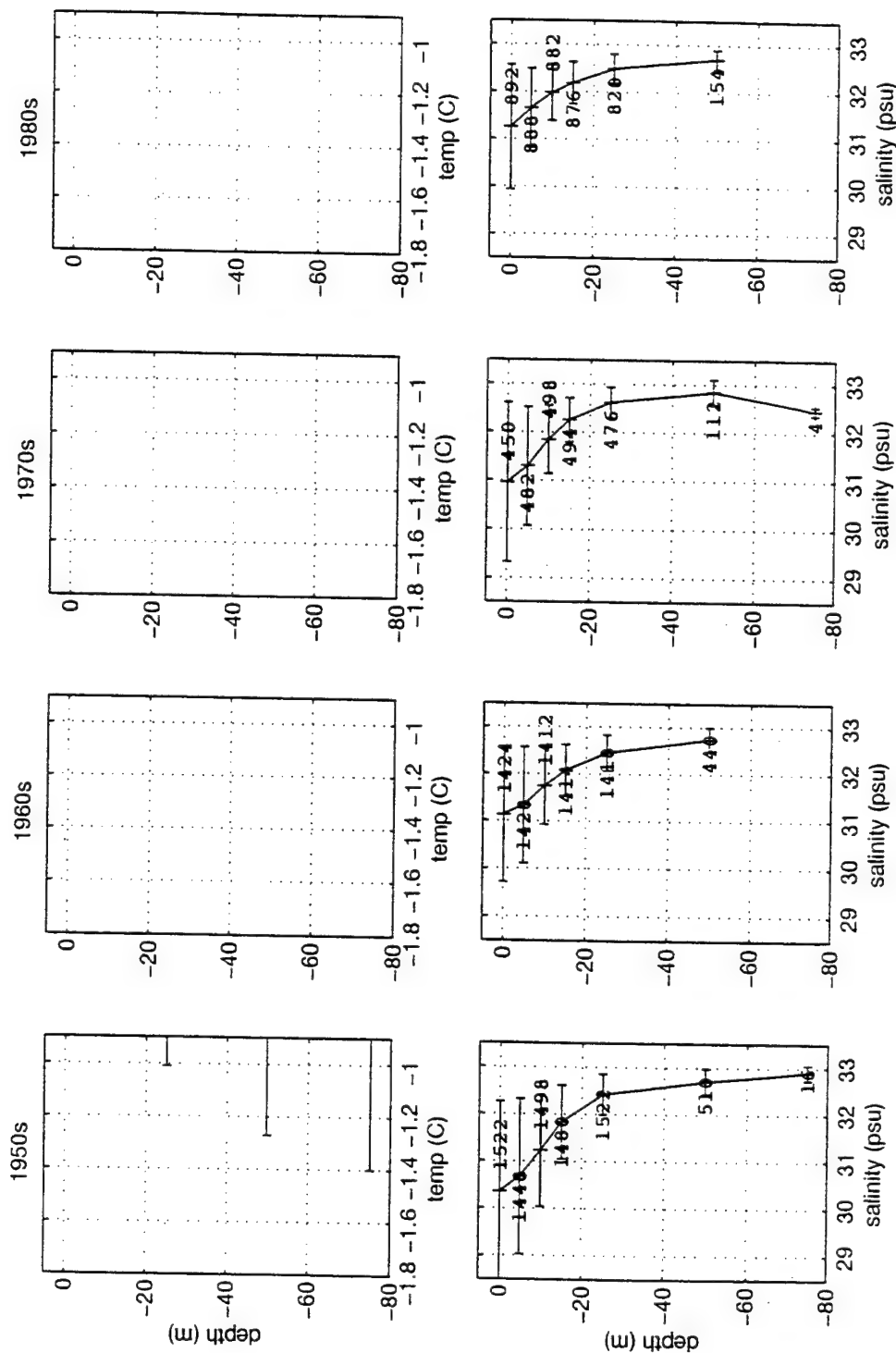


Figure 3.5 (a). Jul-Sep mean temperature and salinity profiles for the Chukchi Sea during the 1950's, 60's, 70's and 80's. Mean values/standard deviations are from the EWG digital atlas. The number of observations at each depth is annotated for each data point. See also Figure 3.5 (b).

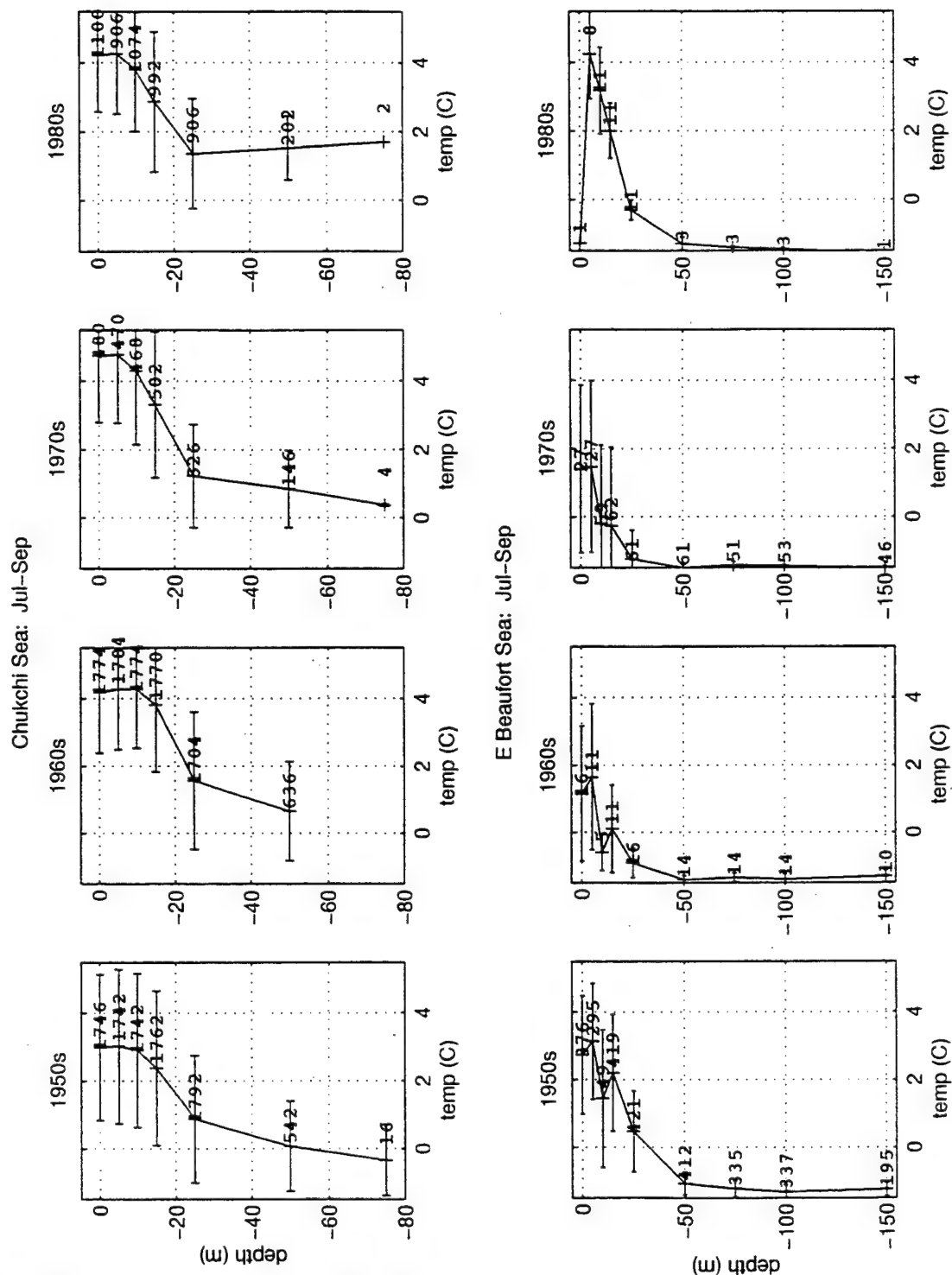


Figure 3.5 (b). Jul-Sep mean temperature profiles for the Chukchi Sea and eastern Beaufort Sea during the 1950's, 60's, 70's and 80's. Mean values/standard deviations are from the EWG digital atlas. The extended scale of the horizontal axes allows depiction of summer heating.

E Beaufort Sea: Jul-Sep

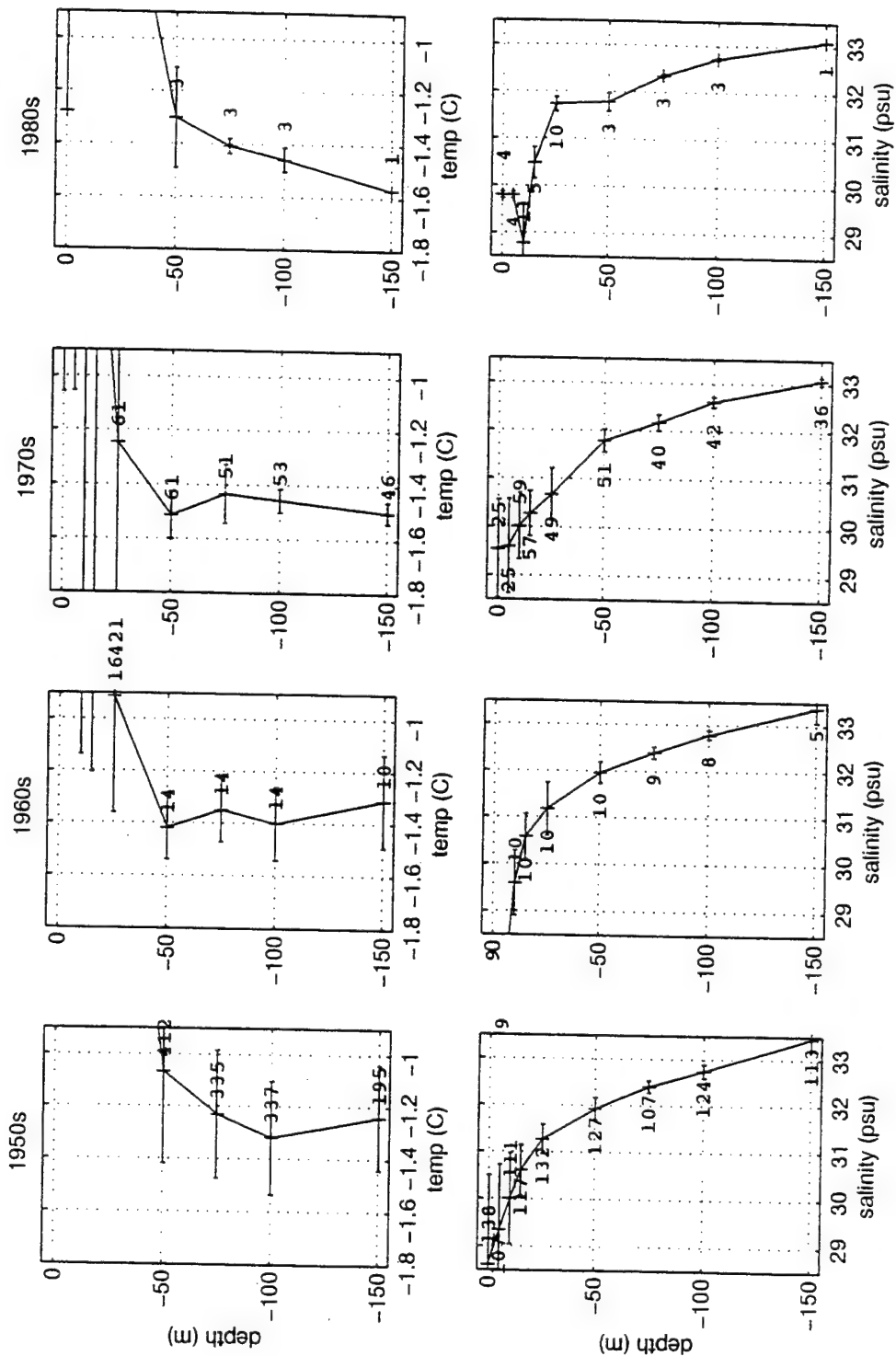


Figure 3.5 (c). Jul-Sep mean temperature/salinity profiles for the eastern Beaufort Sea during the 1950's, 60's, 70's and 80's. Mean values/standard deviations are from the EWG digital atlas. The number of observations at each depth is annotated for each data point. See also Figure 3.5 (b).

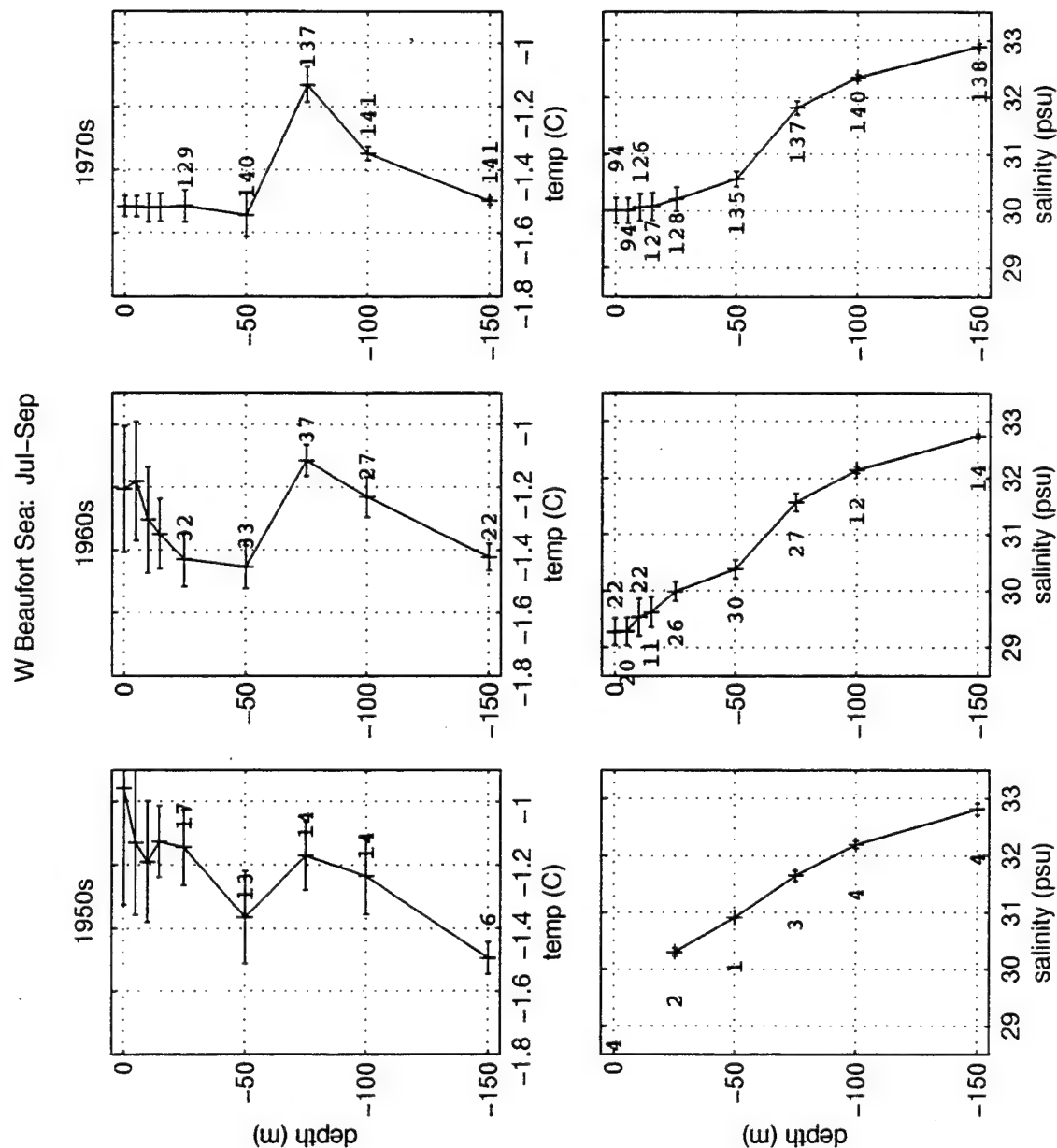


Figure 3.5 (d). Jul-Sep mean temperature and salinity profiles for the western Beaufort Sea during the 1950's, 60's, 70's. Mean values/standard deviations are from the EWG digital atlas. The number of observations at each depth is annotated for each data point.

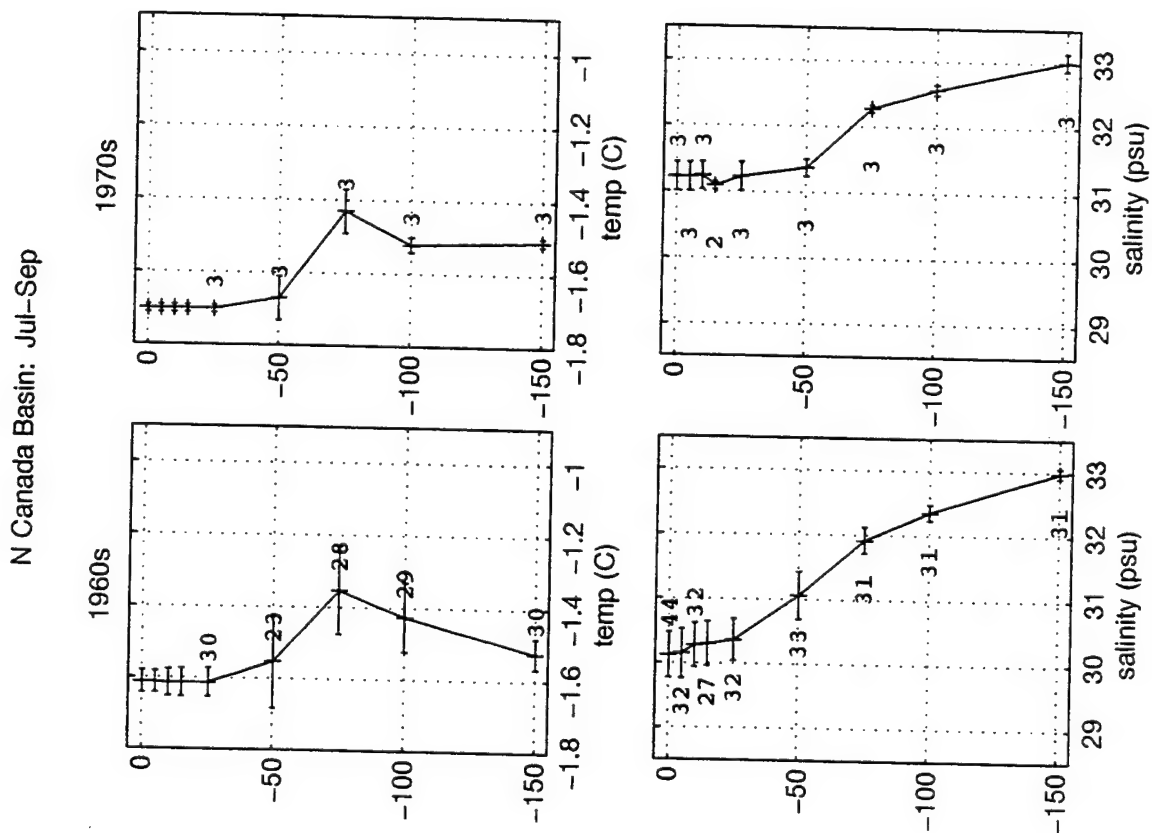


Figure 3.5 (e). Jul-Sep mean temperature and salinity profiles for the northern Canada Basin during the 1950's, 60's, 70's. Mean values/standard deviations are from the EWG digital atlas. The number of observations at each depth is annotated for each data point.

1. 15 m Mar-May analysis (Figures 3.2a-d)

In all decades, temperatures at 15 m are within $+0.2^{\circ}\text{C}$ of the freezing point. Generally, the coldest mixed layer temperatures are in the Chukchi Sea region, with values near -1.8°C . The highest 15 m salinities (between 32 psu and 33 psu) are found in this same region. This is expected since late winter is the period of maximum ice cover in a region where ice melts and reforms annually. In areas of net advection, seasonal ice formation tends to increase the salinity of the surrounding water, thus decreasing the freezing temperature as described in Chapter II.

In the Canada Basin, mean mixed layer salinities were a little lower. Mean mixed layer temperatures were therefore a little warmer, reflecting higher freezing point temperatures for areas removed from the shallow Chukchi Sea. The freshest and warmest mixed layers were in the western Beaufort Sea and in the vicinity of the Chukchi Cap. Here mean temperatures ranged from -1.63°C to -1.67°C , and mean salinities ranged from 29.90 psu to 30.80 psu. The western Beaufort Sea and Chukchi Cap regions are closest to the source of the warm, summertime Pacific input that enters through the Bering Strait and Chukchi Sea. As this Pacific water exits the shallow Chukchi Sea, it is modified and sinks as it interleaves into the water column at the appropriate density equilibrium level as described in Chapter II. In the eastern Beaufort Sea and northwest Canada Basin, farther removed from the summertime Pacific input, mean temperatures were slightly cooler (mostly between -1.67°C and -1.72°C) and salinities were slightly higher (30.37-31.49 psu).

2. 50 m Mar-May analysis (Figures 3.2a-d)

At 50 m depth, the coldest temperatures were also in the Chukchi Sea area, where their values were within 0.03°C of the 15 m temperatures (usually cooler). Mean salinities

at 50 m in the Chukchi Sea were generally equal to or slightly higher than their 15 m values.

In the Canada Basin, 50 m mean temperatures were warmer and 50 m mean salinities were higher than their 15 m values. This is consistent with the summertime Pacific inflow. The warmest 50 m mean temperatures were in the western Beaufort Sea and over the Chukchi Cap, ranging from -1.08°C to -1.61°C . Within this range, the warmer temperatures were generally to the south - closer to the Chukchi Sea while remaining over deep water. In the eastern Beaufort Sea 50 m temperatures ranged from -1.27°C to -1.70°C , and in the northwest Canada Basin they ranged from -1.46°C to -1.70°C .

The mean salinity range at 50 m varied notably from region to region. The saltiest water (>32.1 psu) was in the Chukchi Sea, consistent with both the theory of dense water formation on shallow shelves, and with relatively saline Bering Sea water flowing across the Chukchi Sea into the Beaufort. The next saltiest region was the southeastern Beaufort Sea (>31.5 psu). Moving westward across the Beaufort Sea, the water at 50 m rapidly freshens. The western Beaufort Sea, which is the deepest part of the Canada Basin, contains the freshest water at 50 m (<30.8 psu). This is also consistent with Chapter II, as 50 m is shallower than the historical level of maximum temperature (approximately 75 m), where relatively saline Pacific water historically reaches its density equilibrium point after leaving the shallow shelf area. Just west of the Beaufort Sea, the bathymetry abruptly rises to form the Chukchi Cap, where salinity at 50 m varies between 31 and 32 psu, with the higher salinity values found to the south, closer to the Chukchi Sea, and the lower salinity values found to the northeast, closer to the central Canada Basin. In the central Canada Basin, 50 m salinity values range from 31.0-31.3 psu. In the northwest Canada Basin, approaching the

Mendeleev Ridge, 50 m salinities rise slightly, ranging from 31.2-31.6 psu.

3. 100 m Mar-May analysis (Figures 3.2a-d)

There is no 100 m data for the Chukchi Sea, as it is shallower than 100 m at nearly all points. Throughout the Canada Basin there is far less variation in temperature and salinity at 100 m than at 15 m or 50 m. The western Beaufort Sea again contains the warmest ($\sim -1.3^{\circ}\text{C}$) and freshest (32.2 to 32.4 psu) water. Over the Chukchi Cap the mean water temperature is $\sim -1.4^{\circ}\text{C}$ and the mean salinity is 32.4 to 32.7 psu. In the northern Canada Basin the mean temperature is -1.4°C to -1.5°C , with a small mean salinity range of 32.4 to 32.6 psu, indicating relatively few advective or decadal changes in this region. In the eastern Beaufort, mean temperatures also range from -1.4°C to -1.5°C , but mean salinity ranges more broadly, from 32.4 to 32.9 psu. The larger variability in the eastern Beaufort may be related to the proximity of the Beaufort Undercurrent discussed in Chapter II.

4. 15 m Jul-Sep analysis (Figures 3.3a-d)

Summer mixed layer temperatures vary widely over the Canada Basin because the Chukchi Sea and southern Beaufort Sea become ice-free while the northern Canada Basin remains ice-covered. Summertime mean mixed layer temperatures over the Chukchi Sea are all above the freezing point, ranging from -0.7°C to $+5.0^{\circ}\text{C}$, with warmer temperatures tending towards the south, away from the ice edge. Summertime mean salinities in the Chukchi Sea range from 30.6 to 32.4 psu, with higher salinity values also tending towards the south. This is consistent with the relatively warm, salty inflow through Bering Strait as described in Chapter II.

Over the Chukchi Cap, limited observations indicate a mean temperature range from -0.4°C to -1.5°C , and a mean

salinity range between 29.3 psu and 29.4 psu. In the western Beaufort Sea mean temperatures ranged from roughly -1.1°C to -1.5°C , and mean salinities range from 29.5 to 30.3 psu. The warmer, fresher water is found nearest the Chukchi Sea and Alaskan coastline, and the cooler, saltier water is found to the north in the vicinity of the ice edge. In the north Canada Basin (within the permanent ice pack), water temperatures are very near the freezing point, with salinities ranging from 30.1 to 30.5 psu.

In the eastern Beaufort Sea, 15 m temperatures vary greatly, from as warm as 3.0°C to the southeast, to as cold as -1.61°C near the central Beaufort Sea. The 15 m salinities in this region vary from 29.4 psu to 30.7 psu. The grid box in the southeast Beaufort Sea bounded by $1200 < y \text{ km} < 1400$ and $-1600 < x \text{ km} < -1400$ contains by far the warmest 15 m temperatures during all four decades. The likely source of this warm, relatively fresh water is outflow from the MacKenzie River in northwest Canada, in combination with summer ice melt. The peak springtime discharge of this river normally occurs in early June, and falls off in the following months (Becker, 1995). The summertime MacKenzie river outflow may form a lens of relatively fresh, warm water that moves northward across the MacKenzie shelf and into the Beaufort Sea (Kulikov et al., 1998). As the lens moves farther seaward, the warm temperatures extend slightly deeper, while cooling slightly at the surface. Salinities well below 20 psu are common to the southeast, but salinity increases rapidly with depth and distance from the river mouth, climbing toward 30 psu. Summer data for June from the digital atlas is extremely limited and non-robust, and does not illustrate this effect. However, the July-September mean temperature and salinity data from the digital atlas for the surface, 5 m, and 10 m in the eastern Beaufort Sea (including grid boxes just east of those shown in Figure 3.3) illustrate this scenario quite

well. This data demonstrates that during summer in this southeast portion of the Beaufort Sea, there is no distinct surface mixed layer. The effects of the MacKenzie River outflow are not readily evident below 25 m.

5. 50 m Jul-Sep analysis (Figures 3.3a-d)

In the Chukchi Sea the 50 m mean temperatures are much cooler than at 15 m, ranging from -0.7°C to 1.6°C . The mean salinities are slightly higher, between 32.6 psu and 32.9 psu. The warmest water is again to the south within the Chukchi. Although much cooler than the 15 m water, these values are still consistent with relatively warm Pacific water entering the Arctic through Bering Strait. Over the Chukchi Cap and along the north Alaskan coastline, temperatures cool and salinities decrease slightly in comparison with the Chukchi Sea. In the western Beaufort Sea the water is yet colder (-1.3°C to -1.6°C) and fresher (30.2 psu to 30.7 psu). Moving east, temperatures and salinities slightly increase again in the eastern Beaufort Sea, approaching coastal waters.

6. 100 m Jul-Sep analysis (Figures 3.3a-d)

Mean temperatures in the northern Chukchi Sea and along the northern Alaskan coastline vary from about -0.9°C to -1.6°C . Over the rest of the Canada Basin, the range is more limited, from about -1.1°C to -1.5°C , with the warmest temperatures occurring in the Beaufort Sea. Mean salinities at 100 m vary only slightly across the Canada Basin, from 32.1 psu to 32.8 psu. Generally, the fresher values appear in the western Beaufort Sea and central Canada Basin.

D. ANALYSIS OF REGIONAL DECADEAL MEAN PROFILES

As another approach to determining regional and seasonal characteristics in the Canada Basin, the following

discussion of statistical, regional vertical profiles (Figures 3.4a-d and 3.5a-e) is presented. The regions analyzed in this section are shaded in Figure 3.1. Again, robust data is not available for all regions in all decades, and only mean values derived from five or more observations are used for statistical comparisons. Where sufficient data is available, inter-decadal comparisons have been made.

1. Chukchi Sea (Mar-May, Figure 3.4a)

Sufficient data is available for the 1960's, 70's and 80's in this region. In winter the shallow Chukchi Sea is nearly isohaline and isothermal with temperatures at or near the freezing point, as expected from the discussion in Chapter II. At all depth levels the mean salinity decreases each decade from the 60's to the 80's, with the larger decrease occurring from the 70's to the 80's. For example, at 25 m mean salinity decreases from 32.92 psu in the 60's to 32.89 psu in the 70's to 32.57 psu in the 80's. The maximum decadal difference (between the 60's and 80's) is larger than the decadal standard deviations at the surface and 5 m, but less than the decadal standard deviations below 5 m, and therefore is barely statistically significant.

2. Eastern Beaufort Sea (Mar-May, Figure 3.4b)

Sufficient data is available only for the 70's and the 80's in this region. Both decades show a 25 m mixed layer depth. The decrease between decades in mean mixed layer temperatures at 10 m and 15 m are slightly larger than the standard deviation of 0.04°C in both decades. The mean mixed layer salinity, based on 15 m values, increases 0.35 psu (from 31.08 psu to 31.43 psu) between the 70's and the 80's, but this increase is less than the decadal standard deviations of 0.56 psu and 0.78 psu, respectively. However, the standard deviations of decadal salinities in the mixed layer of the eastern Beaufort Sea are relatively large.

This is likely related to interannual variations in the spring outflow of the MacKenzie River, which starts during this late winter period and peaks in June (Becker, 1995; Aagaard and Carmack, 1989; Melling and Lewis, 1982). (Although the grid boxes nearest the river mouth were excluded from these profiles, much of the eastern Beaufort Sea is effected by the outflow.)

Generally T_{\max} is less distinct in the eastern Beaufort Sea than in other regions of the Canada Basin, probably because it is the farthest removed from the Pacific input. The mean T_{\max} in the 70's is -1.39°C at 75 m depth. In the 80's the mean temperature at 75 m drops 0.33°C to -1.62°C , a very large decrease in comparison with the standard deviations of 0.07°C and 0.12°C at this level. However, the mean T_{\max} in the 80's (-1.48°C) is at 150 m, much deeper than expected based on the regional description in Chapter II. The mean salinity at 75 m increases by 0.33 psu, significantly more than the decadal standard deviations of 0.14 and 0.22 psu.

The temperature and salinity profiles in the eastern Beaufort Sea appear to have changed significantly from the 70's to the 80's. The water is saltier at all depths. The maximum decadal mean salinity difference exceeds the standard deviation range for depths greater than 25 m - except at 100 m where this difference equals the largest decadal standard deviation. Significant salinity changes within the mixed layer could possibly exist but are likely masked by the large natural variability there. The average slope of the halocline between 25 m and 150 m is 0.017 psu/m in the 70's and 0.015 psu/m in the 80's. Temperatures are cooler in the 80's at all levels above 150 m, and the maximum decadal difference exceeds the standard deviation from 10 m to 75 m, except at 25 m, where again the difference equals the largest deviation.

3. Western Beaufort Sea (Mar-May, Figure 3.4c)

Numerous observations from the 70's are available, but robust data from other decades is limited to just a few depths in the 60's. There is an apparent discontinuity between observations in the upper 15 m and observations at or below 25 m in the 70's. This is an artifact of the process of forming mean profiles from incomplete profiles with large variability. It appears as an artificial unstable salinity gradient between 15 m and 25 m.

From the 60's to the 70's, the mean mixed layer salinity increases 0.34 psu (from 30.06 psu to 30.40 psu), which is significantly higher than the decadal standard deviations of 0.06 psu and 0.14 psu. At 50 m the mean salinity is virtually unchanged between decades. Robust salinity data is not available below 50 m in the 60's. The mixed layer temperature increases by 0.02°C between the two decades, which is equal to the largest decadal standard deviation.

The mean T_{\max} decreases from -1.14°C in the 60's to -1.18°C in the 70's, a slightly larger decrease than both decadal standard deviations. T_{\max} appears to be at 75 m during both decades, but in the 60's no data is available below 75 m. The halocline appears relatively constant during these two decades.

4. Northern Canada Basin (Mar-May, Figure 3.4d)

Observations from the 50's, 60's, and 70's are available for this region. In the 50's and 60's the mixed layer depth is just above 50 m, but in the 70's it is at 25 m. The maximum decadal difference in the mean mixed layer salinity is only 0.23 psu, which is within the standard deviation range for this level (0.13 psu to 0.40 psu). The mean mixed layer temperature (just above the freezing point) therefore also remains relatively constant.

In the 50's, mean T_{\max} is at 100 m, and in both the 60's

and 70's the mean T_{\max} is at 75 m. However, for both the 50's and 60's, the difference between the 75 m and 100 m values is well within the standard deviation range for those depth levels. The actual T_{\max} may lie between 75 and 100 m in all decades. At 75 m, the maximum decadal mean temperature difference is near zero. At both 100 m and 150 m, however, the water cools each decade, and the maximum decadal differences exceed the standard deviation ranges for those levels.

For all levels below 25 m, the maximum decadal difference in mean salinity exceeds the largest standard deviation at that level. However, there is no clear overall trend, as all salinity observations decrease from the 50's to the 60's and increase from the 60's to the 70's. At 50 m, 75 m, and 100 m, the maximum decadal difference occurs between the 70's and 80's. The average slope of the halocline between 25 m and 150 m is .017 psu/m in both the 50's and 60's, and steepens to 0.15 psu/m in the 70's.

5. Chukchi Sea (Jul-Sep, Figures 3.5a-b)

Robust data is available for all four decades. The entire depth of the Chukchi Sea warms up so much during the summer that all mean temperatures are off the standard temperature axis used for the winter profiles. The top portion of Figure 3.5b depicts the mean summer temperature profiles in the Chukchi Sea on a shifted (warmer) horizontal axis. Although all levels warm, the surface warms substantially more than the bottom due to the combined effects of warm inflow from the Pacific and solar insolation. At all depths in all decades, the standard deviations were quite large, indicating significantly larger annual variability than the western Beaufort Sea or north Canada Basin. This is likely the result of mesoscale and temporal variability in the surface heating. Few

observations are available below 50 m because very little of the Chukchi Sea is more than 50 m deep.

The mean surface temperature ranges from a low of 2.99°C in the 50's to 4.74°C in the 70's. Although the 50's mean surface temperature is more than 1.2°C cooler than all other decades, the standard deviation in all decades exceeds $\pm 1.6^\circ\text{C}$. The maximum decadal difference of 1.76°C is also within the range of surface standard deviations (1.65°C to 2.17°C). The maximum summer mean temperatures extend to 10 m in the 50's and 60's, but just to 5 m in the 70's and 80's, suggesting a shallower surface mixed layer in summer.

The mean temperatures drop off sharply between 10 m and 25 m, and then continue to gradually decrease towards the bottom. Although the mean temperatures at 50 m increase each decade, the maximum decadal difference is 1.45°C, which is just within the standard deviation range for this level (0.94°C to 1.48°C).

The summer mean salinity profile (Figure 3.5a) also changes markedly from its relatively isohaline winter structure. The water at the surface is much fresher, primarily due to ice melt, with mean salinities ranging from 30.36 psu in the 50's to 31.25 psu in the 80's. The maximum difference at the surface of 0.89 psu is well within the range of standard deviations at the surface (1.4 to 1.9 psu). Salinity increases markedly with depth to about 25 m, and then increases much more gradually below 25 m. The salinity at 50 m varied little, remaining between 32.7 and 32.8 psu in all decades.

6. Eastern Beaufort Sea (Jul-Sep, Figures 3.5b-c)

The temperature and salinity profiles of the eastern Beaufort Sea also change markedly from winter to summer due to melting ice, solar insolation, and fresh water outflow from the MacKenzie River. There is no regional-scale mixed layer present during summer, and both temperature and

salinity vary widely at each depth level above 25 m. Also, there is no clear T_{\max} that could be associated with Pacific input in any decade. The temperatures above 50 m were off the standard axis (Figure 3.5c) in most cases, and are better depicted on an expanded temperature axis in the bottom portion of Figure 3.5b. Robust data is not available below 25 m in the 80's.

Mean surface temperatures range from 1.15°C to 2.73°C, but this maximum decadal difference of 1.58°C is less than the standard deviation for any decade, as expected in ice-free, solar heated conditions. Temperatures decrease rapidly to about 25 m, more gradually between 25 m and 50 m, and are nearly isothermal below 50 m. At and below 15 m, mean temperature decreases each decade from the 50's to the 70's, and at 15 m, 25 m, 50 m and 150 m, the maximum decadal differences exceed the standard deviations for all decades. Then, in the 80's, mean temperatures increase at 15 m and 25 m, but are not available below 25 m. Over all four decades, the variation exceeds the standard deviations, but no clear trend is present. At 75 m and 100 m, the temperatures may be affected by fluctuations in the Beaufort Undercurrent discussed in Chapter II.

Mean salinities at and above 25 m vary widely. They range from 28.61 psu to 29.54 psu at the surface, and then increase rapidly to about 25 m, where they range from 30.67 psu to 31.26 psu. At the surface, 5 m, 10 m, and 25 m the maximum decadal differences were higher than the standard deviations for all decades, but there was no consistent trend from decade to decade or from depth to depth. Above 15 m, mean salinity increases and decreases every other decade, but the differences between consecutive decades were less than the standard deviations. Below 25 m salinity increases more gradually. Below 50 m, the maximum decadal differences exceed the standard deviations, and the 70's

values are the freshest. (No robust data is available at these levels in the 80's.)

7. Western Beaufort Sea (Jul-Sep, Figure 3.5d)

Robust temperature data is available for the 50's through 70's, but robust salinity data is only available for the 60's and 70's. During the 50's and 60's, the temperature observations vary widely at each level, especially above 15 m, but in the 70's the temperature observations have much lower standard deviations. There is relatively little variation in the salinity observations. In the 60's and 70's, there appears to be weak stratification almost to the surface.

At all depth levels, the salinity increased from the 60's to the 70's, with a mean decadal difference that exceeded the standard deviation for both decades. Below 25 m the salinity gradient remained nearly the same, but above 25 m the water was more stratified in the 60's than in the 70's.

From the surface through 50 m depth, the water was progressively colder in each of the three decades, and the maximum decadal difference exceeded the largest standard deviations at all levels. There was no significant change at 75 m. At 100 m and 150 m the coldest temperatures were in the 70's, but an inter-decadal trend was not present. At 150 m the maximum decadal difference again exceeded the largest standard deviation for that level. The T_{\max} resulting from Pacific input through the Bering Strait was at 75 m for each decade. The 100 m temperatures were in all decades much closer to the 75 m temperatures (warmer) than the 50 m temperatures, suggesting that T_{\max} may be deeper than 75 m. This data suggests that while the Pacific input may have been relatively unchanged in comparison with previous years, the mixed layer above it was slightly cooler and saltier.

8. Northern Canada Basin (Jul-Sep, Figure 3.5e)

Robust data is only available for the 60's in the northern Canada Basin, so no decadal comparisons can be made. In the 60's, the mixed layer depth is only 5 m, with a mean temperature of -1.61°C and mean salinity of 30.15 psu. The upper ocean is isothermal down to 25 m (the Mar-May mixed layer depth), but is slightly salinity stratified below 10 m. From 25 m to 75 m, the salinity gradient is much stronger, while below 75 m it begins to decrease again. T_{max} is -1.35°C at 75 m depth. Below 50 m, the Mar-May and Jul-Sep mean temperature and mean salinity profiles are nearly identical.

E. WINTER-SUMMER COMPARISONS

The two preceding analysis sections demonstrate that although there is large seasonal variability in the Chukchi Sea, the eastern Beaufort Sea, and along the Alaskan Coast, conditions in the northern Canada Basin experience little seasonal change. Following the discussions in Chapter II, this is expected due to the effects of Pacific inflow, retreating/reforming ice cover, MacKenzie River outflow, and the Alaskan Coastal Current and Beaufort Undercurrent - all of which predominantly impact the more southerly and coastal areas. Although changes in solar insolation influence all regions, the effects are greater over open water areas due to the the albedo differences between water and ice. Bathymetry changes within regional areas also may play a significant role in regional and sub-regional variability, because the barotropic flow is topographically steered.

Significant seasonal changes occur in the eastern Beaufort Sea and over the Chukchi Cap, but the extreme shortage of data makes the precise extent of this variability difficult to determine. Compounding the data shortage problem is the fact that even where data is

available, it is often not available for the both the Mar-May and Jul-Sep seasons within the same decade, making seasonal comparisons within the same decade nearly impossible. The one exception to this is the large amount of data available during the 70's, much of which likely comes from the AIDJEX ice camps.

F. HISTORICAL VARIABILITY SUMMARY (Figures 3.6 and 3.7)

The sparseness of this data set must be kept in mind when considering these results, as more ideally the averages would have been based on frequent, spatially varying temperature and salinity profiles taken throughout each decade. The lack of temporal and vertical resolution, and the lack of information about the spatial (horizontal) spread of individual observations within grid boxes further complicate the analysis process. However, in the absence of other inter-decadal data, areas of high variability and slow regional trends have been identified. Decadal differences are related to higher frequency fluctuations, and the decadal standard deviations are related to lower frequency inter-decadal fluctuations.

Figures 3.6 and 3.7 summarize the Jul-Sep and Mar-May variability of the four analyzed regions. They demonstrate very little seasonal, decadal, or inter-decadal variability within the northern Canada Basin. The western Beaufort Sea also experiences little variability, although the large scale (low frequency) inter-decadal variability was more prominent than the decadal (<10 years) variability during the summer months. The eastern Beaufort Sea has the highest historical wintertime variability, dominated by decadal (higher frequency) differences. The Chukchi Sea and the eastern Beaufort Sea both demonstrated high summertime variability, but while low frequency inter-decadal differences dominated in the eastern Beaufort Sea during

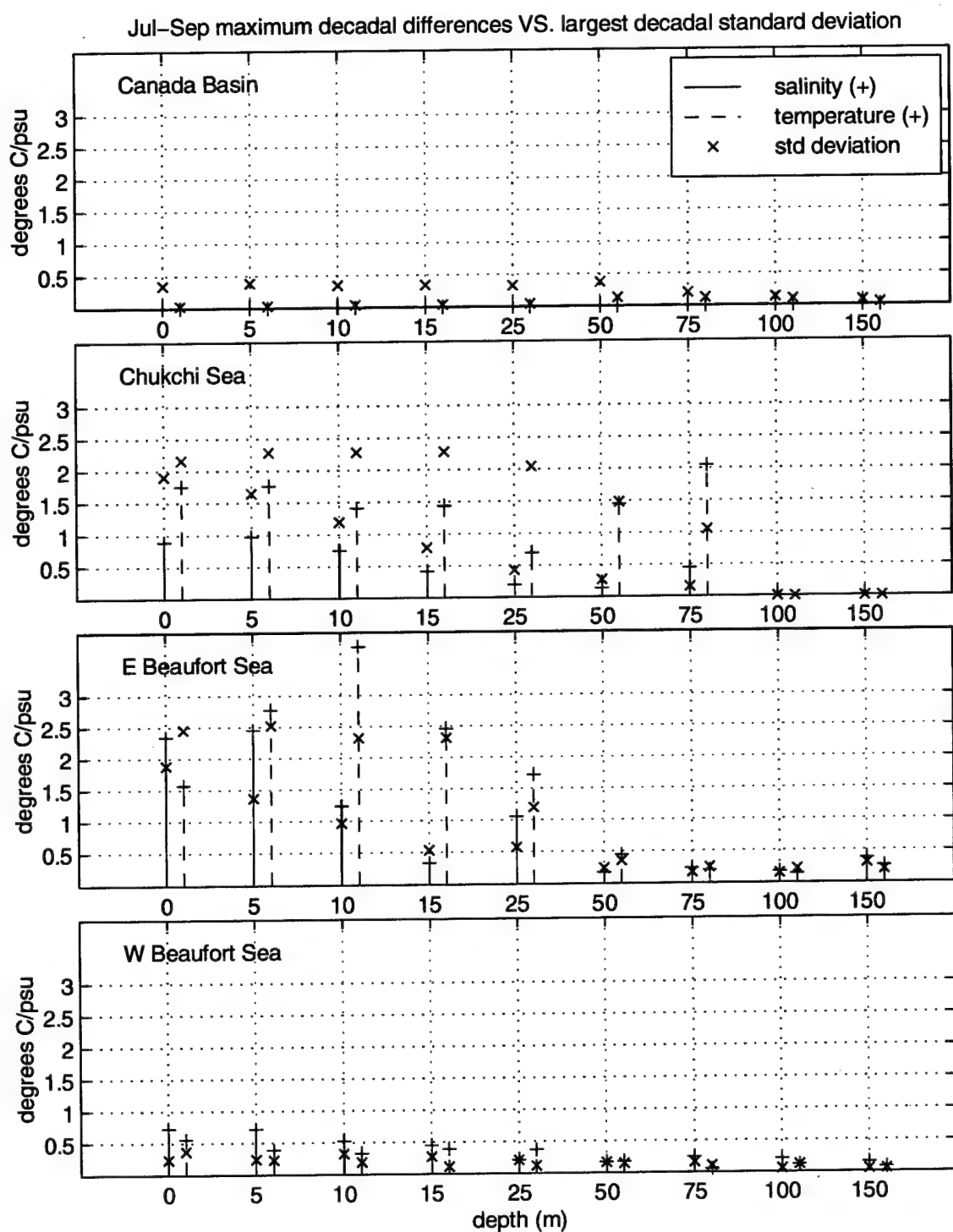


Figure 3.6. Jul-Sep comparison plots of largest decadal standard deviation (from the digital atlas) and maximum inter-decadal differences for both temperature and salinity.

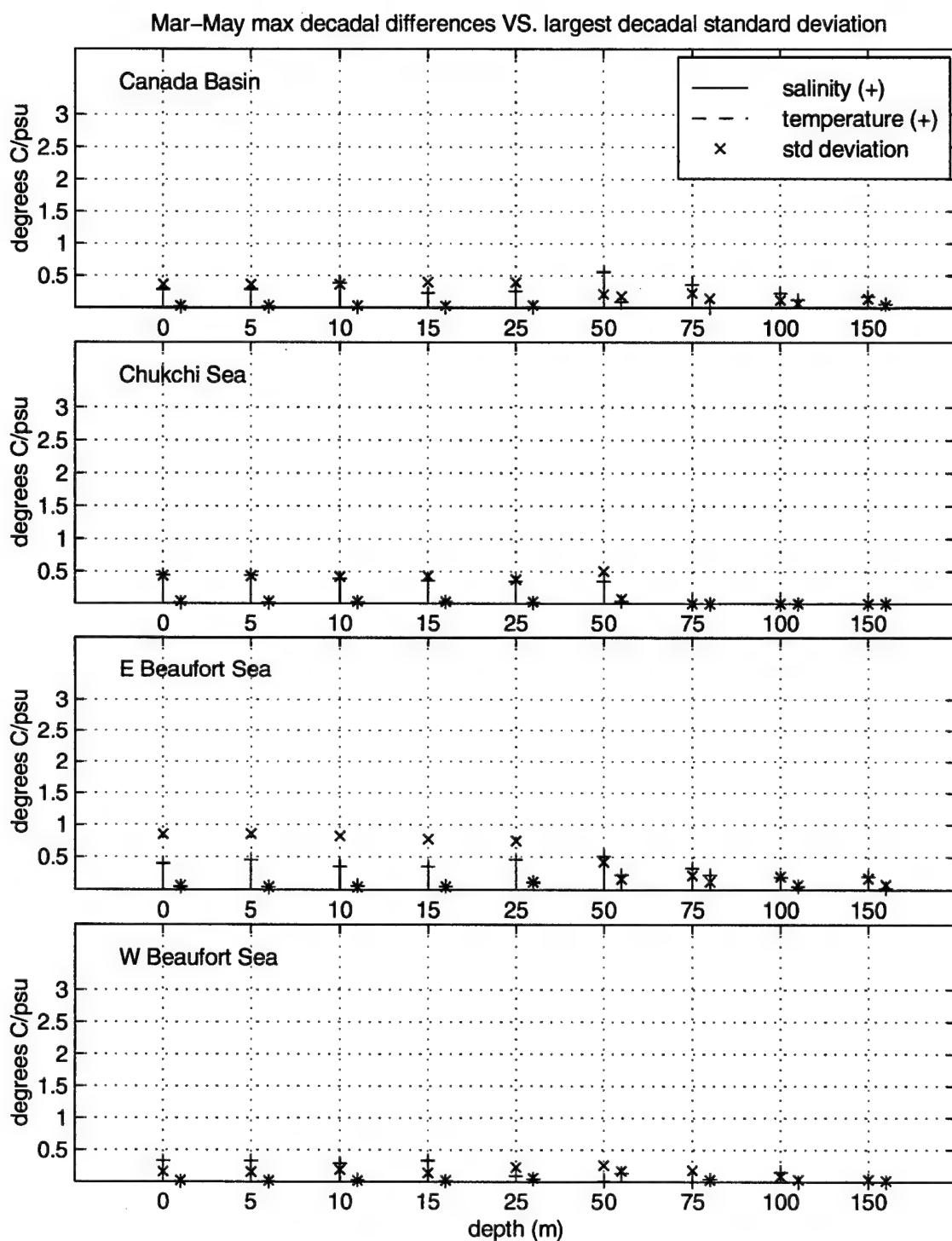


Figure 3.7. Mar-May comparison plots of largest decadal standard deviation (from the digital atlas) and maximum inter-decadal differences for both temperature and salinity.

summer, higher frequency decadal variability was more prominent in the Chukchi Sea during summer.

No consistent decadal trends or oscillations were found in this nearly 40-year data collection. In almost all cases, trends (if any) observed were not statistically significant. Even where results were statistically significant, it was by very small margins, or there were "data holes" in the form of decades with no robust data. It appears that any existing trends and oscillations are of a small scale in comparison with the values and variability observed. Therefore, 40-year (1950-1989) means of this historical data may justifiably be compared with new (SHEBA) observations to determine whether anomalies exist.

IV. ANALYSIS OF SHEBA DATA IN COMPARISON WITH HISTORICAL DATA

A. OVERVIEW

As part of the Surface Heat Budget of the Arctic (SHEBA) experiment, a nearly continuous time series of temperature and salinity profiles was collected between 07 Oct 1997 and 22 September 1998. For this analysis, only data from the upper 150 m of the water column was considered. Each individual temperature and salinity profile was reviewed for data spikes and lags caused by equipment malfunctions and biological fouling of the sensors. This yielded over 12,000 profiles for each parameter. The temperature and salinity measurements were then averaged over one meter depth intervals and one day time intervals.

Mean profiles of temperature and salinity from the SHEBA time series are plotted against the 1950's through 1980's decadal means over the eight SHEBA track boxes (indicated on Figure 3.1) in two different formats, in order to address both regional and decadal variability. Both formats also depict winter-summer seasonal variability. In both representations, the SHEBA data (averaged over one meter intervals) is plotted as a continuous profile, while the historical data is plotted as discrete data points representing the nine depth levels for which mean data is available in the digital atlas (0, 5, 10, 15, 25, 50, 75, 100, and 150 m). Winter means for each box are indicated by "+", and summer means for each box are indicated by "x". Both representations illustrate the lack of historical data over the Beaufort Sea and Chukchi Cap. During most decades there are boxes where no data is available. Appendix A contains summary plots of historical data from the climatological atlas for both temperature and salinity

during Mar-May and Jul-Sep. These summaries show mean profile plots for each SHEBA box during each decade, and indicate the number of observations used to generate these means at each level. Again, means based on less than five observations were not used for this analysis.

In the first presentation format, mean decadal temperature/salinity profiles for each box are plotted together on one graph for each decade (50's -80's). Mean SHEBA profiles for each box were overlaid on each of these four decadal plots. This presentation depicts the range of regional and seasonal variability of historical profiles along the SHEBA track for each decade, in contrast with the range of regional and seasonal variability of the SHEBA data. Figure 4.1 presents temperature data by decade, and Figure 4.2 displays salinity data by decade.

The second format for comparing historical data with SHEBA data indicates the range of decadal variability within a single box. For this presentation, all Mar-May and Jul-Sep decadal means available for a box are plotted together with the Feb-May, Jul-Sep, and regional mean SHEBA profiles for that box. Because SHEBA was never in the same box from Feb-May as it was from Jul-Sep, the same legend code (a continuous line) is used to depict both seasonal averages. Feb-May was used to represent winter SHEBA data instead of Mar-May, which was used by the digital atlas as the best estimate of maximum winter conditions over the entire Arctic. In the vicinity of SHEBA, winter conditions are expected to be fully developed by February. Using Feb-May vice Mar-May to represent SHEBA winter provided more opportunity for seasonal comparisons between the SHEBA and historical data. The title of each plot indicates the dates during which SHEBA was in that particular box. A continuous dash-dot line is used to represent the mean of all SHEBA observations taken within that particular box. This presentation allows comparison of both decadal and seasonal

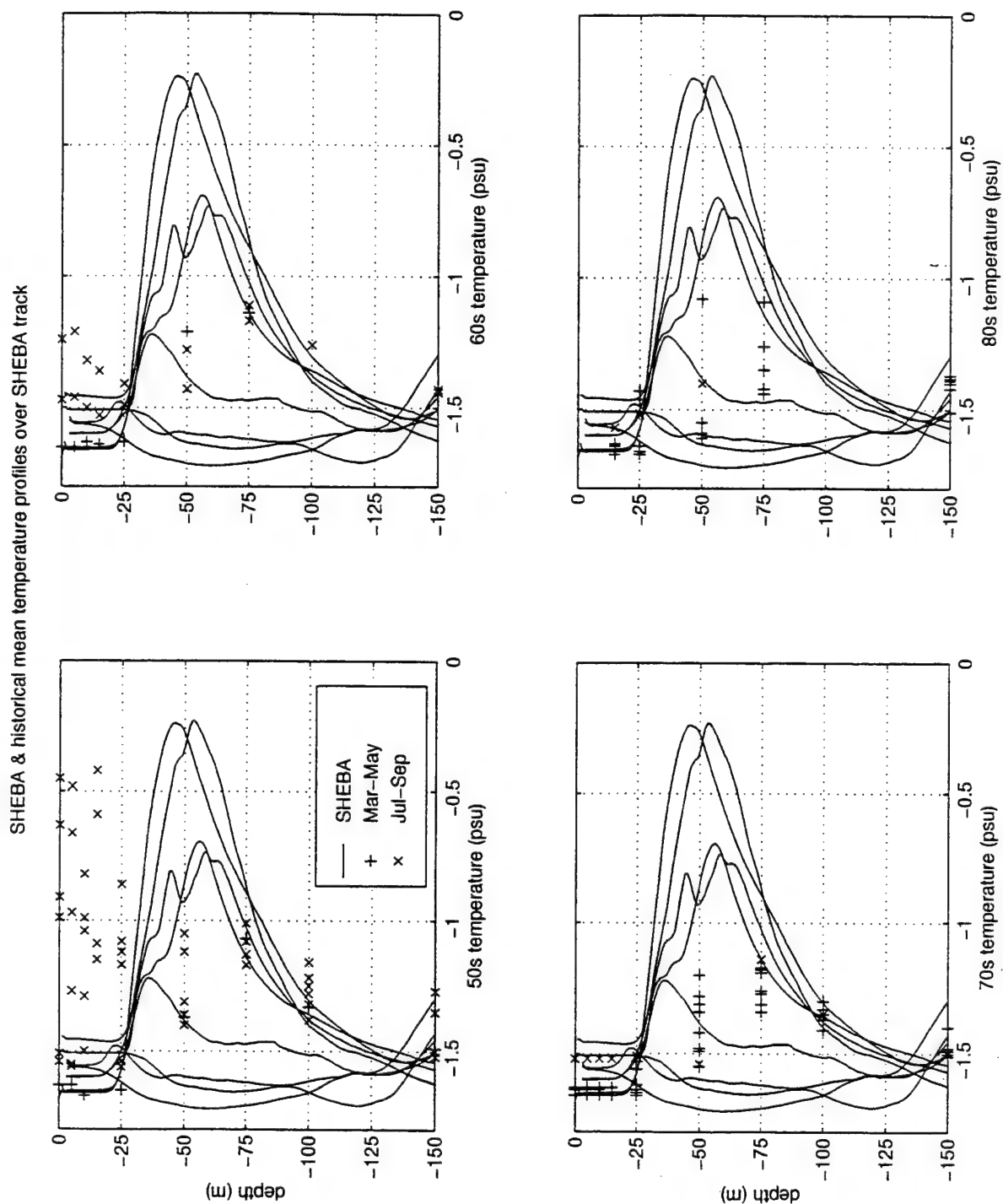


Figure 4.1. Mean SHEBA temperature profiles in all eight boxes are plotted against all available Mar-May and Jul-Sep historical mean temperature values for the 50's, 60's, 70's, and 80's in the four subplots, respectively.

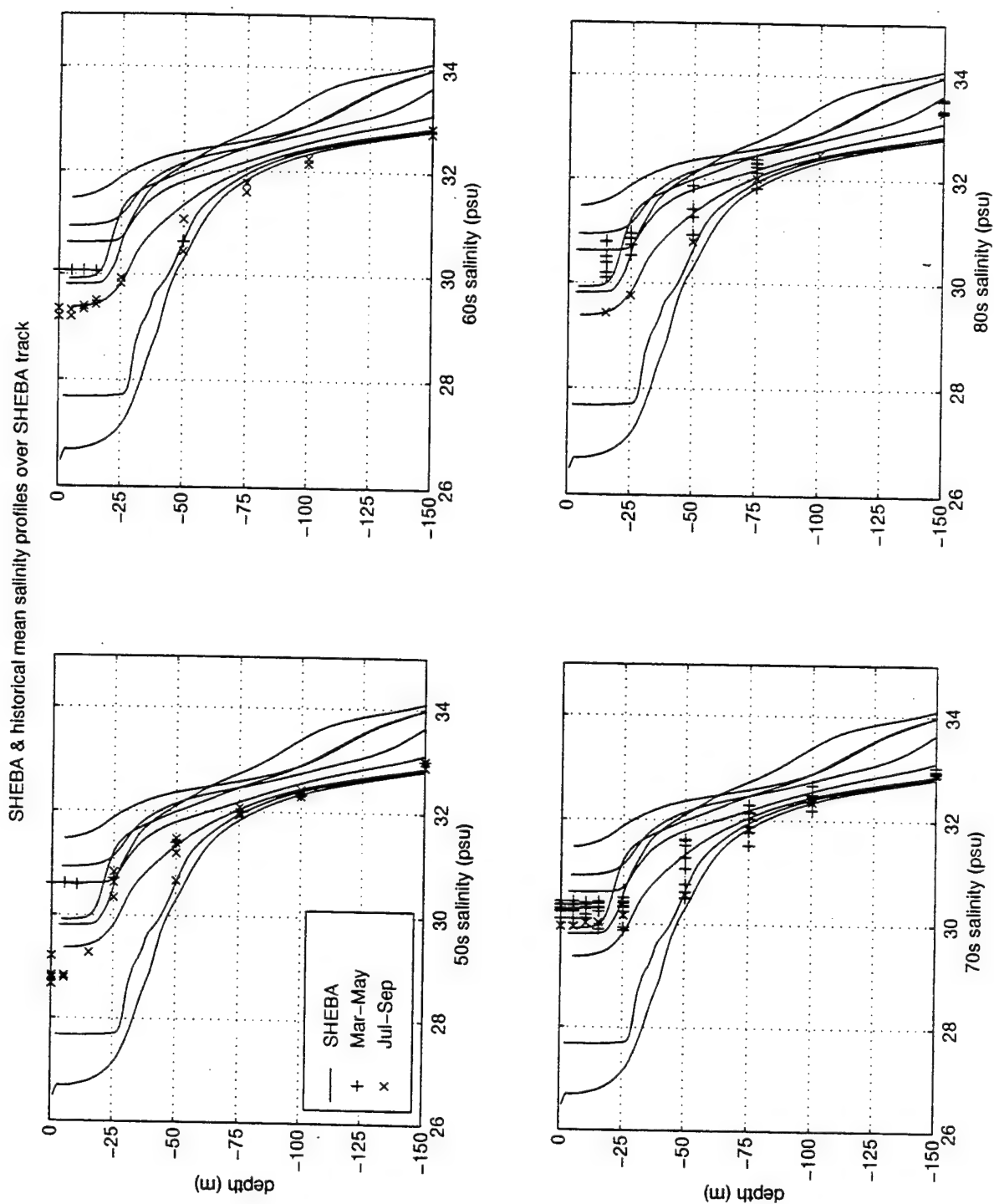


Figure 4.2. Mean SHEBA salinity profiles in all eight boxes are plotted against all available Mar-May and Jul-Sep historical mean temperature values for the 50's, 60's, 70's, and 80's in the four subplots, respectively.

variability of SHEBA and historical data. Figure 4.3 presents temperature data by grid box, and Figure 4.4 displays salinity data by grid box.

B. DECADAL AND GRID BOX COMPARISONS

1. Decadal temperature plots (Figure 4.1)

Due to the lack of vertical resolution in the historical data, the mixed layer is poorly resolved. The Mar-May historical data generally indicates a mixed layer depth of approximately 25 m depth in all four decades in all SHEBA boxes. The SHEBA profiles indicate mixed layer depths ranging from 15 m to 30 m.

As discussed in Chapter II, the mixed layer temperature in winter is at the freezing point, and is therefore a function of salinity (see Figure 2.4). Large fluctuations within the mixed layer occur primarily as a result of relatively short-term changes (seasonal or annual) in forcing variables such as solar insolation. Solar insolation contributes largely to melting ice and surface warming, but its impact varies significantly from region to region depending on season, ice cover, and atmospheric conditions. The mean Jul-Sep temperature observations at and above 25 m (for all decades) in Figure 4.1 are above the freezing point inferred from the corresponding salinity observations in Figure 4.2. Large variations in mixed layer temperature are readily apparent during the 1950's and 1960's, as all but one set of observations plotted were taken from Jul-Sep. In the 1970's and 1980's, Jul-Sep mean observations were only available for one SHEBA box.

Within the subsurface layer, where the upper halocline and pycnocline are located, all mean historical observations (from both winter and summer and all four decades) had

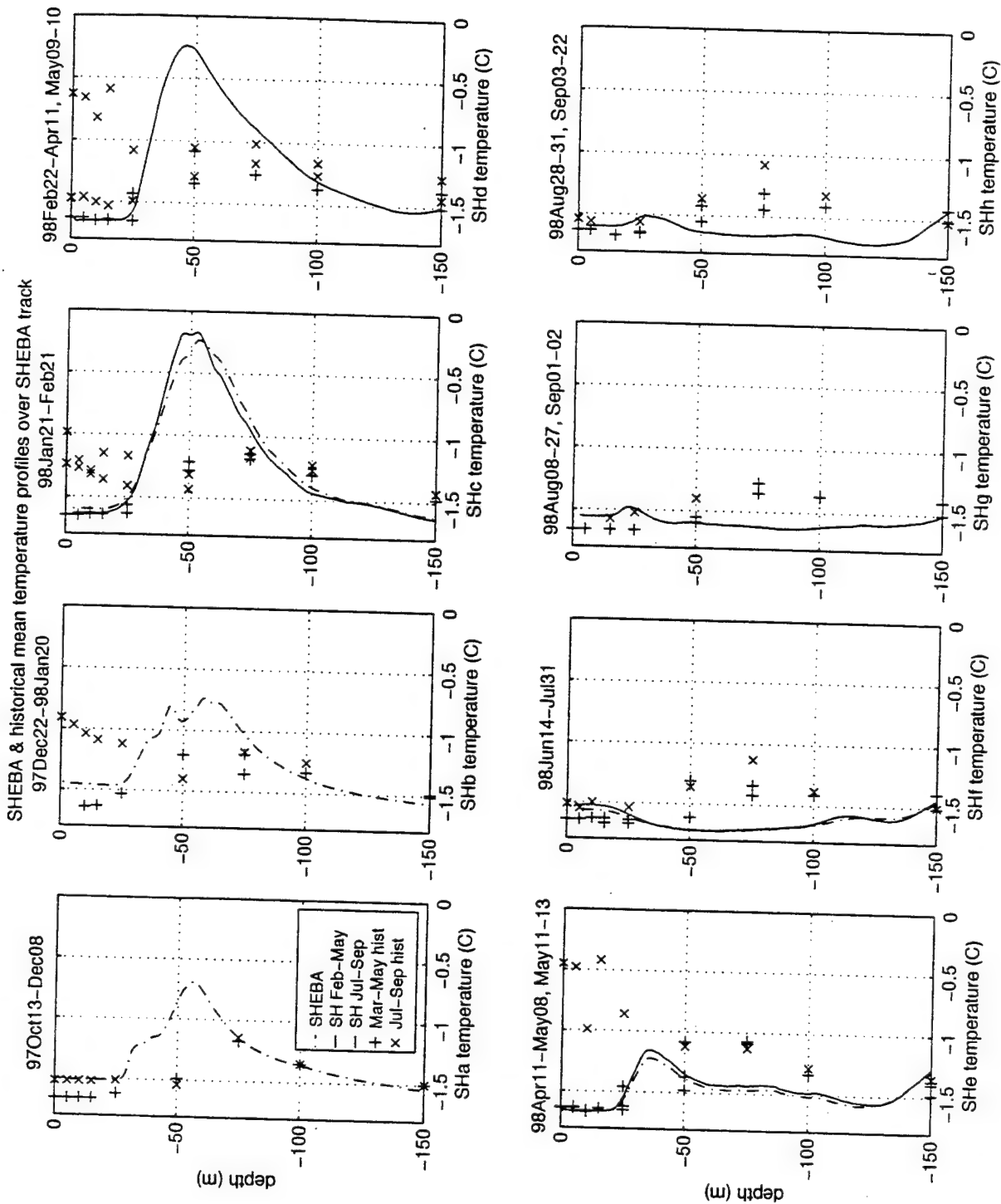


Figure 4.3. For each grid box along the SHEBA track, the mean, mean Feb-May, and mean Jul-Sep SHEBA temperature profiles are plotted with all available Mar-May and Jul-Sep historical mean data (50's-80's) for that grid box. The dates SHEBA was in each box are listed above each subplot.

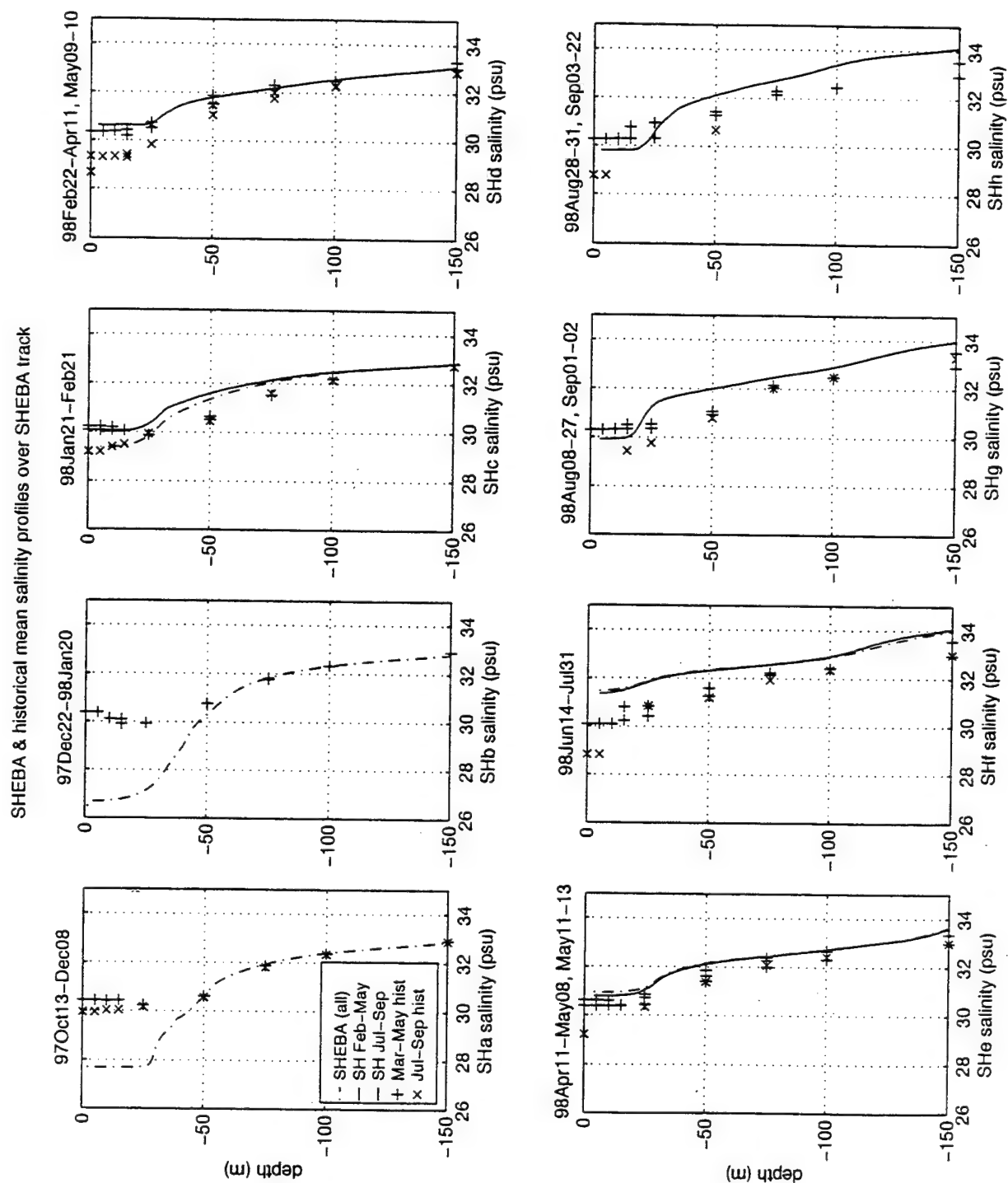


Figure 4.4. For each grid box along the SHEBA track, the mean, mean Feb-May, and mean Jul-Sep SHEBA salinity profiles are plotted with all available Mar-May and Jul-Sep historical mean data (50's-80's) for that grid box. The dates SHEBA was in each box are listed above each subplot.

temperature values below -1°C . A T_{max} (with a value $<-1^{\circ}\text{C}$) was apparent near 75 m or between 50 m and 75 m in all decades, which is consistent with previous studies reviewed in Chapter II. The regional ranges of 75 m mean decadal temperatures collected over all eight boxes during the 1950's, 1960's, 1970's, and 1980's are 0.16°C , 0.06°C , 0.20°C , and 0.35°C , respectively. The regional range of 75 m decadal mean temperatures across these eight boxes over all four decades is 0.43°C .

The range of all SHEBA temperatures at 75 m, measured during a one-year cycle over these same eight boxes, is 0.84°C (from -1.71°C to -0.87°C) - nearly twice the range found in the 40-year decadal averaged climatology. However, in all SHEBA boxes, T_{max} is found above 75 m, at depths ranging from 20 m to 60 m, with the warmest peaks around 50 m. The largest subsurface layer temperature range across the eight boxes, at a given depth, is 1.44°C at 50 m. For the SHEBA data, the depth with the largest range of temperatures is also the depth where the warmest temperatures (of all eight boxes in the SHEBA region) occurred.

The largest historical mean temperature range across all eight boxes also occurs at 50 m for each decade, although this does not coincide with the depth where the maximum sub-surface layer temperatures are found. For the 1950's, 1960's, 1970's, and 1980's, these 50 m decadal averaged regional ranges are 0.35°C , 0.22°C , 0.35°C , and 0.53°C , respectively - only 15-37% of the range found in the single year of SHEBA observations.

2. Decadal salinity plots (Figure 4.2)

The historical mean Mar-May salinity values also indicate a mixed layer depth of approximately 25 m throughout the region, while the SHEBA data depicts mixed layer depths ranging from 15 m to 30 m. The historical mean

Jul-Sep salinity values are consistent with the seasonal halocline expected during the summer in response to melting ice. Again, this feature is more noticeable during the 1950's and 1960's when more Mar-May data is available.

The horizontal variability of salinity decreases with depth in all boxes, during the 1950's, 1980's, and during SHEBA. Based on the available data, this variability was notably larger during SHEBA than during any other decade. At 25 m, the regional range of salinity values over the eight boxes is 0.49 psu, 0.10 psu, 0.63 psu, 1.19 psu, and 4.74 psu for the 1950's, 1960's, 1970's, 1980's, and SHEBA respectively. At 50 m, the ranges are 0.80 psu, 0.62 psu, 1.12 psu, 1.08 psu, and 2.06 psu, respectively. SHEBA yielded salinity variability ranges roughly four to nine times larger than the historical data at 25 m, and two to three times larger at 50 m. However, a substantial part of these horizontal variability differences may result from the very limited sampling of historical data for this region, the decadal averaging of the historical data, and the 0(1 month) averaging used in the SHEBA observations.

In the subsurface layer below 25 m, the salinity gradient is relatively constant from the 1950's through the 1980's, but the amount of data available is insufficient to make any firm conclusions about decadal trends. In all cases (SHEBA and historical), the steepest halocline gradient occurs between 25 m and 75 m.

3. Temperature plots for each SHEBA box (Figure 4.3)

Figure 4.3 also shows the large temperature variability in the mixed layer. Jul-Sep mixed layer temperatures above the freezing point (calculated as a function of salinity) occur in all eight boxes. As expected based on Chapter II, the Jul-Sep historical mixed layer temperatures in boxes SHa, SHf, SHg, and SHh are just above the freezing point. These boxes represent the deeper, more northerly areas of

the SHEBA track, where ice cover is expected year round, and little warming occurs in the mixed layer. The seasonal thermocline is clearly pronounced in boxes SHb, SHc, SHd, and SHE. These are the southernmost boxes of the SHEBA track, closest to land and the shallow Chukchi Sea, through which warm summertime Pacific inflow enters the Arctic (as discussed in Chapter II). Box SHb is interesting in that it depicts peak temperatures at two depths - a primary T_{\max} at 58 m, and a secondary (presumably transient) T_{\max} at 45 m, suggesting complicated interleaving in this area.

The SHEBA profiles do not indicate a seasonal thermocline in boxes SHb-e, because SHEBA drifted through these regions during the winter months. SHEBA was located in boxes SHf, SHg, and SHh during the peak summertime warming. The mean Jul-Sep SHEBA temperature profile in box SHf indicates a small seasonal thermocline, closely aligned with the only Jul-Sep historical mean profile available (from the 1950's). Box SHf is over the northernmost part of the Chukchi Cap - shallower and more southerly than boxes SHg and SHh. The mean Jul-Sep SHEBA profiles over boxes SHg and SHh (the two northernmost boxes) do not have a seasonal thermocline, but do reflect temperatures slightly higher than the freezing point, very similar to the historical Jul-Sep mean temperatures.

The SHEBA data varied significantly from the historical pattern in several ways. In four of the eight boxes, SHa-SHd, the mean SHEBA T_{\max} values exceeded the largest historical T_{\max} values for all four decades. They also exceeded -1°C , reaching values of -0.6923 , -0.7344 , -0.2296 , and -0.2381 , respectively. Boxes SHc and SHd have the warmest mean T_{\max} values, both historically and during SHEBA. However, mean T_{\max} during SHEBA was 0.88°C warmer than the historical mean T_{\max} of -1.11°C in box SHc, and 0.77°C warmer than the historical mean T_{\max} of -1.01°C in box SHd. These differences are 4.5 to 6.3 times larger than the maximum

inter-decadal differences and maximum standard deviations for the western Beaufort Sea shown in Figure 3.6. (Box SHc is within the western Beaufort Sea region; box SHd is adjacent to it).

Another significant difference between the SHEBA data and the historical data was the depth of T_{\max} in boxes SHa-e. T_{\max} of the mean SHEBA data was found at depths of 57 m, 59 m, 54 m, 47 m, and 37 m, in boxes SHa-e respectively. T_{\max} of the mean historical data occurred at approximately 75 m in boxes SHa-c, and between 50 m and 75 m in boxes SHd-e. In all cases, T_{\max} was significantly shallower during SHEBA, although it followed a similar pattern as the historical data in that the depth of T_{\max} was shallower in boxes SHd-e than boxes SHa-c. (Note that a precise determination of historical T_{\max} values is not feasible since observation values were only available at 25 m increments in the subsurface layer).

In boxes SHf-SHh, the mean SHEBA temperatures between 50 m and 100 m were cooler than the mean historical values for all decades. In these three boxes, the historical data indicates a T_{\max} at approximately 75 m depth. The SHEBA profiles, however, do not depict a T_{\max} at all. At 75 m, the regional differences between the mean SHEBA temperatures and the coldest historical mean temperatures are 0.29°C, 0.25°C and 0.19°C in boxes SHf-h, respectively. These differences are higher than the maximum standard deviation of 0.12°C in the northern Canada Basin just north of these boxes. The small temperature maxima in boxes SHg and SHh are presumed to be trapped heat in the mixed layer, as discussed in Chapter II, and not maxima of Pacific origin.

The differences between the SHEBA and historical mean temperatures in box SHE appear to be a combination of the differences noted in boxes SHa-d and boxes SHf-h. A T_{\max} is apparent during SHEBA at 37 m depth, roughly 25 m shallower than the historical data would suggest. However, the value

of mean T_{\max} during SHEBA is slightly less than the historical value. Between 50 m and 150 m, the mean SHEBA temperatures are less than the mean historical temperatures at the same depths.

4. Salinity plots for each SHEBA box (Figure 4.4)

The mean salinity profiles for individual boxes show relationships between SHEBA and historical mean data varying between regions. In boxes SHa and SHb, in the western Beaufort Sea, mean salinity measured during SHEBA in the mixed layer was 2 and 3 psu fresher than the freshest historical mean data available. Below 50 m the SHEBA and historical profiles were very similar in these same two boxes. Therefore, the halocline between 25 m and 50 m was much stronger during SHEBA. All of the SHEBA data in these two boxes was collected in early winter, after the peak ice melting season, when new ice was beginning to form (thus expelling brine). Based on the review in Chapter II, it is possible that the salinity gradient was even stronger in these two boxes a month or two earlier in the year. This 2 to 3 psu difference between the SHEBA and historical mixed layer values is significantly larger than the maximum summer inter-decadal difference (0.73 psu) or the maximum standard deviation (0.32 psu) for the mixed layer of the Western Beaufort as shown in Figure 3.7.

In box SHc, the Feb-May SHEBA salinity profile is very similar to the historical Mar-May profile in the mixed layer and below 100 m. Between 25 m and 75 m, it is up to 1 psu more saline than the historical data. A significant difference exists between the Feb-May SHEBA mean values and the mean of all SHEBA measurements within this box, even though the total mean includes only 10 more days of data (for a total of 31 days in SHc). This suggests that mixed layer conditions within this box were still changing rapidly in late January - becoming denser as new ice was formed.

The mean Feb-May SHEBA profiles in boxes SHd and SHE are slightly more saline than the saltiest of the historical profiles. However, the difference is less than 0.5 psu, which is less than both the maximum decadal standard deviation and the maximum inter-decadal difference for all three surrounding regional areas (Chukchi Sea, western Beaufort Sea, and northern Canada Basin) as shown in Figure 3.6.

The mean SHEBA profile in box SHf is more saline at all levels than the saltiest historical mean observations - 1.37-1.40 psu in the mixed layer, 0.76-1.03 psu between 15 m and 50m, and 0.34-0.47 between 50 m and 150 m. SHf is between the northern Canada Basin, western Beaufort Sea, and Chukchi Sea regions described in Chapter II. The minimum SHEBA/historical differences listed above are significant in comparison with the maximum inter-decadal differences and maximum standard deviations for the northern Canada Basin and western Beaufort Sea as shown in Figure 3.7. However, these differences are not significant in comparison with the statistics for the Chukchi Sea region, also shown on Figure 3.7. Box SHf is at the northern edge of the Chukchi Cap, located over relatively shallow water in comparison with the northern Canada Basin and western Beaufort Sea, but relatively deep water in comparison with the Chukchi Sea region. The barotropic nature of the currents in the Arctic Ocean causes them to steer around bathymetric features. Hence, box SHf may represent differences brought about by changes in advective features.

The mean Jul-Sep SHEBA profiles in boxes SHg and SHh are saltier than the historical mean Jul-Sep observations at all levels. They are also more saline than the historical mean Mar-May observations below 25 m. The mixed layer depth during SHEBA appears to be around 15 m; the historical mean mixed layer depth appears around 25 m. A relatively sharp gradient appears between 15 m and 25 m in box SHg and

between 15 m and 35 m in box SHh. The historical data does not indicate a similar gradient, but this may be due to the lack of vertical resolution.

C. SHEBA ANALYSIS SUMMARY

Figures 4.5 and 4.6 show the mean SHEBA temperature and salinity profiles, respectively, for each of the eight SHEBA boxes along the SHEBA drift track. Annotated near the top of each SHEBA box are the differences between mean SHEBA and 40-year mean historical mixed layer temperatures and salinities for both winter and summer. (Winter was considered March through May for historical data, and February through May for SHEBA data; summer was considered July through September for all data). The mixed layer parameter values were based on historical data at 15 m, and SHEBA data between 14 m and 16 m. In boxes where mixed layer differences are not annotated, no SHEBA data was available between 5 m and 25 m for the desired season (winter or summer), and/or robust inter-seasonal comparisons were not possible.

SHEBA drifted through boxes SHa and SHb in early winter, when neither Feb-May nor Jul-Sep SHEBA data was available. To accomodate this short-coming, the mean early winter (Oct13-Dec08) SHEBA profile for box SHa is compared with historical summertime expectations, keeping in mind that the mixed layer is generally freshest in late summer. The mean Dec22-Jan20 SHEBA profile for box SHb is compared with historical wintertime expectations. The difference for these two boxes is marked with an asterik (*) on Figures 4.5 and 4.6, indicating that direct seasonal comparisons were not possible.

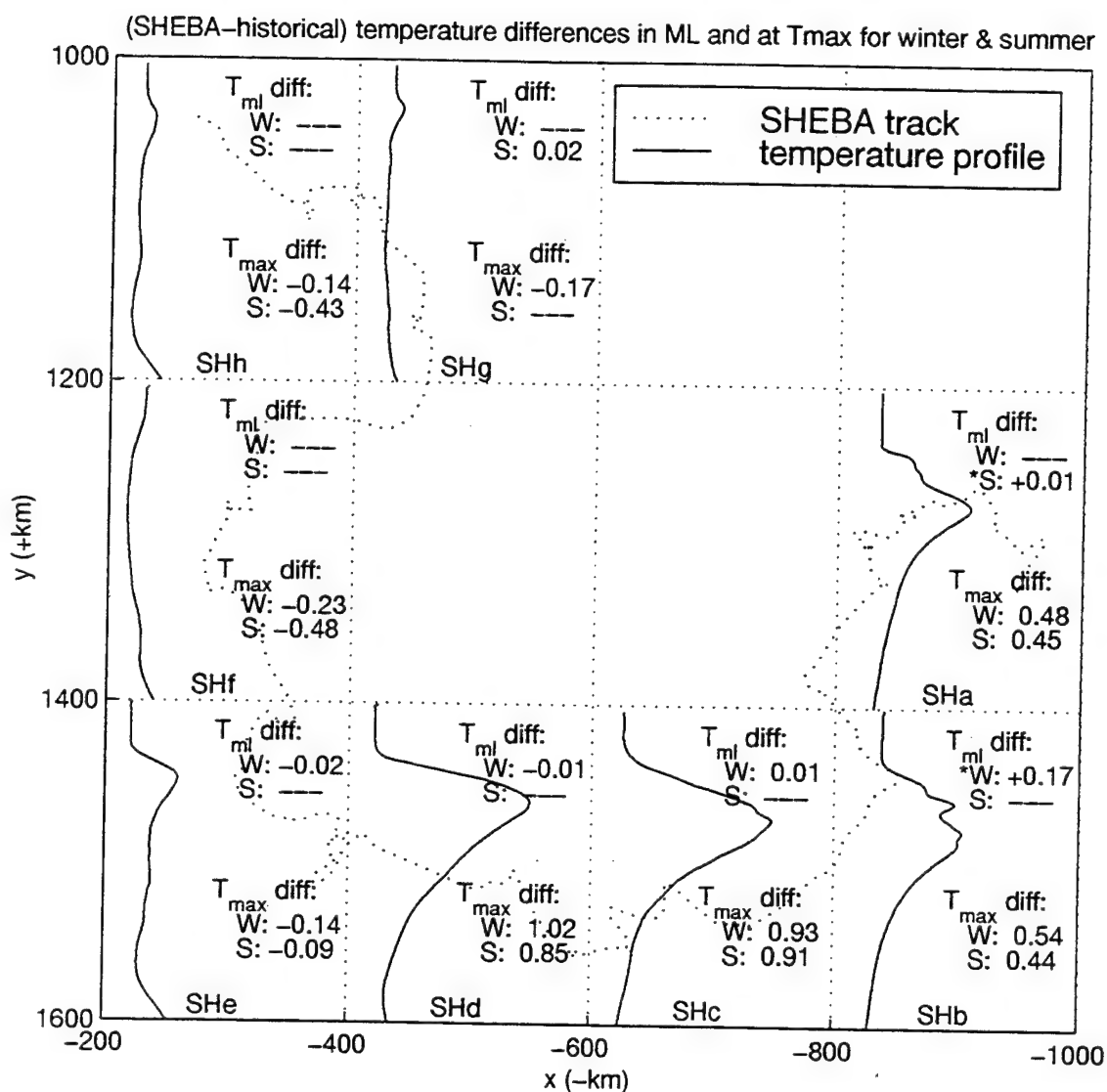


Figure 4.5. Mean SHEBA temperature profiles are plotted for each grid box. The SHEBA-historical temperature ($^{\circ}\text{C}$) difference in the mixed layer and at T_{max} are annotated for winter and summer in each box. At T_{max} , mean SHEBA temperatures for the entire box are compared with seasonal historical means. In the mixed layer, seasonal means are used for both SHEBA and historical data unless marked with an asterik (*) - ("*" indicates total mean SHEBA data used). Profiles are from the surface to 150 m, normalized to the 200 unit vertical scale of each grid box.

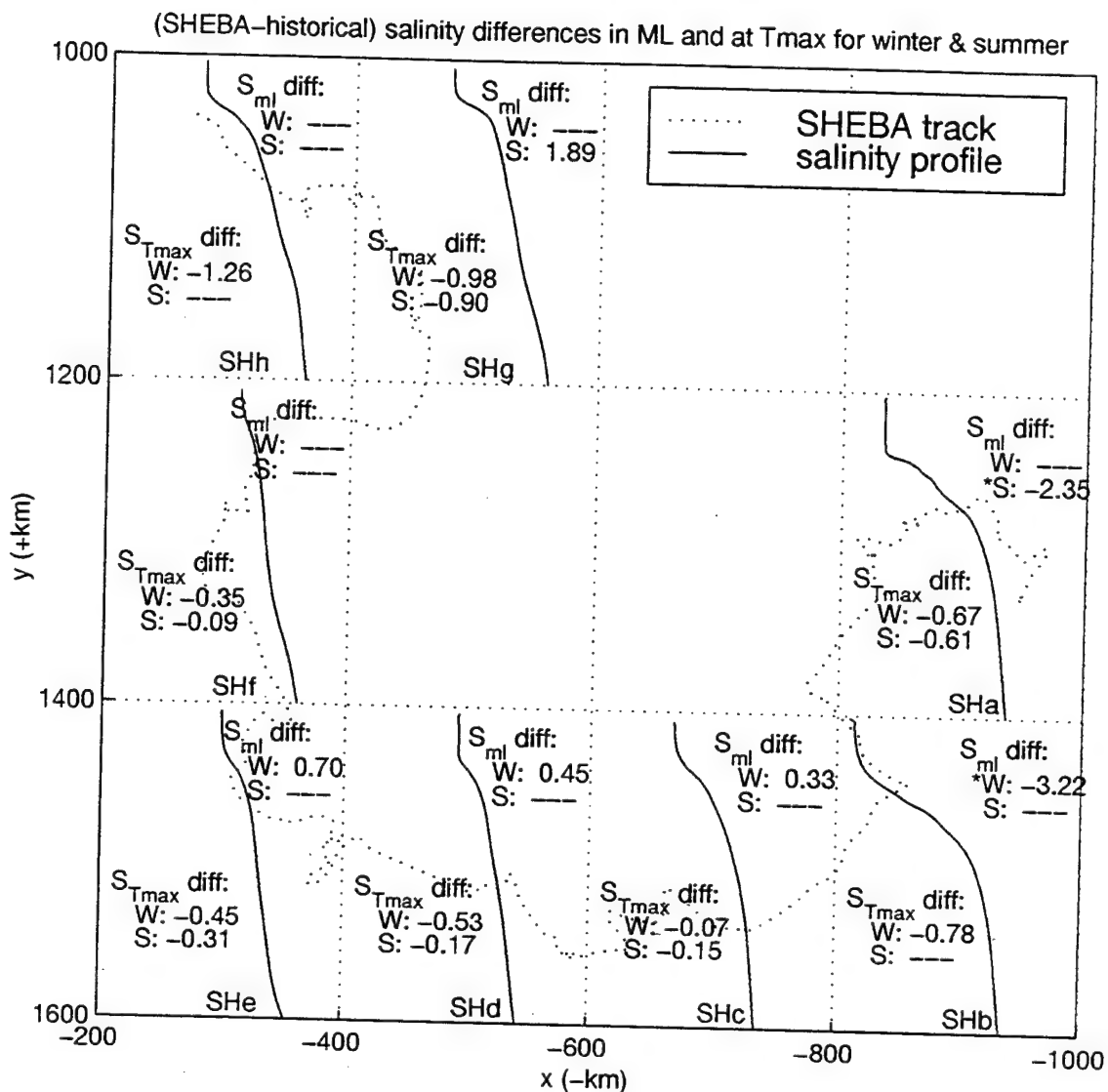


Figure 4.6. Mean SHEBA salinity profiles are plotted for each grid box. The SHEBA-historical salinity (psu) difference in the mixed layer and at T_{max} are annotated for winter and summer in each box. At T_{max} , mean SHEBA temperatures for the entire box are compared with seasonal historical means. In the mixed layer, seasonal means are used for both SHEBA and historical data unless marked with an asterisk (*) - ("*" indicates total mean SHEBA data used). Profiles are from the surface to 150 m, normalized to the 200 unit vertical scale of each grid box.

Table 4.1 summarizes mean SHEBA minus mean historical data differences for the mixed layer where direct seasonal comparisons or robust inter-seasonal comparison were possible. In all boxes except SHb, mean mixed layer temperatures varied only slightly (within $\pm 0.02^{\circ}\text{C}$) in comparison with historical data. In box SHb the mean SHEBA temperature was $+0.17^{\circ}\text{C}$ warmer, but this is not considered significant because this Dec-Jan value falls between the historical Jul-Sep and Mar-May values.

SHEBA - HISTORICAL
MIXED LAYER TEMPERATURE/SALINITY DIFFERENCES

Mean Seasonal Differences	SHa mixed*	SHb mixed*	SHc winter	SHd winter	SHe winter	SHg summer
ΔT_{ml} ($^{\circ}\text{C}$)	+0.01	+0.17	+0.01	-0.01	-0.02	+0.02
ΔS_{ml} (psu)	-2.35	-3.22	+0.33	+0.45	+0.70	+1.89

Table 4.1. Seasonal differences between mean SHEBA mixed layer values and 40-year historical mean values for boxes SHc-e, and g. The asterik (*) indicates boxes where direct seasonal comparisons were not possible. For box SHa, Oct-Dec SHEBA values are compared with Jul-Sep 40-year historical means. For box SHb, Dec-Jan SHEBA values are compared with Mar-May 40-year historical mean values.

In boxes SHa-b the mixed layer salinity *decreased* significantly. In SHa the SHEBA mean was 2.35 psu fresher - even though this value used Oct13-Dec08 SHEBA data in comparison with historical summer values. Summer values are generally the freshest within a given year, suggesting that the actual salinity anomaly in Jul-Sep 1998 within this box was probably even fresher than the +2.35 psu difference. In SHb the Dec22-Jan20 SHEBA mean was 3.22 psu fresher than the Mar-May historical mean. Although late winter salinity values are normally greater than early-mid winter values, this 3.22 psu difference is larger than the historical annual salinity range for neighboring boxes SHa and SHc,

again suggesting a robust low salinity anomaly. The 15 m Dec-Jan SHEBA salinity value is 26.78 psu. This is significantly fresher than every available Jul-Sep historical salinity value in every grid box immediately surrounding SHb, as shown on Figures 3.3(c) and (d). The lowest historical Jul-Sep mixed layer salinity of all decades and all surrounding boxes is 29.47 psu, 2.69 saltier than the Dec-Jan SHEBA value of 26.78 psu. The combination of these anomalously low salinities and relatively unchanged temperatures suggests thinner ice thickness or lower ice concentrations, likely due to excessive ice melt during the summer of 1997, just before SHEBA began. McPhee et al. (1998) noted that sea ice thicknesses during SHEBA were significantly less than the expected mean values of 2 m to 3 m, making it difficult to find ice floes thicker than 1.5 m; the thickest unridged ice rarely exceeded 1.8 m on the relatively thick flow chosen for the SHEBA site.

Mixed layer salinity, however, *increased* significantly in SHEBA boxes SHc-e and SHg, with increases ranging from 0.33 to 1.89 psu. The 1.89 psu increase in the Chukchi-Mendeleev boundary region far exceeds the increases in the southern boxes nearer the Chukchi Sea (Table 4.1). The combination of increased salinity and relatively unchanged temperature might suggest more sea ice, but this has not been observed. These observed changes might be related to the shoaling of the Atlantic (intermediate) layer or a shift in the Atlantic/Pacific water boundary, and will be addressed in Chapter V.

Annotated near the bottom of each SHEBA box (on Figures 4.5 and 4.6) are the differences between mean SHEBA and mean historical temperatures (salinities) at the level of T_{\max} for both winter and summer. The depth of T_{\max} used for historical data was 75 m. The depth of T_{\max} for SHEBA data was calculated as the depth of the maximum mean temperature value between 25 m and 100 m in boxes SHa-e. These SHEBA

T_{\max} depths are displayed in Table 4.2. (There was no T_{\max} in boxes SHf-h). This analysis treats the warm Pacific layer as a distinct tracer, and considers the water property changes within this layer (between historical and SHEBA data). Because temperature and salinity conditions at the depth of T_{\max} experience relatively little seasonal change, the mean of all SHEBA data collected in a particular box, regardless of season, was compared to the winter and summer historical data at this level.

DEPTH OF T_{\max}						
	HIST	SHa	SHb	SHc	SHd	SHe
depth of T_{\max}	~75 m	57 m	59 m	54 m	47 m	37 m

Table 4.2. Depth of T_{\max} for historical Canada Basin data and for SHEBA data in various grid boxes.

This comparison indicates warming (0.44°C to 1.02°C) at the depth of T_{\max} in boxes SHa-d, and cooling (-0.09° to -0.48°C) at T_{\max} in boxes SHe-h (see Figure 4.5). The greatest warming occurred in boxes SHc and SHd, and the greatest cooling occurred in box SHf. The magnitude of the warming in boxes SHa-d was approximately twice as large as the magnitude of the cooling in boxes SHe-h. In boxes SHf-h, the cooling was much greater for summer data than winter data. Boxes SHf-h also highlight the absence of a defined layer of Pacific origin, as no T_{\max} is apparent.

Figure 4.6 demonstrates freshening of the water at T_{\max} , ranging from -0.07 psu to -1.26 psu, in all SHEBA boxes. The greatest freshening (-0.90 to -1.26 psu) occurred in the northernmost boxes, SHg and SHh, near the northern Canada Basin. Substantial freshening (-0.61 to -0.78 psu) also occurred in boxes SHa and SHb, over the deepest portion of the western Beaufort Sea. These changes are likely related to long-term (decadal scale) shifts in atmospheric circulation patterns, and are addressed in Chapter V.

V. DISCUSSION AND CONCLUSIONS

A. COMPARISON SUMMARY OF SHEBA AND HISTORICAL DATA

The Chapter III analysis of historical temperature and salinity data from the 1950's through the 1980's did not reveal any consistent, significant decadal trends or oscillations. It demonstrated little seasonal, decadal, or inter-decadal variability within the northern Canada Basin and the western Beaufort Sea. The eastern Beaufort Sea had the highest historical wintertime variability, and both the Chukchi Sea and the eastern Beaufort Sea demonstrated high summertime variability. Due to the sparseness of historical data sampling in time and space, this does not eliminate the possibility that decadal trends or oscillations exist. It does, however, indicate that any such trends have a small magnitude compared with the changes observed in the SHEBA data as presented in Chapter IV. For this reason 40-year means of historical data were used for comparisons with the SHEBA data.

The platform for SHEBA, CCGS *Des Groseilliers*, was initially located in the western Beaufort Sea, and drifted within the Beaufort Gyre, ending up near the northern Canada Basin - both of these endpoints being in relatively deep water. However, during its transit, SHEBA passed over the Chukchi Cap, a shallower region with rapidly varying, shallow bathymetry north of the Chukchi Sea. (Refer to the bathymetry plot, Figure 2.1.) The SHEBA data showed significant departures from the available historical observations across most of its track, but the nature of these departures from historical data were quite different in the sample areas located east of the Chukchi Cap than the areas located over and north of the Chukchi Cap. Possible explanations for the apparently anomalous SHEBA observations on different sides of the Chukchi Cap follow. Figure 5.1

illustrates the salinity and temperature profiles for each grid box along the SHEBA track. Figures 4.5 and 4.6 show these same profiles, along with the computed difference in reference to historical 40-year means.

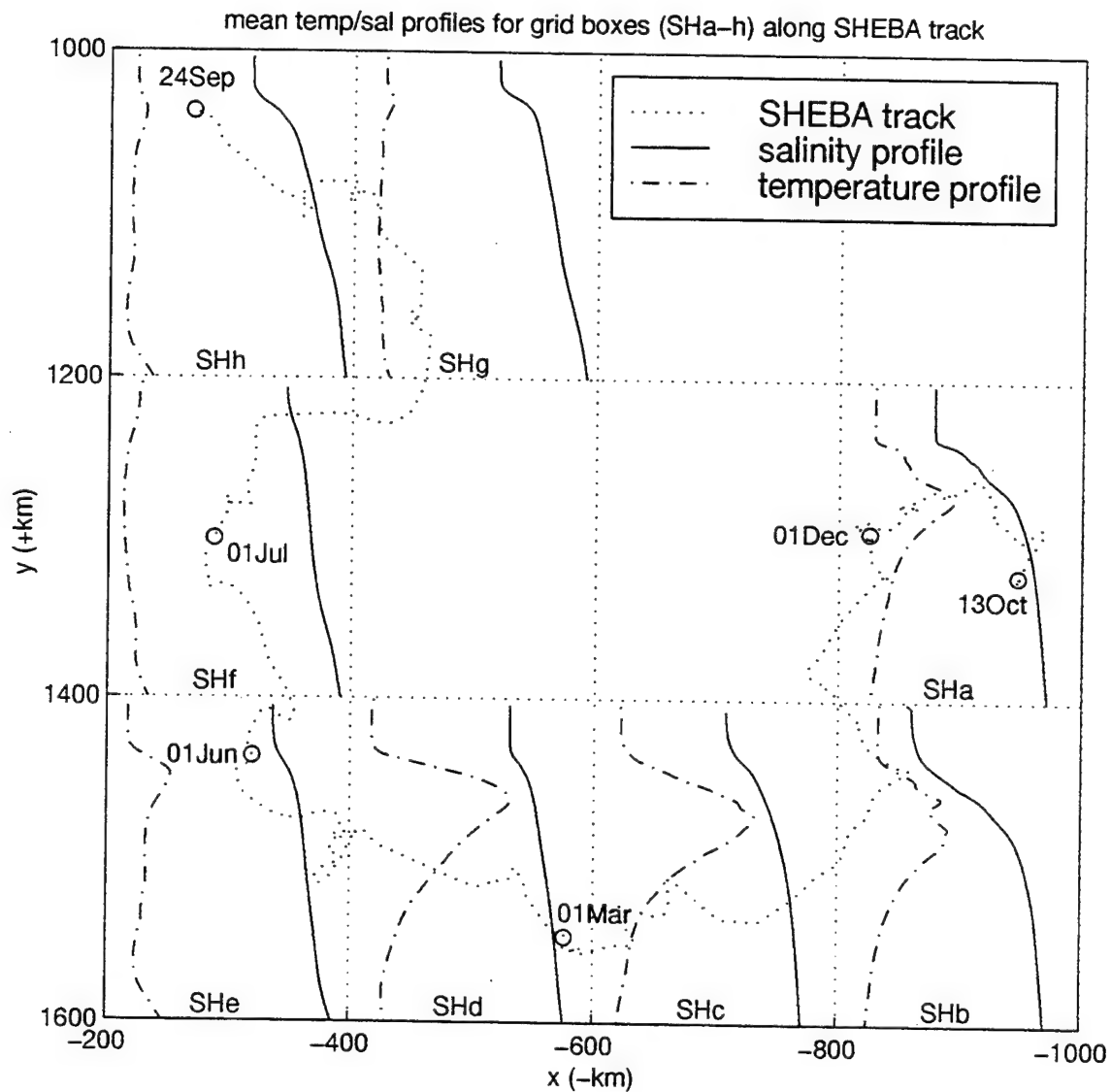


Figure 5.1. Mean SHEBA temperature and salinity profiles for each grid box along the SHEBA track. Profiles are from the surface to 150 m, normalized to the 200 unit vertical scale of each grid box.

B. SHEBA ANOMALIES AND PROPOSED EXPLANATIONS

1. Temperature and salinity at the depth of T_{\max}

a. Temperature at the depth of T_{\max}

Historical information based on both the atlas and the literature reviewed in Chapter II indicates that the water layer of Pacific origin has a T_{\max} of less than -1°C at approximately 75 m, with a corresponding salinity near 31.9 psu. These sources also indicate that this Pacific layer is normally found throughout the entire Canada Basin, although the magnitude of T_{\max} may decrease with distance from the source. In all boxes east of the Chukchi Cap (SHa-d), T_{\max} exceeded -1°C , with increases of 0.44°C to 1.02°C over mean values for the previous four decades. These temperature increases were more than twice the historical decadal and inter-decadal variations in these areas. In box SHe, the temperature of T_{\max} was notably cooler, and in boxes Shf-h, in the northern Canada Basin, there was no evidence of a Pacific layer at all.

There is no major source of heating or cooling below the Pacific layer, and the intrusive Pacific layer is separated and largely protected from surface effects by the strong upper halocline. Previous research has indicated that the upper halocline, where the Pacific layer is found, is maintained by lateral advection (Melling and Lewis, 1982; Aagaard et al., 1981). Therefore, it is likely that changes in advection patterns, such as a change in the flow rate through the Bering Strait or a shift in the Atlantic/Pacific front, are primarily responsible for the large departures from historical patterns in the Pacific layer/upper halocline.

As discussed in Chapter II, the Beaufort Gyre is driven by the atmospheric Beaufort High pressure system. Changes in the intensity and location of the Beaufort High

ultimately lead to changes in the Beaufort Gyre circulation, which extends as deep as 150 m. Walsh et al. (1996) studied Arctic mean sea level pressure data. They found that the mean 1987-1994 central pressure of the Beaufort High had decreased from the 1979-1986 mean, and that the center had shifted southeast nearer to the north Canadian coastline (see Figure 5.2). They noticed that the 1979-1986 mean magnitude and location of the Beaufort High pressure center were very similar to the corresponding features of the 1952-1989 mean determined by Serreze et al. (1993), indicating relatively little change over this nearly four-decade period. The post-1987 decrease in the intensity of the Beaufort High was found to be seasonally robust, with the largest decreases occurring during winter months. Further, their examination of annual sea level pressure anomalies (increases and decreases relative to the 1950-1994 mean) indicated seven consecutive years of negative values from 1988-1994. This is unprecedented, as negative anomalies have never previously persisted for more than 3-4 years during this 45-year period. They also found a corresponding decrease in anti-cyclonic wind-forcing, implying less surface convergence over the Beaufort Gyre.

The findings of Walsh et al. (1996) correspond well with the results of the comparison of SHEBA and historical data. Both data sets indicated no persistent large scale trends during the 1950's through 1980's, but large anomalies in the 1990's. Walsh et al. (1996) found that the most pronounced pressure decreases - the onset of the current trend of weaker pressures - occurred in 1987 and 1988. Morison et al. (1998) also studied yearly average pressure maps in conjunction with their analysis of data from a 1993 Arctic cruise of the submarine, *USS Pargo*. Their results were consistent with Walsh et al. (1996), and indicated that the temporal shift in Arctic atmospheric circulation roughly corresponds to their estimate of the

onset of recent ocean circulation changes. The period 1989 through 1997 would be sufficient time for the Beaufort Gyre to adjust to the weakened and shifted Beaufort High as shown in Figure 5.2. The adjusted circulation pattern of the Beaufort Gyre would be a weaker flow, limited to the Canada Basin - no longer extending into the Makarov Basin.

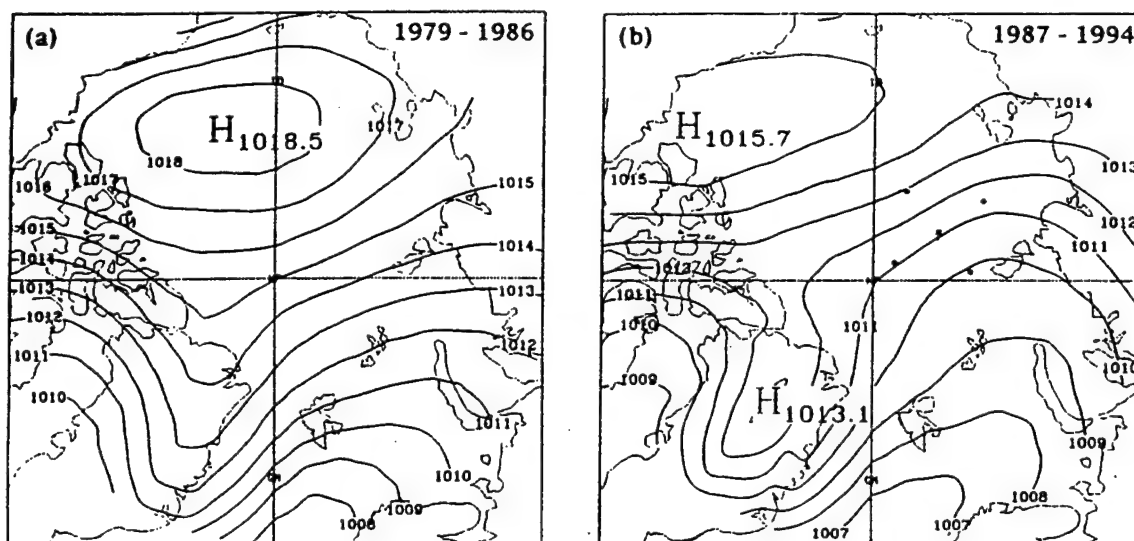


Figure 5.2. Annual mean sea level pressure (mb) in the Arctic for (a) 1979-1986 and (b) 1987-1994 (from Walsh et al. 1996).

Swift et al. (1997) and Carmack et al. (1997) examined water properties along a cross-section across the Canadian Basin from the AOS94 expedition (see Figure 5.3). They noted changes in the location of water masses that suggest a shift in Arctic circulation patterns consistent with a weakened Beaufort High circulation. They found that the nutrient maximum (at salinity ~33.1 psu) associated with Bering Sea (Pacific) water was absent from the Makarov Basin, apparently displaced by water from the Eurasian Basin.

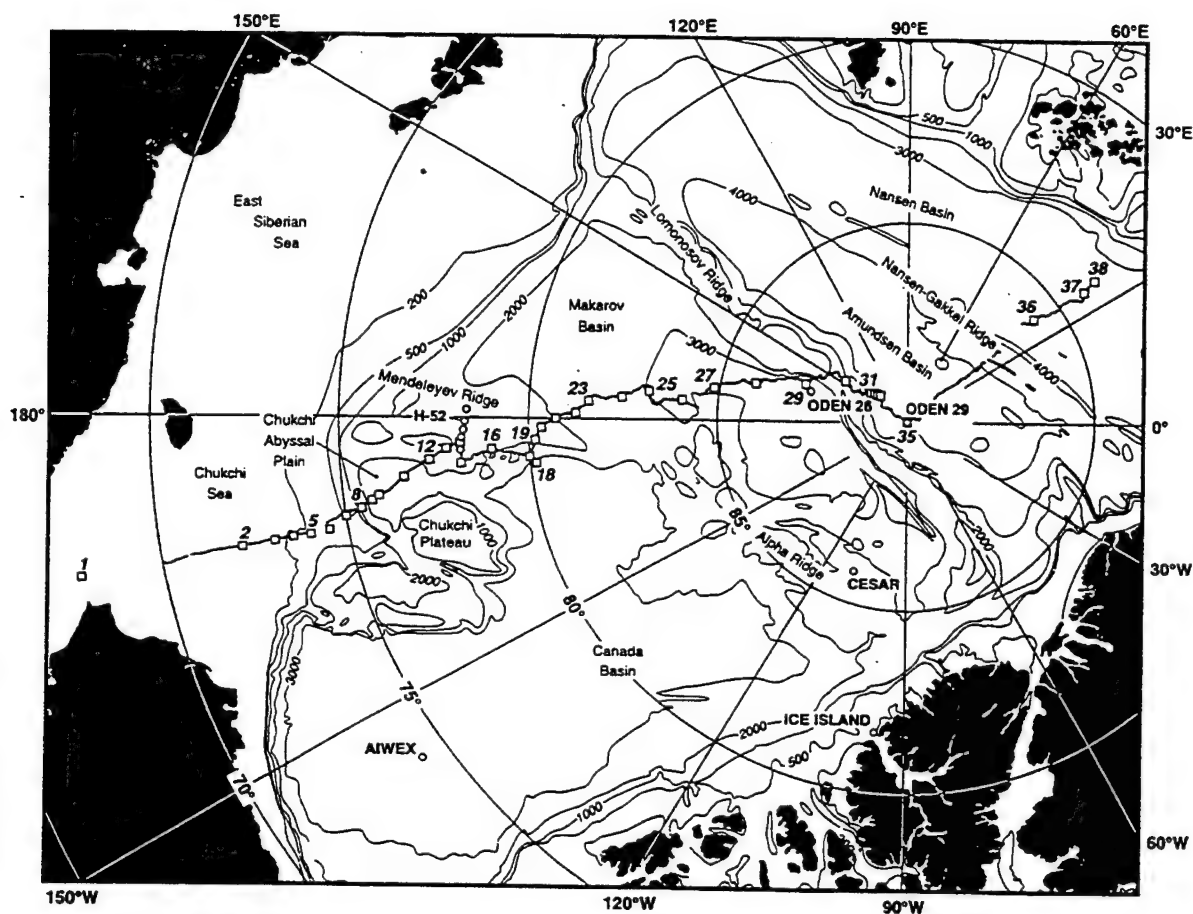


Figure 5.3. Locations of CCGS Louis S. St-Laurent Stations 1 to 38 of the AOS94 expedition across the Arctic Ocean. The cruise track is illustrated by the positions where soundings were collected from USCGC Polar Sea during AOS94. Also included are positions of hydrographic stations from other expeditions mentioned in the text. The term "Chukchi-Mendeleyev boundary region" refers to the complex bathymetry crossed by AOS94 from the Chukchi Sea self break to the Makarov Basin. (From Swift et al., 1997).

Morison et al. (1998) and Steele and Boyd (1998) examined SCICEX '93 and SCICEX '95 data, respectively, and also found no influence of Pacific water in the Makarov Basin. McLaughlin et al. (1996) defined the Atlantic/Pacific front as the boundary between waters characteristic of the eastern and western Arctic Ocean. Their work studied water mass characteristics of data collected in 1993 aboard the CCGS *Henry Larsen*, and suggests that while the Atlantic/Pacific front was historically located roughly over the Lomonosov Ridge, it had recently shifted to a location roughly over the Mendeleev Ridge by 1993. Morison et al. (1998) suggested a similar substantial shift in the location of the front between the waters of the eastern and western Arctic ocean.

The Beaufort Gyre is strongly influenced by topography. The circulation corresponding to its weaker intensity and shifted location may be limited in its westward extent by the eastern edge of the Chukchi Cap. This may focus the warm Pacific input through Barrow Canyon into the Beaufort Sea, as illustrated by the SHEBA data where the warmest values of T_{\max} are all in the western Beaufort Sea. The expanded counter-clockwise circulation reflecting a deeper Eurasian Low may curtail warm inflow through Herald Canyon into the Chukchi-Mendeleyev boundary region, as illustrated by the lack of a Pacific layer in SHEBA data from the Makarov Basin. Steele and Boyd (1998) plotted contours of maximum temperature with salinity less than 33 psu (indicative of T_{\max} for Bering Sea Water) based on four different data sets: the EWG digital atlas, Oden '91, SCICEX '93, and SCICEX '95. Their plots depict the retreat of Bering Sea Water from the Makarov Basin. Only their plot for SCICEX '95 included a -1.0°C contour, indicating temperatures warmer than -1.0°C in the western Beaufort Sea/eastern Chukchi Cap region - consistent with the areas of above -1.0°C water found during SHEBA. Their

research suggested a roughly 0.5°C warming of Bering Sea Water in the Canada Basin in comparison with historical values (compared to the 0.44 to 1.02°C warming found in this region during SHEBA). Melling (1998) also studied data from hydrographic surveys in the Canada Basin and found significant upper halocline warming.

The cause for the temperature increase within the Pacific Layer is uncertain, but it is likely to be the result of an increase in the temperature and/or volume of Bering Sea inflow. Roach et al. (1995) measured Bering Strait transport from 1990-1994. They found the mean annual transport measured over these four years (0.83 Sv northward) to be near historical values, but the transport of 1.14 Sv measured during the first nine months of 1994 was the largest flow rate measured during the previous 50 years.

b. Salinity at the depth of T_{\max}

The upper halocline salinity at the depth of T_{\max} decreased in all boxes along the SHEBA drift track. This freshening is most pronounced in boxes SHa,b,g, and h - the boxes over the deepest waters along the track - and also results from the changes in large scale advection patterns. As the Beaufort High pressure system weakened and shifted southeast, the Eurasian Low Pressure over the eastern Arctic strengthen and extended into the Canadian Basin as in Figure 5.2 (Walsh et al. 1996; Steele and Boyd, 1998). This results in an expansion into the Canadian Basin of the counterclockwise circulation associated with the Eurasian Low.

Steele and Boyd (1998) compared 40-60 m averaged 1990's salinities (from ODEN '91, SCICEX '93, and SCICEX '95) with 40-year means and minimums from the digital atlas. They identified increased salinities in the Makarov and Amundsen Basins, but freshening in the central Canada Basin of about 0.5 psu relative to the 40-year minimum. They

proposed that the result of the counterclockwise circulation driven by the Eurasian Low should be Ekman transport onto the shelf, and/or transport along the shelf with the ice motion. This explains the retreat they identified of fresh surface waters from the Amundsen Basin into the Makarov Basin. This also may explain the large salinity decreases found in the SHEBA data near the Northern Canada Basin. This advected water is relatively fresh due primarily to river runoff, which varies seasonally and annually, but remains on the shelves through the winter ice production season. The expanded counterclockwise circulation and resulting transport advect relatively fresh water from the Russian shelves primarily into the Makarov Basin, instead of the Amundsen Basin.

Swift et al. (1997) used alkalinity to trace river runoff, and found its presence at all stations in the Canadian Basin and Amundsen Basin during AOS94. AOS94 stations roughly followed a line from the Chukchi Sea, over the Mendeleev Ridge just northwest of the Chukchi Cap, to just across the Lomonosov Ridge. By examining water mass properties, they identified a Chukchi-Mendeleev boundary region with many water properties similar to the Eurasian Basin. They propose that this Chukchi-Mendeleev boundary region may be a primary injection site for the interior Canada Basin waters.

The above scenarios lend themselves well to the observed anomalies in SHEBA salinity data. Relatively fresh shelf water may be advected into the Canadian Basin by the counterclockwise flow associated with a strengthened and expanded Eurasian Low. The Chukchi-Mendeleev boundary region may then be the primary injection point for this flow to enter into the Canada Basin, where it would then move clockwise with the Beaufort Gyre. This could explain why boxes SHg-h, in the Chukchi-Mendeleev boundary region, showed the largest upper halocline salinity decreases (-0.98

psu to -1.26 psu), why boxes SHa-b in the western Beaufort Sea also experienced the large upper halocline salinity decreases (-0.61 psu to -0.78 psu), and why boxes SHc-f, nearer the Chukchi Sea and southeast of the Chukchi Cap showed the smallest upper halocline salinity decreases (-0.07 psu to -0.53). The low salinity anomalies in boxes SHa-d may be related to interannual fluctuations in the Pacific inflow as well, which is also relatively fresh compared with the Arctic Ocean.

c. Reason for temperature and salinity anomalies at T_{\max}

The temperature and salinity anomalies observed during SHEBA suggest that the Atlantic/Pacific front, marking the extent of upper halocline water, may have retreated even farther from its 1993 position over the Mendeleev Ridge described by McLaughlin et al. (1993). The Atlantic/Pacific front is most likely now located over the Chukchi-Mendeleev boundary region described by Swift et al. (1997), but nearer the Chukchi Cap. This eastward push may have significantly reduced the northward flow of relatively warm Pacific water through Herald Canyon, thus increasing the flow through Barrow Canyon. The temperature anomalies observed during SHEBA (described in the previous section) support this hypothesis. Historical and current (proposed) synoptic scale flow patterns are shown in Figure 5.4.

2. Depth of T_{\max}

In SHa-e (all boxes where Pacific inflow water was observed) the depth of T_{\max} from the SHEBA data was significantly shallower than expected (~50 m versus ~75 m) based on comparison with the digital atlas data and previous observations. However, the SHEBA salinity profiles below 50 m in these five boxes closely resemble available historical data (see Figure 3.4). This suggests that the Pacific

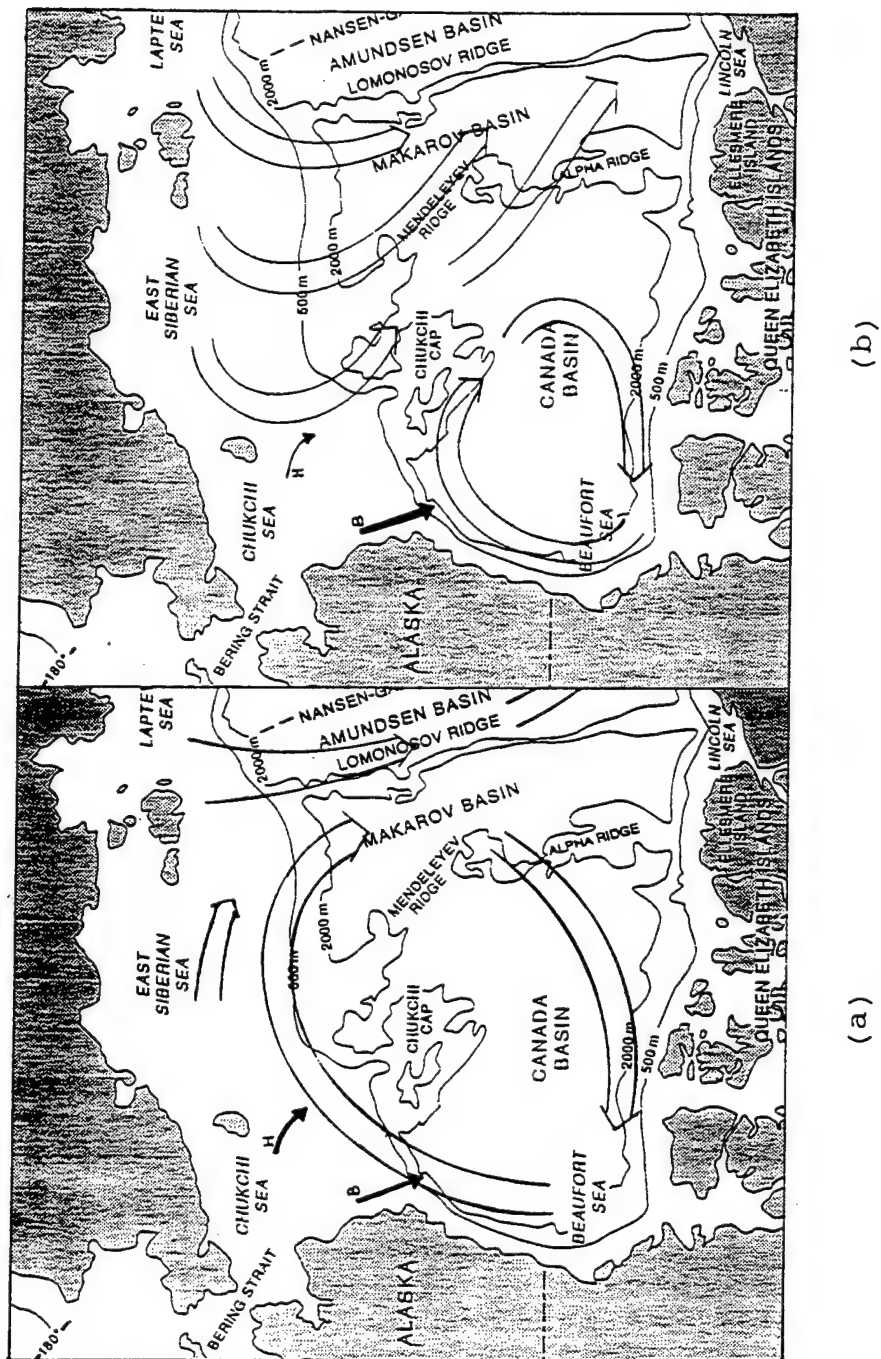


Figure 5.4. (a) Historical and (b) current (proposed) synoptic scale flow patterns in the Canadian Basin. Small arrows indicate Pacific inflow through Barrow (B) and Herald (H) canyons. This figure incorporates concepts from Morison et al. (1998), Swift et al. (1997), Carmack et al. (1997), Walsh et al. (1996), and Kwok et al. (1996).

inflow is fresher (less dense) than it was prior to 1990, and therefore interleaves into the water column at a shallower (less dense) equilibrium level. The salinity values of the summertime Pacific input at the depth of T_{\max} ranged from 31.02 psu in SHb to 31.78 psu in SHe, all of which are lower than the historical value of ~31.9 psu (Jones and Anderson, 1986) cited in Chapter II. Recent works (Steele and Boyd, 1998; McLaughlin et al., 1996) cite lower and broader salinity ranges for T_{\max} (31 to 32 psu). Roach et al. (1995) measured the salinity of Bering Strait inflow from 1990-1994 and found wintertime 1993-1994 salinities to be significantly lower than wintertime 1990-1991 salinities. However, data from several more years is needed to determine whether a trend exists.

Processes that lead to a thinner mixed layer may be secondary contributors to the shoaling of the upper halocline. A thinner mixed layer could result from a decrease in the mean intensity of winter storms. For example, the small temperature maxima near 25 m in boxes SHg-h are likely due to a relatively mild winter storm season failing to completely re-mix the seasonal thermocline formed by summer heating. Another potential contributor to a thinner mixed layer is a retreating annual ice edge. If the maximum winter and minimum summer extent of the ice edge were both displaced farther north for several consecutive years, the region of new ice formation and summer ice melting would then be shifted northward. Therefore, the region where summer ice melt adds to the relatively fresh mixed layer would also shift northward. The shallowest depths of T_{\max} were 46 m and 36 m in boxes SHd and SHe, respectively - the boxes closest to the warm Pacific inflow. Finally, the weakened Beaufort High may have a small influence on the mixed layer depth, as a weaker central pressure and surface pressure gradient results in reduced wind forcing at the air-sea interface.

3. Mixed layer temperature and salinity

Due to the limited seasonal coverage of SHEBA data over various boxes, direct seasonal comparisons of mixed layer temperature and salinity with respect to mean Mar-May and Jul-Sep values are only available for boxes SHc-e in winter and SHg in summer (refer to Figure 4.6 and Table 4.1). Temperature changes were negligible, but in all four cases the salinity increased significantly during SHEBA. The 1.89 psu summertime increase in SHg (the Chukchi-Mendeleev boundary region) is roughly three times the increase in the boxes to the south. These increases may all be related to warming or shoaling of the Atlantic layer (Aagaard and Swift, 1998), and entrainment of salt into the mixed layer.

The effect of warming or shoaling of the Atlantic layer would likely be largest in SHg, where the largest increase was found, due to its location north of the Chukchi Cap, closer to source of Atlantic water. Following the previous discussion, atmospheric circulation changes may have led to a shift in the location of the Atlantic/Pacific front and the retreat of Pacific water from the northern Canada Basin. This removal of upper halocline waters from the northern Canada Basin would weaken the overall halocline, thus weakening the primary barrier to entrainment from the Atlantic layer. Figure 4.3 shows a temperature increase between 125 m and 150 m in boxes SHe-h, over the Chukchi-Mendeleev boundary region, which may be consistent with the increase to the deeper Atlantic layer maximum. If so, this increase appears at least 25 m higher than expected based on the discussion in Chapter II. Analysis of SHEBA profiles below 150 m is required to substantiate this. Also, this very large increase was observed during the summer (Jul-Sep) in only one grid box (SHg). No comparable information is currently available in any of the surrounding grid boxes for either winter or summer. Therefore, further analysis must also determine whether this is a regional or local anomaly.

Although direct seasonal comparisons between SHEBA and historical data were not possible in boxes SHa-b, the inter-seasonal comparisons made in Chapter IV demonstrate that the mixed layer salinity is anomalously fresh in both of these boxes (see Figure 4.6 and Table 4.1). McPhee et al. (1998) also noted anomalously fresh SHEBA (Oct-Nov 1997) mixed layer salinities in comparison with AIDJEX observations taken 22 years earlier over the same location. Their comparison was also inter-seasonal, accounting for expected seasonal changes in mixed layer salinity and temperature between mid-summer (when AIDJEX was conducted) and late fall/early winter (when this SHEBA data was obtained).

The low salinities measured in boxes SHa-b during SHEBA are likely due to excessive ice melting during the preceeding summer 1997. This ice melt would not yet have been convectively mixed by significant winter ice growth or winter storms. Thinning pack ice and/or a retreating ice edge may account for these mixed layer observations from SHEBA. Increased basal melting would both thin the ice, as observed by McPhee et al. (1998), and freshen the mixed layer. If the ice edge were to shift northward, then the region where annual thawing adds fresh water to the mixed layer may account for both the decreased salinities in the mixed layer of the western Beaufort Sea, and the increased salinities nearer the Chukchi Sea.

C. POTENTIAL EFFECTS OF OBSERVED ANOMALIES

1. Surface Layer Freshening

Surface layer freshening strengthens the upper halocline (assuming relatively unchanged salinity in the Atlantic layer). A stronger halocline would provide even more stability to the water column and less chance for exchange between mixed layer waters and the Pacific layer below.

2. Lack of Pacific Input in SHf-h

The lack of waters with a Pacific signature in these boxes may result in these water masses more closely resembling water masses originating in the Eurasian Basin. Such similarities have already been observed in the Makarov Basin and Chukchi-Mendeleyev boundary region (Steele and Boyd, 1998; Carmack et al., 1997; Morison et al., 1998; and Swift et al., 1997). The absence of the strong, cold halocline layer in the northern Canada Basin could result in an increase in upward heat flux from the intermediate (Atlantic) layer.

3. Effect of Changes in Depth and Magnitude of T_{\max}

Because the magnitude of T_{\max} is notably increased, and the depth of T_{\max} is notably decreased in boxes SHa-d, the upward heat flux by turbulent transport through the pycnocline (during winter ice cover) will increase over historical values, and consequently, heat flux into the bottom of the ice is increased (Stanton, 1999). This effect might be reflected in decadal statistics and trends of ice edge, percent ice cover, and ice thickness. The largest decreases in ice cover would be expected where T_{\max} is warmest and nearest the surface.

D. RELATED TOPICS FOR FURTHER INVESTIGATION

1. Properties of Northern Canada Basin Waters

The origin of a water mass can be traced by examining its properties. For example, river runoff can be traced by its alkalinity content, and Pacific water can be traced by its high nutrient maximum (Jones and Anderson, 1986; Swift et al., 1997). A detailed analysis of water mass properties in all SHEBA boxes may reveal more conclusive evidence regarding the changes in surface layer advection patterns, and affirm the suggestion that the Chukchi-Mendeleyev

boundary region may be a primary injection site. It would be interesting to trace the amount or existence of river runoff in all SHEBA boxes and compare this with observed salinity decreases (and ice edge data).

2. Ice Cover/Thickness Changes

Exploration of the relationship between SHEBA temperature and salinity anomalies and ice data (i.e., coverage and thickness) would be an appropriate subject for further investigation. Additionally, studies of changes in ice drift patterns and regions of active pressure ridge formation would provide more evidence related to the accuracy of current theories about changes in Arctic circulation patterns.

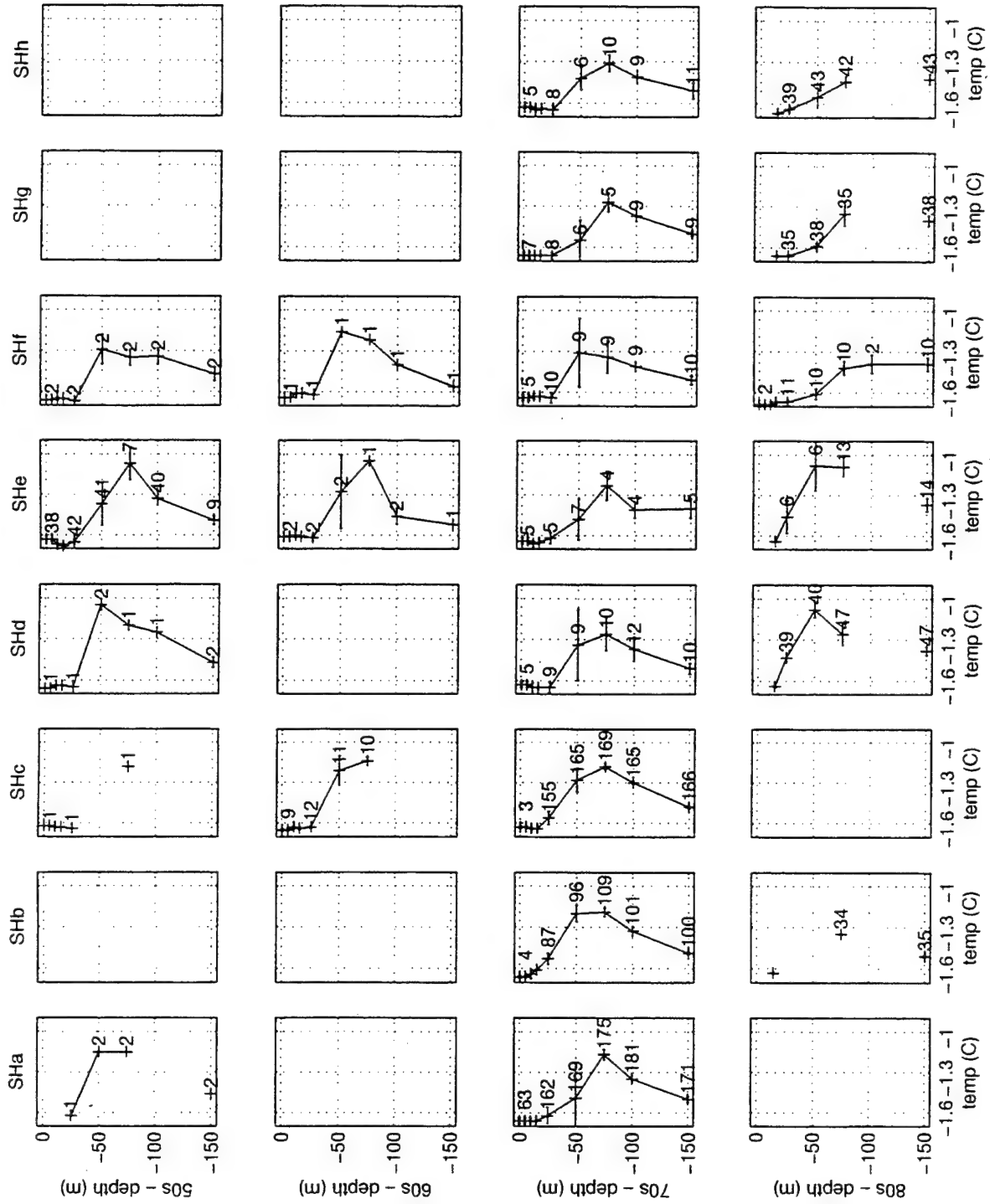
3. Impacts on Marine Life

Changes in circulation and advection patterns, as well as temperature, salinity, and nutrient content at a given depth (pressure) level may significantly impact the location and even survival of marine plants, animals and birds at all levels of the food chain. This could potentially lead to altered migration patterns, or otherwise effect various life cycle stages in both positive and negative ways.

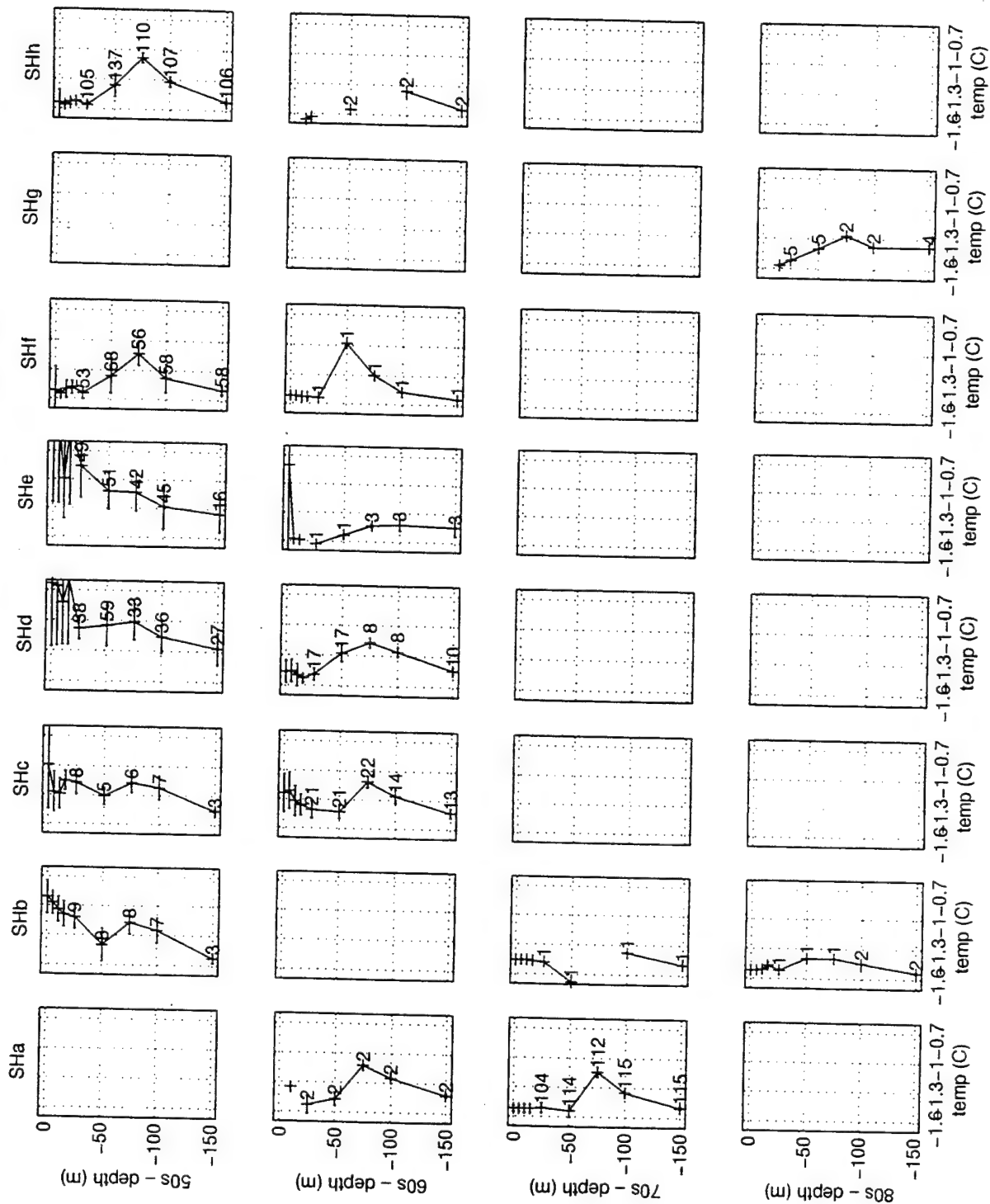
APPENDIX A

SUMMARY PLOTS OF MAR-MAY AND JUL-SEP HISTORICAL DATA FROM THE EWG DIGITAL ATLAS FOR TEMPERATURE AND SALINITY

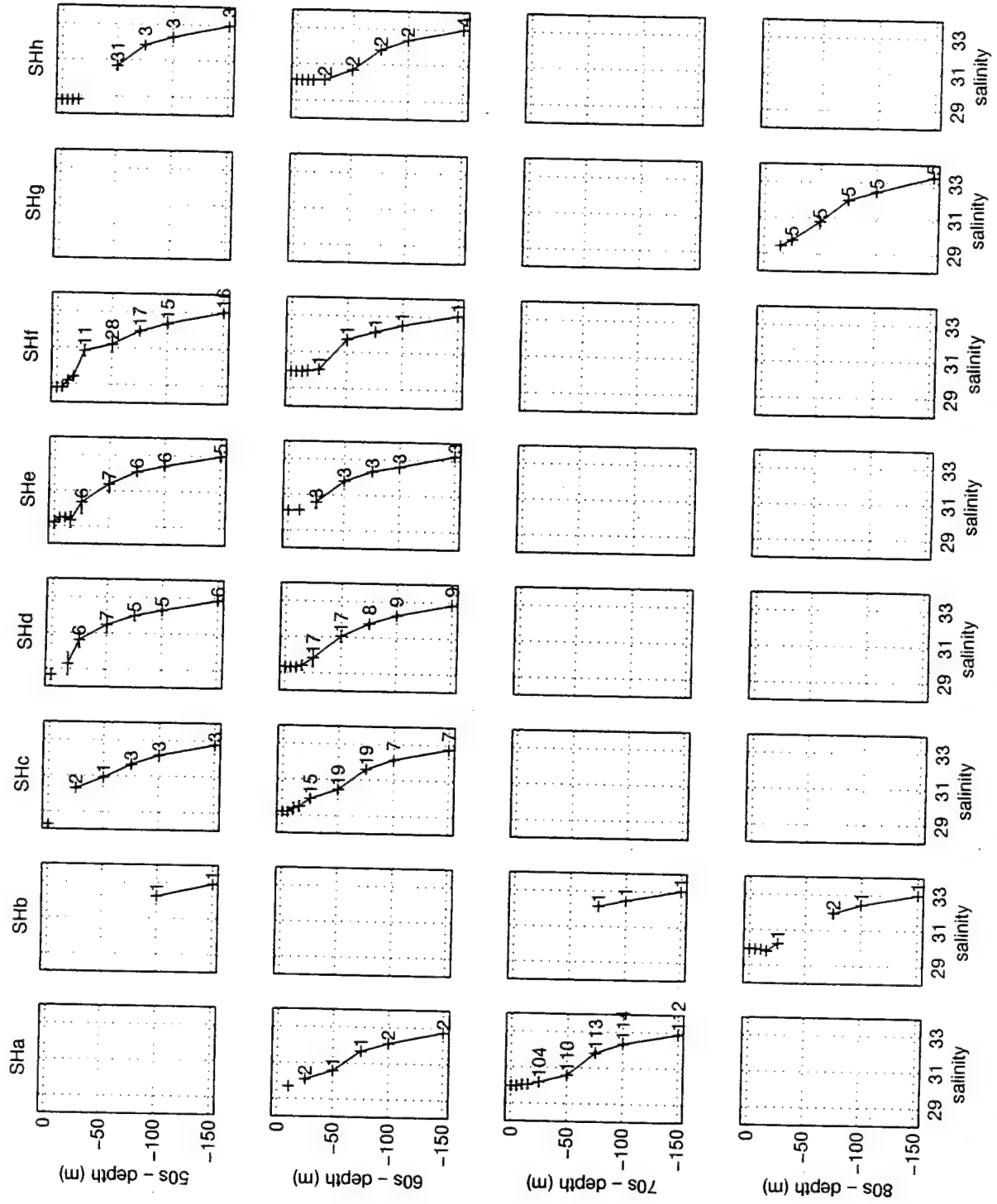
All decades Mar-May temperature over 8 SHEBA track boxes



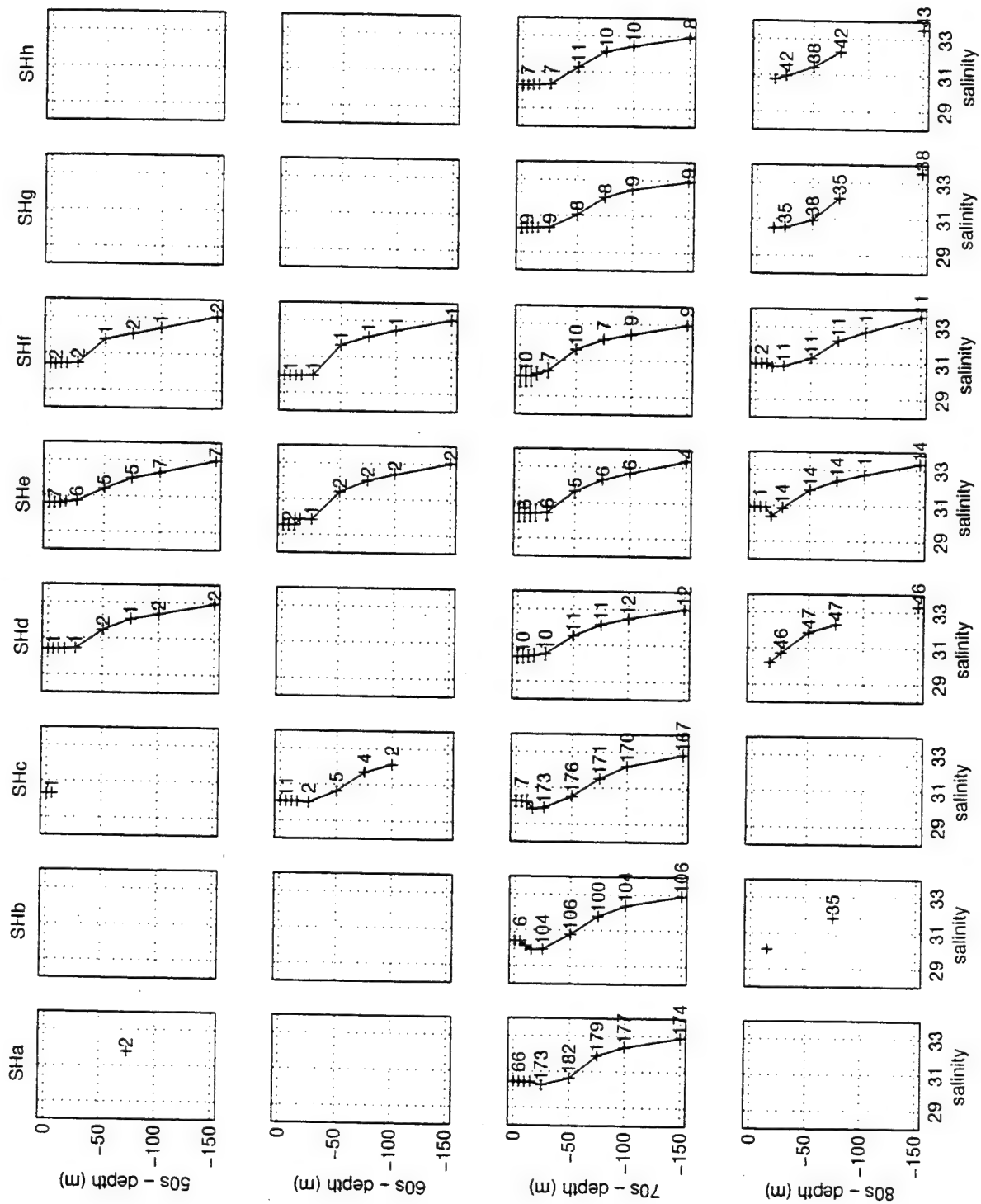
All decades Jul-Sep temperature over 8 SHEBA track boxes



All decades Jul-Sep salinity over 8 SHEBA track boxes



All decades Mar-May salinity over 8 SHEBA track boxes



LIST OF REFERENCES

- Aagaard, K., The Beaufort Undercurrent, in The Alaskan Beaufort Sea, edited by P. W. Barnes et al., Academic Press, FL, 47-74, 1984.
- Aagaard, K., and E. C. Carmack, The Role of Sea Ice and Other Fresh Water in the Arctic Circulation, *J. Geophys. Res.*, 94, 14485-14498, 1989.
- Aagaard, K., L. K. Coachman, and E. Carmack, On the Halocline of the Arctic Ocean, *Deep-Sea Res., Part A*, 28, 529-545, 1981.
- Aagaard, K., and J. H. Swift, Atlantic Water Warming in Study of the Arctic Change Workshop, edited by J. Morison, K. Aagaard, and M. D. Steele, APL/UW/Seattle, 10-12 November 1997, 46-47, August 1998.
- Becker, P., The Effect of Arctic Hydrological Cycles on Arctic Ocean Circulation, Ph.D. Dissertation, Old Dominion University, Norfolk, VA, 1995.
- Bourke, R. H., Currents, Fronts and Fine Structure in the Marginal Ice Zone of the Chukchi Sea, *Polar Record*, 21(135), 569-575, 1983.
- Carmack, E. C., and K. Aagaard, On the Deep Water of the Greenland Sea, *Deep-Sea Res.*, 20, 687-715, 1973.
- Carmack, E. C., K. Aagaard, J. H. Swift, R. W. MacDonald, F. A. McLaughlin, E. P. Jones, R. G. Perkin, J. N. Smith, K. M. Ellis, and L. R. Killius, Changes in Temperature and Tracer Distributions within the Arctic Ocean: Results from the 1994 Arctic Ocean Section, *Deep-Sea Res., Part II*, 44, 1487-1502, 1997.
- Cavalieri, D. J., and S. Martin, The Contribution of Alaskan, Siberian, and Canadian Coastal Polynyas to the Cold Halocline Layer of the Arctic Ocean, *J. Geophys. Res.*, 99, 18343-18362, 1994.
- Coachman, L. K., and K. Aagaard, Physical Oceanography of Arctic and Subarctic Seas, in Marine Geology and Oceanography of the Arctic Seas, edited by Y. Herman, Springer-Verlag, NY, 1-72, 1974.
- Coachman, L. K., and C. A. Barnes, The Contribution of Bering Sea Water to the Arctic Ocean, *Arctic*, 14(3), 146-161, 1961.

D'Asaro, E. A., Observations of Small Eddies in the Beaufort Sea, *J. Geophys. Res.*, 93, 6669-6684, 1988a.

D'Asaro, E. A., Generation of Submesoscale Vortices: A New Mechanism, *J. Geophys. Res.*, 93, 6685-6693, 1988b.

Environmental Working Group (EWG), *Joint U.S.-Russian Atlas of the Arctic Ocean* [CD-ROM], Natl. Snow and Ice Data Cent., Boulder, CO, 1997.

Hunkins, K. L., Subsurface Eddies in the Arctic Ocean, *Deep-Sea Res.*, 21, 1017-1033, 1974.

Jones, E.P. and L.G. Anderson, On the Origin of Chemical Properties of the Arctic Halocline, *J. Geophys. Res.*, 91, 10,759-10,767, 1986.

Kulikov, E. A., E. C. Carmack, and R. W. Macdonald, Flow Variability at the Continental Shelf Break of the MacKenzie Shelf in the Beaufort Sea, *J. Geophys. Res.*, 103, 12,725-12,741, 1998.

Kwok, R., J. C. Comiso, and G. F. Cunningham, Seasonal Characteristics of the Perennial Ice Cover of the Beaufort Sea, *J. Geophys. Res.*, 101, 28417-28439, 1996.

Manley, T. O., and K. Hunkins, Mesoscale Eddies of the Arctic Ocean, *J. Geophys. Res.*, 90, 4911-4930, 1985,

Maykut, G. A., and M. G. McPhee, Solar Heating of the Arctic Mixed Layer, *J. Geophys. Res.*, 100, 24691-24703, 1995.

McLaughlin, F. A., E. C. Carmack, R. W. Macdonald, and J. K. B. Bishop, Physical and Geochemical Properties Across the Atlantic/Pacific Water Mass Front in the Southern Canadian Basin, *J. Geophys. Res.*, 101, 1183-1197, 1996.

McPhee, M. G., T. P. Stanton, J. H. Morison, and D. G. Martinson, Freshening of Upper Ocean in the Central Arctic: Is Perennial Sea Ice Disappearing?, *J. Geophys. Res.*, 25, 1729-1732, 1998.

Melling, H., Hydrographic Changes in the Canada Basin of the Arctic Ocean, 1979-1996, *J. Geophys. Res.*, 103, 7637-7645, 1998.

Melling, H. and E. L. Lewis, Shelf Drainage Flows in the Beaufort Sea and Their Effect on the Arctic Ocean Pycnocline, *Deep-Sea Res.*, 29, 967-985, 1982.

- Muench, R. D., Mesoscale Phenomena in the Polar Oceans, in Polar Oceanography, Part A: Physical Science, edited by Walker Smith, Jr., Academic Press, NY, 223-285, 1990.
- Morison, J., M. Steele, and R. Anderson, Hydrography of the Upper Arctic Ocean Measured From the Nuclear Submarine U.S.S. Pargo, *Deep-Sea Res. I*, 45, 15-38, 1998.
- Padman, L. and T. M. Dillon, Vertical Fluxes Through the Beaufort Sea Thermohaline Staircase, *J. Geophys. Res.*, 92, 10799-10806, 1987.
- Paquette, R. G., and R. H. Bourke, Observations on the Coastal Current of Arctic Alaska, *J. Mar. Res.*, 32, 195-207, 1974.
- Paquette, R. G., and R. H. Bourke, Ocean Circulation and Fronts as Related to Ice Melt-Back in the Chukchi Sea, *J. Geophys. Res.*, 86, 4215-4230, 1981.
- Roach, A. T., K. Aagaard, C. H. Pease, S. A. Salo, T. Weingartner, V. Pavlov, and M. Kulakov, Direct Measurements of Transport and Water Properties Through the Bering Strait, *J. Geophys. Res.*, 100, 18443-18457, 1995.
- Serreze, M. C., J. E. Box, R. G. Barry, and J. E. Walsh, Characteristics of Arctic Synoptic Activity, 1952-1989, *Meteor. Atmos. Phys.*, 51, 147-164, 1993.
- Stanton, T. P., Ocean Heat Fluxes and Pycnocline Entrainment During SHEBA, in Proceedings of Fifth Conference on Polar Meteorology and Oceanography, 10-15 January 1999, Dallas, 372-375, Am. Meteor. Soc., Boston, 1999.
- Steele, M., and T. Boyd, Retreat of the Cold Halocline Layer in the Arctic Ocean, *J. Geophys. Res.*, 103, 10419-10435, 1998.
- Swift, J.R., E. P. Jones, K. Aagaard, E. C. Carmack, M. Hingston, R. W. MacDonald, F. A. McLaughlin, and R. G. Perkin, Waters of the Makarov and Canada Basins, *Deep-Sea Res. II*, 44, 1503-1529, 1997.
- Untersteiner, N., On the Mass and Heat Budget of Arctic Sea Ice, *Arch. Meteorol. Geophys. Bioklimatol.*, A12, 151-182, 1961.
- Walsh, J. E., W. L. Chapman, and T. L. Shy, Recent Decrease of Sea Level Pressure in the Central Arctic, *J. Climate*, 9, 480-486, 1996.

Weingartner, T. J., D. J. Cavalieri, K. Aagaard, and Y. Sasaki, Circulation, Dense Water Formation and Outflow on the Northeast Chukchi Shelf, *J. Geophys. Res.*, 103, 7647-7661, 1998.

INITIAL DISTRIBUTION LIST

1. Defense Technical Information Center 2
8725 John J. Kingman Rd., STE 0944
Ft. Belvoir, VA 22060-6218
2. Dudley Knox Library 2
Naval Postgraduate School
411 Dyer Rd.
Monterey, CA, 94943-5101
3. LCDR Robin D. Tyner 2
3012 Tammy Street
Bellevue, NE 68123
4. Timothy P. Stanton 3
Code OC/St
Naval Postgraduate School
Monterey, CA 93943
5. Dr. R. H. Bourke 2
Code OC/St
Naval Postgraduate School
Monterey, CA 93943
6. Chairperson, Dept. Of Oceanography 1
Code OC
Naval Postgraduate School
Monterey, CA 93943
7. Yuxia Zhang 1
Code OC
Naval Postgraduate School
Monterey, CA 93943
8. CWO4 (Ret.) Thomas Brown 1
92-1191 Hookeha Street
Makakilo, HI 96707
9. Edwin & Marilyn Buxton 1
25 Kickapoo Place
Charleston, IL 61920